

College of Engineering, Design and Physical Sciences  
Department of Electronic and Computer Engineering  
PhD. Electronics and Electrical Engineering



Brunel University London

Wireless Power Transfer for Electric Vehicles  
using Variable Capacitor Technique in  
Compensated Circuit

Name: Muhammad Salman Sikandar

February, 2024

## Abstract

The Wireless Power Transfer (WPT) systems provide a platform by which the electric energy from the power grids can be conveyed to Electric Vehicles (EVs) by only using the electromagnetic fields, i.e. without necessarily the contacts. Other enhancements that WPT offers include: its ability to address some issues inherent in the "plug-in" charging technique like vulnerability to vandalism, power inefficiencies, and the dangers of exposed connectors as well as loose wires, among other things. Additionally, this technology makes it convenient for EVs to be charged while they are moving or parked.

Comprehensive research has been carried out in the last decades in the development of wireless power transfer technologies for electric vehicles. Literature review in the field of wireless power transferred has revealed that inductive resonance with series-series compensation circuit is the most efficient compensated circuit in inductive resonant technology as it plays important role in the system resonance. The resonance frequency is the key point which could be disturbed because of external and internal disturbance of the inductor values. To overcome this limitation a variable capacitor technique is used to achieve the required resonance frequency.

A proposed variable capacitor technique implemented in wireless power transfer circuit is designed, simulated and practically implemented with 87.75% efficiency. In this research the fixed capacitor in the proposed compensation circuit is replaced with a controlled variable capacitor in order to achieve a fine-tuned resonance frequency. Also, the speed of selecting the required tuned capacitor is achieved using high frequency (100kHz). The main idea is to select different values of the resonant capacitor in order to achieve different resonance frequencies.

Inductor coil design is also presented in this research using Ansys Electronic software in order to find the optimum inductor and optimum airgap used in the design of the variable-capacitor compensated circuit.

A circuit using the proposed technique is built in the lab to verify the design and simulation results. Overall, this research is based on static wireless charging.

## **Acknowledgment**

Firstly, I would like to thank Almighty Allah (God) and then my academic supervisor Dr. Mohamed Darwish, for providing me with the best supervision, guidance and enthusiastic support during the entire period of my dissertation for his immense support and guidance. His knowledge and expertise greatly aided me in completing my PhD research and thesis successfully.

I would also like to thank lab technicians for their great support and guidance. I would also like to thank the department of electronics and computer engineering for their continuous support over the course of my academic study.

I would also like to say thank you to all my friends for their great support and motivation. I would also like to say thank you to my parents for their utmost interest in my education. They are a source of inspiration for me in my life. Thank you to my beloved brother and sisters for their constant love throughout my master's journey.

I would like to dedicate my PhD degree to My beloved Mamu (Uncle) Late Farhan ul Haq Faisal Hashmi and my grandma Late Farman-e-Elahi.

## Table of Contents

Abstract.....	ii
Acknowledgment .....	iii
List of Figures .....	vii
List of Tables .....	ix
Abbreviations.....	x
List of Symbols .....	xii
Chapter 1: Introduction .....	1
1.1 Aim and Objectives .....	3
1.2 Scope of the Research.....	4
1.3 Publications.....	4
1.4 Contributions .....	5
1.4.1 Review of methods for charging of Electric Vehicle. ....	5
1.4.2 Review of different compensative circuit topologies for resonance circuit.....	5
1.4.3 Design of Variable Capacitor for WPT.....	5
1.4.4 Simulation design of wireless power transfer for EV including variable capacitor. ....	6
1.4.5 Simulation design of inductive coil. ....	6
1.4.6 Hardware Design of wireless charging system. ....	6
1.5 Thesis Layout.....	6
Chapter 2: Literature Review .....	8
2.1 Introduction .....	8
2.2 Concept of Electric Vehicle .....	8
2.3 Types of Electric Vehicles.....	8
2.4 Types of EV Charging.....	10
2.4.1 Conductive Charging .....	11
2.4.2 Battery Swapping .....	12
2.4.3 Wireless Charging .....	13
2.5 Modes of Wireless Charging .....	14
2.5.1 Static Charging .....	14
2.5.2 Dynamic Charging .....	15
2.6 Challenges of Wireless Charging .....	15
2.7 Different Methods of Wireless Power transfer .....	16
2.7.1 Capacitive Charging.....	17
2.7.2 Inductive Charging .....	18
2.7.3 Magnetic gear wireless power transfer .....	18
2.7.4 Hybrid Charging System .....	19

2.8 Compensation topologies .....	21
2.8.1 Series-Series Compensation.....	21
2.8.2 Series-Parallel Compensation .....	22
2.8.3 Parallel-Series Compensation .....	23
2.8.4 Parallel-Parallel Compensation.....	23
2.9 Summary .....	24
Chapter 3: Design of variable capacitor .....	25
3.1 Introduction .....	25
3.2 Function of Variable Capacitor .....	25
3.3 Proposed variable Capacitor .....	26
3.3.1 C-effective Calculation .....	26
3.4 Summary .....	33
Chapter 4: Design of Wireless charging System of Electric vehicle .....	35
4.1 Introduction .....	35
4.2 Design of WPT System .....	35
4.3 Equivalent Circuit and derivations .....	36
4.4 Summary .....	41
Chapter 5: Simulation of WPT with fixed and variable capacitor .....	42
5.1 Introduction .....	42
5.2 Simulation Design .....	42
5.3 Results .....	45
5.4 Variable Capacitor Simulation.....	51
5.5 Summary .....	60
Chapter 6: Inductor coil design .....	61
6.1 Introduction .....	61
6.2 Single Inductor Coil Design Simulation .....	61
6.3 Two Coil design Primary and Secondary.....	68
6.4 Simplorer/ Twin builder Design .....	74
6.5 Summary .....	76
Chapter 7: Hardware Implementation.....	78
7.1 Introduction .....	78
7.2 Hardware Implementation .....	78
7.3 Results.....	79
7.3.1 Test 1.....	80
7.3.2: Test 2.....	81
7.4 Comparison between Simulation and Hardware.....	82

7.5 Summary .....	83
Chapter 8: Conclusions and Future Work .....	84
8.1 Conclusions .....	84
8.2 Future Recommendation Work .....	85
References .....	86
Appendixes.....	91

## List of Figures

Figure 2-1:Different Types of EVs [18] .....	9
Figure 2-2:Primary Methods of EV Charing [18].....	10
Figure 2-3:Basic block diagram of wireless charging for Electric Vehicles [23].....	14
Figure 2-4:Different technologies for wireless charging system [23].....	16
Figure 2-5:Diagram of Capacitive Wireless Power Transfer [23] .....	17
Figure 2-6:Diagram of Inductive Wireless Power Transfer [23] .....	18
Figure 2-7:Diagram of magnetic Gear based Wireless Power Transfer [23].....	19
Figure 2-8:Diagram of Hybrid Charging System [23].....	20
Figure 2-9:Series-Series Compensation Circuit.....	21
Figure 2-10:Series-Parallel Compensation Circuit .....	22
Figure 2-11:Parallel-Series Compensation Circuit .....	23
Figure 2-12:Parallel-Parallel Compensation Circuit.....	23
Figure 3-1:Basic diagram of Variable Capacitor .....	25
Figure 3-2:Diagram of Proposed Variable Capacitor .....	26
Figure 3-3:C-effective values at different duty cycle and N by using other equation (3.9).....	32
Figure 3-4:C-effective values at different duty cycle and N by using other equation (3.10).....	33
Figure 4-1:Circuit Diagram of wireless power transfer by using SS-Compensation topology.....	35
Figure 4-2:Equivalent Circuit Diagram of wireless power transfer by using SS-Compensation topology .....	36
Figure 5-1:Wireless power transfer design with fixed capacitor .....	42
Figure 5-2:H-Bridge Output Voltage Waveform.....	45
Figure 5-3:Primary Side Current waveform .....	46
Figure 5-4:Secondary Side Current waveform .....	47
Figure 5-5:Primary Side Voltage Waveform.....	48
Figure 5-6:Secondary Side Voltage Waveform .....	48
Figure 5-7:Secondary Side Rectifier Input Voltage waveform.....	49
Figure 5-8:Output Power at load Side RL .....	50
Figure 5-9:Average Input and Output Powers .....	51
Figure 5-10:Variable Capacitor Circuit Diagram .....	52
Figure 5-11:Result Graph for Variable Capacitor.....	53
Figure 5-12:Variable Capacitor Circuits with different duty cycles .....	54
Figure 5-13:Results Graph of Variable capacitor with different duty cycles .....	56
Figure 5-14:Variable Capacitor design with same C values.....	56
Figure 5-15:Result Graph for Variable Capacitor with same capacitor values.....	57
Figure 5-16:Circuit diagram of WPT with variable capacitor .....	58
Figure 5-17:Graph for C-effective values at more different resonance frequency .....	59
Figure 6-1:Graphical User Interface of Ansys Software.....	62
Figure 6-2:Current Excitation (in and out) .....	63
Figure 6-3:Design List dialog box .....	64
Figure 6-4:Different Parameter sitting dialog box (Length).....	65
Figure 6-5:Simulation Validation dialog box .....	66
Figure 6-6:Measurement report of designed coil.....	67
Figure 6-7:Simulation environment of Primary and secondary coil.....	68
Figure 6-8:Current Excitation diagram (In and out) .....	69
Figure 6-9:Design List for Mutual Induction.....	70

Figure 6-10:Measurements results of Designed Coils .....	71
Figure 6-11:Graphical representation results of designed coil .....	72
Figure 6-12:Magnetic field distribution of designed coil .....	73
Figure 6-13:Different views of magnetic field representation .....	74
Figure 6-14:Simplorer/ Twin Builder circuit of WPT .....	75
Figure 6-15:Result graph of Simplorer/ Twin builder design .....	76
Figure 7-1:Hardware of WPT System .....	79
Figure 7-2:Result of Test .....	80
Figure 7-3:Result of Test 2 .....	82



## List of Tables

Table 1:EVs charging levels and Specification [18].....	12
Table 2:Comparing EV charging using dynamic and static wireless methods [18] .....	15
Table 3:Overview of different methods of WPT for EV's [23].....	17
Table 4:Variable used in the all above equations (3.1) - (3.11).....	29
Table 5:Calculation of N value .....	31
Table 6:Value used in V-Pulse for H-Bridge.....	44
Table 7:WPT design Components Values used.....	44
Table 8:V-Pulse value used for variable capacitor design .....	52
Table 9:Components and their values used in variable capacitor design with different C values .....	52
Table 10:Duty cycle set for design A-I.....	55
Table 11:Components and their values used in variable capacitor design with equal C values .....	57
Table 12:C-effective values for different resonance frequency .....	58
Table 13:Labelled hardware description.....	79

## Abbreviations

WPT	Wireless Power Transfer
WCS	Wireless Charging System
WEVCS	Wireless Electric Vehicle Charging System
EVs	Electric Vehicles
CO	Carbon Monoxide
NO <sub>x</sub>	Nitrogen Oxides
SO <sub>2</sub>	Sulphur Dioxide
ICE	Internal Combustion Engine
NEVs	New Energy Vehicles
HEVs	Hybrid Electric Vehicles
PEVs	Pure Electric Vehicles
FCEVs	Fuel Cell Electric Vehicles
PHEVs	Plug-in Hybrid Electric Vehicles
FCVs	Fuel Cell Vehicles
BEVs	Battery Electric Vehicles
SOH	State of Health

SS	Series-Series
SP	Series-Parallel
PS	Parallel-Series
PP	Parallel-Parallel
MCS	Megawatt Charging System
V2G	Vehicle-to-Grid
HF	High Frequency
MGWPT	Magnetic Gear Wireless Power Transmission
RIPT	Resonant Inductive Power Transfer
CWPT	Capacitive Wireless Power Transfer
IPT	Inductive Power Transfer
PFC	Power Factor Correction
UART	Universal Asynchronous Transmitter-Receiver
KVL	Kirchhoff Voltage Law
FEA	Finite Element Analysis
GUI	Graphical User Interface
AI	Artificial Intelligence

## List of Symbols

V	Voltage
I	Current
A	Ampere
kW	Kilowatt
kHz	Kilohertz
kVA	Kilo volt ampere
VA	volt ampere
R	Resistance
L	Inductor
C	Capacitor
nF	Nano Farad
uF	Micro Farad
uH	Micro Henry
mH	Milli Henry
us	Micro Seconds
ns	Nano Seconds
PW	Pulse width
PER	Period
TR	Time Rise
TF	Time Fall
TD	Time delay
$Z_1$	Primary side Impedance
$Z_2$	Secondary side Impedance

$Z_r$	Reflected impedance
$\omega$	Frequency
$\omega_o$	Resonance frequency
$i_p$	Primary side current
$i_s$	Secondary side current
$V_p$	Primary side voltage
$V_s$	Secondary side voltage
$L_p$	Primary side inductance
$L_s$	Secondary side inductance
$C_p$	Primary side capacitance
$C_s$	Secondary side capacitance
$M$	Mutual Inductance
$Q_s$	Quality factor
$K$	Coupling factor

# Chapter 1: Introduction

One of the main causes of environmental contamination is the increase in the number of fossil fuel-powered vehicles, including cars, trucks, buses, and motorcycles. Due to the release of dangerous air pollutants such as carbon monoxide ( $CO$ ), nitrogen oxides ( $NO_x$ ), and sulphur dioxide ( $SO_2$ ), the quality of the air deteriorates and it also causes global warming. These pollutants affect almost every organ system in the human body negatively in addition to endangering the environment. Researchers and governmental organisations have expressed concerns about the aforementioned environmental difficulties, which has resulted in a major focus on reducing reliance on fossil fuels and replacing them with cleaner alternatives. One of the best examples of this transition is provided by electric cars (EVs). Over the past few decades, electric vehicles (EVs) have gradually gained popularity due to their benefits, which include reduced greenhouse gas emissions, no emissions of pollutants, and increased economy [1].

Electric vehicles (EVs) are seen as a viable replacement that can help with the air pollution crisis as well as the scarcity of fossil resources. The availability of necessary charging facilities has a significant impact on the general adoption of electric vehicles. Although at the moment wired charging is more common, wireless charging technology is developing quickly. As a result, for the foreseeable future, wired and wireless charging EVs will coexist. For this reason, it is considered essential to have charging stations that support different kinds of electric vehicles in both wired and wireless modes. But the expenses of making and installing these two charging systems separately might be too high. The shared usage of some components in both charging models, such as workspaces, electrical, and electronic devices, is thought to be more economical than building wired and wireless charging facilities separately, especially when considering the investment in civil infrastructure and gadgets [2].

The Electric Vehicle (EV) business has gained more attention in the past few years, most especially with the elevating cost of petroleum. Mainly, the surge of interest is driven by the rapid growth of the industry in an attempt to provide an alternative to conventional motorization based on internal combustion engine (ICE) [3]. Transportation expedites an economy in as much as it makes it expansive, but it is also a very big contributor to greenhouse emissions. The exclusive use of Internal Combustion Engine (ICE) cars for travel, especially in high fuel periods, can be detrimental to economic progress. This has made the Electric

Vehicles (EVs) to be seen as viable alternatives in not only electrifying transportation, but as well in decarbonising it [4].

It is increasingly difficult for the world to be grappling with the environmental and the energy challenges. Electric vehicles (EVs), compared to vehicles using conventional fuel, have many advantages. They help in preserving oil reserves and substantially reduce carbon emissions. This has increased the attention from governments and automotive companies across the globe in the deployment of EVs, which is continuously growing. [5] [6]. Nonetheless, the recurrent instances of spontaneous combustion and fires in Electric Vehicles (EVs) have resulted in substantial economic losses for both car owners and operators of charging facilities. These incidents of charging safety have posed significant impediments to the advancement of EVs and their associated industries [7]. The comprehensive enactment of the national big data strategy has increasingly underscored the trend towards digitalization and intelligence within the automotive sector. Employing big data research as a means to address safety concerns in Electric Vehicles (EVs) has emerged as a crucial approach. The profound amalgamation of EVs with big data is anticipated to expedite the evolution of automotive safety regulatory technology, consequently enhancing the high-quality development of China's EV industry [8].

Recently, the development and extensive acceptance of alternative energy sources have captured substantial global interest. Consequently, this has resulted in an increased popularity of electric vehicles (EVs), which are now regarded as indicators of the advancement and application of these emerging energy technologies [9]. In the pursuit of fostering economic transformation, optimising the energy mix, and enhancing air quality, New Energy Vehicles (NEVs) – encompassing Hybrid Electric Vehicles (HEVs), Pure Electric Vehicles (PEVs), and Fuel Cell Vehicles (FCVs) – have been recognised as key initiatives. These vehicles have now entered a phase of rapid development [10]. China has emerged as the largest national market globally for New Energy Vehicles (NEVs). In 2021, the total sales of NEVs in China reached 3.5 million, marking a 145.6% increase from 2020 and accounting for 53% of the global NEV sales. However, safety concerns have been impeding the extensive adoption of NEVs in the worldwide market. Notably, in 2018, over 40 incidents of spontaneous combustion involving NEVs were reported in China, and the number of recalled NEVs exceeded 130,000. Consequently, it is vital to investigate key technologies such as the state of health (SOH), fault diagnosis, risk assessment, and precise control during NEV operation to enhance the safety regulation of NEVs effectively [11].

For Electric Vehicles (EVs), charging options encompass both contact and wireless methods. Electricity is transmitted via metal contact between plug and socket in contact charging, whereas wireless charging employs an electromagnetic field. Development of wireless charging and its application has kept receiving increasing attention as the benefits such as less contact loss, no mechanical wear, improved safety, and reliability continue to be realised [12]. Electric car charging methods currently in practice include: plug-in charging and wireless charging. Of them, the plug-in charging method is popular, in fact, its high efficiency has even been established as the dominant one. However, this comes with so many disadvantages such as one being prone to tripping over the charging cables, inconveniences of having to manually connect and disconnect the charger, and cable corrosion that would be dangerous to the users. Wireless charging can easily take care of these problems and can add to monitoring systems, hence increasing its functionality [13].

## **1.1 Aim and Objectives**

This research aims to design and develop overall wireless charging system for Electric Vehicle (EV) with design of variable capacitor configuration. The Objectives of the research include:

1. Comprehensive investigation of different wireless power transfer (WPT) technologies for EVs.
2. Full design of variable capacitor configuration.
3. Design of EV charging including variable capacitor.
4. Simulation design of wireless charging for EVs with and without variable capacitor.
5. Simulation design of inductive coil.
6. Hardware implementation of wireless charging system.



## **1.2 Scope of the Research**

The scope of the research will be confined to the Wireless Power Transfer (WPT) technology relevant to Electric Vehicles (EVs). It will commence with an examination of the various existing WPT designs, along with an analysis of their inherent challenges and limitations. It will further aim to design wireless power transfer system for electric vehicle and design of variable capacitor to achieved required resonance frequency. Additionally, inductor coil design will be discussed as well.

The overall system will only take consideration the wireless power transfer of electric vehicle with variable capacitor in order to get the required resonance frequency.

## **1.3 Publications**

During the research process, publications in both conferences and journals were produced.

- 1) M. S. Sikandar, M. Darwish, C. Marouchos “Review of Wireless Charging of EV”, IEEE University Power Engineering Conference (UPEC), September 2022.
- 2) M. S. Sikandar, M. Darwish, “Control of Resonance Frequency by using Variable Capacitor Technique for EV’s”, Journal IEEE Transactions on Vehicular Technology, has been submitted.
- 3) M. S. Sikandar, M. Darwish, “Impact of airgap between Primary and Secondary coil in WPT for Electric Vehicles”, Journal IEEE Transactions on Transportation Electrification, has been submitted.

## **1.4 Contributions**

Contributions of this research are outlined as follows:

### **1.4.1 Review of methods for charging of Electric Vehicle.**

It has been determined that electric vehicles can be charged using two principal methods: the plug-in mode and the wireless power transfer (WPT) mode. The WPT model was chosen after a review of the advantages and disadvantages of both models. Its excellent qualities—such as increased automation, increased safety, increased dependability, and increased flexibility—had an impact on this decision.

Review of technologic techniques was conducted to identify the most adoptive topology of WPT for electric vehicle applications. The magnetic gear wireless power transfer, inductive power transfer, capacitive power transfer, and inductive resonance power transfer are considered of special emphasis in this section. In general, by considering the efficiency, as well as the effectiveness of inductive resonance power transmission, it is generally believed to be the best option for charging electric vehicles.

### **1.4.2 Review of different compensative circuit topologies for resonance circuit**

In order to determine which compensating topology would work best for electric vehicle applications, a thorough analysis of all known Wireless Power Transfer (WPT) technologies topologies was carried out. Discussions encompassed topologies such as Series-Series (SS) compensation, Series-Parallel (SP) compensation, Parallel-Series (PS) compensation and Parallel-Parallel (PP) compensation. Series-Series (SS) compensation topology emerged as the most appropriate choice, being identified and selected for its effectiveness and efficiency in charging electric vehicles.

### **1.4.3 Design of Variable Capacitor for WPT**

This chapter is very critical within the framework of systems that are developed for the transfer of wireless power for electric vehicles. A new paradigm is defined, in that variable capacitors were integrated to maintain the optimum resonance frequencies required to effect energy transfer effectively. In this way, the system will be able to adjust to possible changes in operational conditions, hence increasing efficiency and reliability in the power transfer process. A variable capacitor has been designed to get the required resonance frequency. The value of the capacitor can be controlled by adjusting the duty cycle of the switches (the switching

function of the other switch is a compliment of the first switch).The effective value of the capacitor can be controlled in order to control the resonant frequency without changing the physical value of the capacitor. Simulation has been done in PSpice and MATLAB Simulink.

#### **1.4.4 Simulation design of wireless power transfer for EV including variable capacitor.**

Wireless power transfer design has been proposed with fixed and variable capacitor. Design includes all mathematical equations of wireless power transfer model incorporated with variable capacitor equations. Simulation has been done in PSpice. The contributions made on the details of the design and development of variable capacitor configurations for effective wireless power transfer in electric vehicles. This work highlighted a new way to use variable capacitors to tune resonant frequencies on the fly to increase further energy transfer on its effectiveness via simulation. This work improves the functionalities and reliabilities of wireless power systems, promoting general usage of electric vehicles in consideration of the benefit of improved charging convenience and efficiency

#### **1.4.5 Simulation design of inductive coil.**

In the domain of simulation modelling, a detailed inductive coil has been designed within ANSYS software. Deep analyse has been done by changing the airgap between the primary and secondary coil to see the airgap effect to the efficiency. Important detailed contributions to the electromagnetic modelling and simulation of inductor coils with the help of ANSYS Electronics software. Detailed methodologies and designed a geometric model of the inductor coil so that the simulation results could reflect the actual behaviour of the inductors under different electromagnetic conditions.

#### **1.4.6 Hardware Design of wireless charging system.**

Hardware of wireless power transfer has been designed. Within the confines of a laboratory environment, the implementation of a hardware prototype, designed for the wireless transfer of power to electric vehicles, has been accomplished.

### **1.5 Thesis Layout**

The thesis is divided in to 8 chapters:

**Chapter 1.** This chapter offers an introductory background, elucidating the motivations behind the research. The research aims and objectives, scope of research, publications, contribution and thesis layout are presented.

**Chapter 2.** In this chapter, the justification for utilising a wireless charging system is first addressed, followed by a thorough literature review on various types of wireless EV charging. Subsequently, the most effective configuration will be determined, employing a decision matrix. The limitations of using a fixed capacitor are then discussed, underscoring the necessity for a variable capacitor. This discussion sets the stage for the subsequent chapter

**Chapter 3.** This chapter will encompass the complete design of the variable capacitor configuration. The design encompasses a series of equations that determine the value of the capacitor at varying duty cycles. The outcomes of these equations will be illustrated in an Excel spreadsheet.

**Chapter 4.** This chapter is dedicated to presenting the design of the proposed wireless charging system for Electric Vehicles (EVs), specifically focusing on the variable capacitor component. The design will involve detailing the equations of the wireless system, integrating the variable capacitor equations within it.

**Chapter 5.** This chapter requires the presentation of the simulation work conducted using tools such as PSPICE. It will focus on examining parameters like efficiency, quality factor, mutual induction, compensation circuit, resonance frequency and variable capacitor.

**Chapter 6.** This chapter details the design of an inductive coil using ANSYS software. An extensive analysis has been conducted, focusing on the impact of varying the airgap between the primary and secondary coils on the system's efficiency.

**Chapter 7.** In this chapter, the implementation of a hardware for wireless power transfer has been completed within a laboratory setting. This hardware is specifically implemented for facilitating the wireless transmission of power to electric vehicles.

**Chapter 8.** A concise summary of the research conducted in this thesis has been presented. Discussions have been made regarding the extent of improvements achieved, alongside the presentation of limitations encountered during the research. Additionally, recommendations for future research endeavours have been outlined.

## **Chapter 2: Literature Review**

### **2.1 Introduction**

It is necessary to understand the background and challenges associated to charging system of EV. In the quest to design and develop an optimal WPT topology for EVs, emphasis is placed on a comprehensive understanding of the advancements in wireless charging technologies currently under development and implementation. The acknowledgment of "plug-in" charging methods exists, but the primary focus remains on the progress in wireless charging solutions.

The literature review of this research focuses on types of charging for electric vehicle, different methods of WPT for electric vehicle, types of compensation circuit topologies, modes of charging for electric vehicle and inductive coil design.

The literature review was conducted by synthesizing information from a diverse array of sources. These encompassed various forms of literature, including published thesis, reports, conference proceedings, and company reports. Further insights were derived from additional sources like books, news articles, journals, and select government publications.

### **2.2 Concept of Electric Vehicle**

An Electric Vehicle (EV) is characterized by its reliance not solely on an engine and fuel, but rather on a contemporary electric system comprising motors, power converters, batteries, and controllers. Integration with modern transportation networks can render EVs intelligent systems. Significant progress is required to enhance their affordability. The architecture of an EV encompasses its mechanical construction, the electrical and electronic transmission supplying energy, and the information system managing vehicle control [14].

### **2.3 Types of Electric Vehicles**

EVs are transforming the landscape of personal transportation and exerting an influence on energy grids. As shown in Figure 2-1 four principal varieties of EVs are identified: Battery Electric Vehicles (BEVs), Hybrid Electric Vehicles (HEVs), Plug-in Hybrid Electric Vehicles (PHEVs), and Fuel Cell Electric Vehicles (FCEVs) [15].

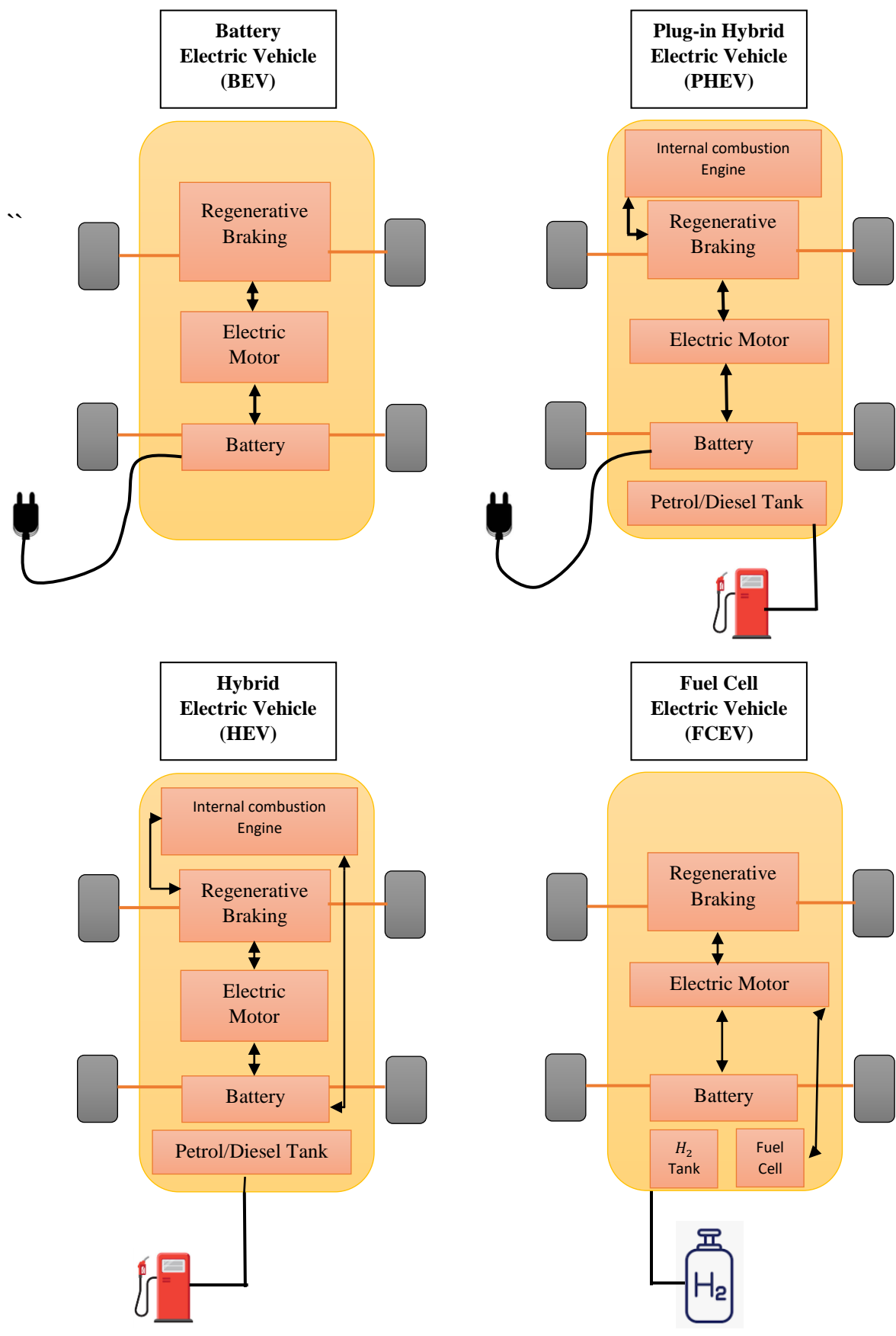


Figure 2-1: Different Types of EVs [18]

## 2.4 Types of EV Charging

The charger for electric vehicles (EVs) is responsible for converting energy from the power grid into a suitable form for the EV or plug-in hybrid EV, while also ensuring the battery's safe reception of this energy [18]. Upon connection of the vehicle to the charger, the initiation of the charging process occurs subsequent to the completion of necessary checks [18]. The battery undergoes an electrochemical transformation facilitated by the delivery of a current during the charging phase. Displayed in Figure 2-2 are the three primary methods of charging an EV battery: conductive charging, inductive charging, and battery swapping [18].

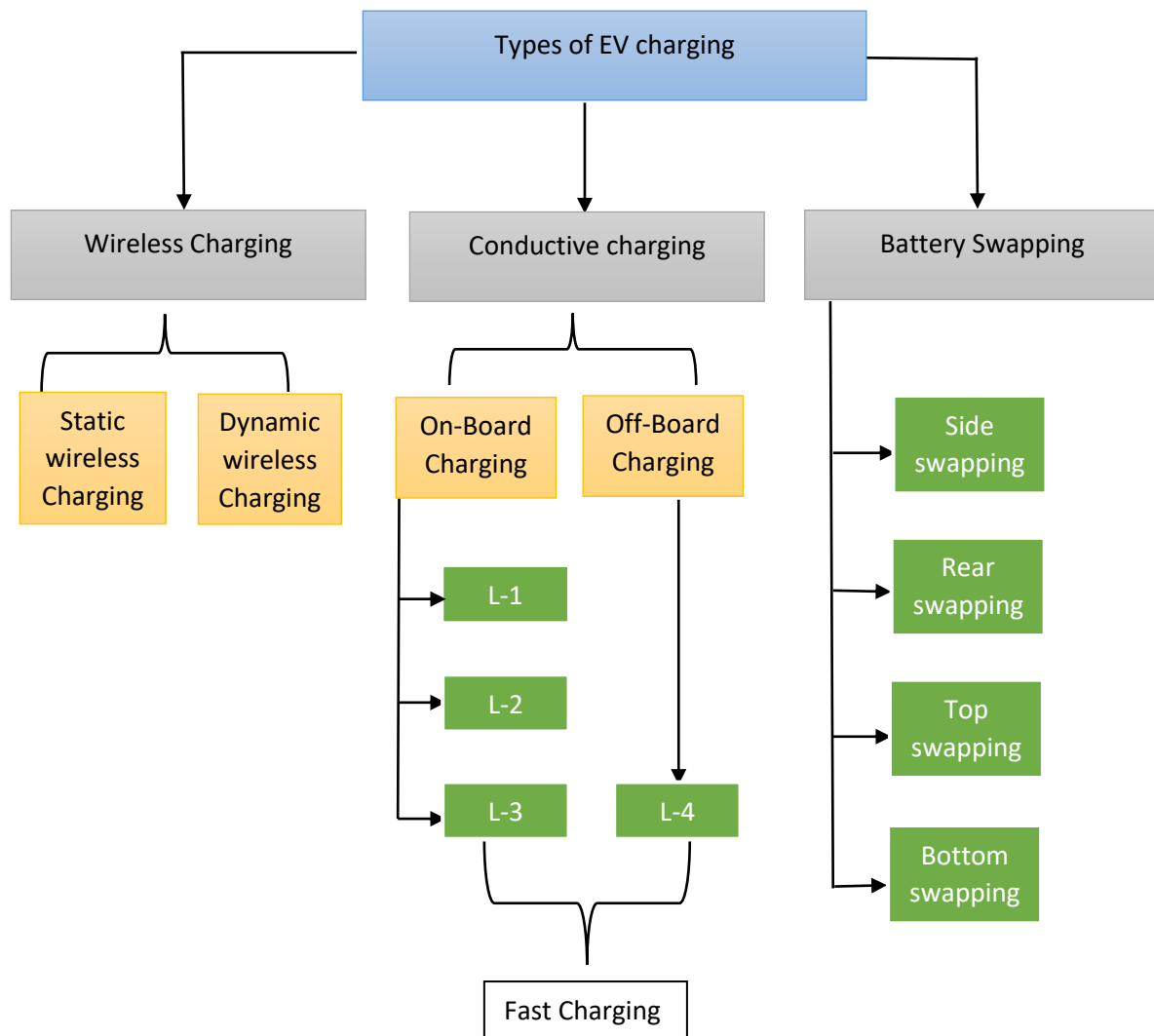


Figure 2-2: Primary Methods of EV Charging [18]

### 2.4.1 Conductive Charging

Conductive charging, commonly referred to as wired charging, is characterised by a system of direct contact for charging between a vehicle and its power supply, as documented in sources [16] [17] [18]. This system incorporates rectifiers and connectors designed to correct power factors. Charging methods fall into two categories: on-board, where the charger is integrated within the vehicle, and off-board, where the charger exists externally. A direct linkage is established between the charger and the electric vehicle's (EV) battery through physical contact, as cited in references [16] [17] [18]. High-power rapid charging may lead to potential adverse effects on the charger or present safety hazards. Moreover, regular charging using a slow charger without the provision for overnight charging could pose issues, as noted in [16]-[17].

Fig.2 illustrated the three distinct tiers of on-board charging options for electric vehicles: L-1, L-2, and L-3. L-1 utilises a conventional 120V power source, offering a charging capacity of 3 to 5 miles per hour, with a complete charge spanning several hours and a rate of 1.4 kilowatts. L-2 necessitates a 208V or 240V power connection, providing an additional range of 12 to 80 miles per hour, and is capable of fully charging an electric vehicle in 2-4 hours with a power rate between 3.7 and 7.2 kilowatts. Typically, L-2 charging facilities are installed in residential homes, offices, and public locations. The quickest on-board charging available for electric vehicles is L-3, or DC fast charging, delivering rates of 50 kilowatts or higher and achieving a full charge within 30 minutes to an hour. These stations are strategically positioned along transportation routes and accommodate various electric vehicle plug connections. There is also mention of L-4 charging, known as the Megawatt Charging System (MCS), which represents the forefront of electric vehicle charging technology. MCS can achieve charging rates up to 3.75 megawatts, dramatically shortening charging times and facilitating rapid charging capabilities. L-4 systems can deliver power at 800 volts or higher, with voltage and current ratings peaking at 1250V DC - 3000A, allowing for a range increase of over 200 miles in just 15 minutes. The deployment of L-4 charging infrastructure is limited due to its ongoing development. Nevertheless, leading charger manufacturers such as ABB, Siemens, Delta Electronics, EVBox, and Tritium are advancing the production of Megawatt Charging Systems featuring multiple ports, responding to the escalating demand for high-capacity EV charging infrastructure [18]. Table 1 offers a detailed account of the characteristics of conductive



charging for electric vehicles, encompassing charge levels, power, voltage, current, types of connections, and durations of charging [18].

**Table 1:EVs charging levels and Specification [18]**

Charging Level	On-Board			Off-Board
	L-1	L-2	L-3	L-4
Power Rating (KW)	1.4 kW	3.7-7.2 kW	50 kW	Max. 3.75 MW
AC Voltage	120 V/240V	208V/240 V	-	-
DC Voltage	-	-	200-800 V	800-1250 V
AC Current	12 A	16-80 A	-	-
DC Current	-	-	50-400 A	400-3000 A
Charging Time	12-24 hours	2-4 hours	30 minutes to 1 hour	15 minutes

### 2.4.2 Battery Swapping

This technique allows for the exchange of a depleted battery for a fully charged one by operators of electric vehicles (EVs). Given that the duration of battery charging can be extensive, the associated waiting time may present a challenge for individuals with constrained time availability [16, 18]. Opting for battery replacement offers advantages such as extended battery longevity, reduced usage duration, and lower operational costs. The requisite infrastructure and apparatus for facilitating battery replacement encompass distribution transformers, AC-DC converters, battery chargers, robotic arms, charging racks, and systems for control and maintenance. A notable advantage of the battery replacement system is its integration with the energy storage system (Vehicle-to-Grid, V2G), which is made possible by enabling bidirectional flow of electricity [16, 18]. The method involves the replacement of an older battery with a new one to support the electric drive. Additionally, battery replacement stations are capable of conducting batch power flow with the power grid, allowing for the injection of stored energy into the grid at times of high demand, thereby enhancing local power efficiency [16, 18].

### 2.4.3 Wireless Charging

WCS have been suggested for high-power uses, like stationary plug-in electric vehicles (PEVs) and electric cars (EVs). When it comes to ease of use, reliability, and simplicity, WCS surpasses plug-in charging systems in its benefits. One drawback of WCS is that it can only be utilised in stationary modes, such as parking lots, garages, or traffic signals, or while the car is parked. Moreover, stationary WCS have challenges from better efficiency, shorter range, hefty designs, restricted power transfer problems. To expand the two domains of range and enough battery storage volume, the dynamic mode of operation of the WCS for EVs has been studied [19]. Battery storage devices can now be charged while the car is moving thanks to this technology. The vehicle has a greater range of travel and requires less expensive battery storage space [20]. A dynamic WCS must, however, overcome two fundamental challenges before it is generally adopted: a large air gap and coil misalignment. The power transfer efficiency is determined by the coil alignment and air-gap distance between the source and receiver [21] [22]. The typical air-gap distance for small passenger cars is between 150 and 300 mm, however it can increase for larger cars. Aligning the ideal driving position on the transmitter coil is easy because the car is driven automatically in dynamic mode [19].

Wireless charging represents a technique for power transmission to the batteries of electric vehicles. The technology employs electromagnetic waves and is utilized where the electric vehicle is stationed in a charging bay [16, 18]. An air gap exists between the primary coil, associated with the vehicle, and the secondary coil, situated within the charging bay, thus obviating the requirement for a galvanic connection. By excluding mechanical components, this approach streamlines the charging procedure and reduces potential hazards [16, 18].

The basic block diagram of the static WCS for EVs is displayed in Figure 2-3. To help with power transfer from the transmission coil to the reception coil, AC/DC and DC/AC converters transform grid-supplied AC mains into high frequency (HF) AC [23].

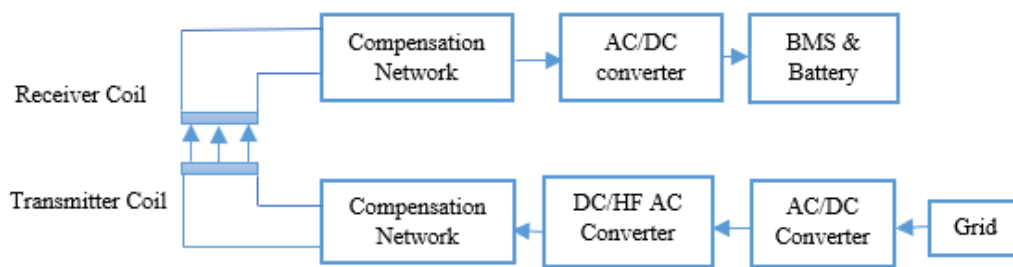


Figure 2-3: Basic block diagram of wireless charging for Electric Vehicles [23]

Compensatory topologies based on series and parallel combinations are employed on both transmitting and receiving sides to improve system efficiency overall [24] [25]. The receiving coil, which is often mounted below the vehicle, transforms the oscillating magnetic flux fields into HF AC. The on-board batteries then use the stable DC supply that was created from the HF AC. The power control, communications, and battery management system (BMS) are also integrated to prevent any risks to health and safety and to guarantee consistent functioning. Magnetic planar ferrite plates are employed on both the transmitter and receiver sides in order to reduce any undesired leakage fluxes and enhance magnetic flux distribution [19].

## 2.5 Modes of Wireless Charging

Wireless charging can be divided into two modes static charging and dynamic charging [16, 18].

### 2.5.1 Static Charging

In the static charging method, energy is transferred from the primary power source to the battery's input. The efficiency of this wireless charging process typically ranges from 85-93%, which may rise to between 95-98% in the presence of an air gap [16, 18]. The primary coil is positioned beneath the floor of the vehicle, and the secondary coil is situated either below or at the vehicle's centre. This advanced technology is suitable for use in various settings, such as parking lots, car parks, residential areas, and shopping centres [16, 18].

## 2.5.2 Dynamic Charging

The dynamic charging technique is employed for electric vehicles while they are moving. The objective of wireless charging systems is to extend the range of vehicles by reducing the necessity for frequent charging or the use of larger batteries [16, 18]. Along specific routes, transmitter coils and power supplies are strategically installed. Nevertheless, the intensity of the electromagnetic field diminishes progressively with increasing distance from the transmitter. The frequency range for wireless charging systems usually lies between 20-100 kHz [16, 18].

## 2.6 Challenges of Wireless Charging

Certain challenges are associated with wireless charging systems, especially concerning transmission efficiency and safety. The efficiency of these systems is influenced by various factors, including the alignment, design of the power pad, operating frequency, compensation topology, and the distance between the transmitter and receiver [16, 18]. Nevertheless, wireless charging represents a promising technology that supports the usage of electric vehicles and contributes to the extension of battery life [16, 18]. Comparison between static and dynamic charging system is shown in Table 2.

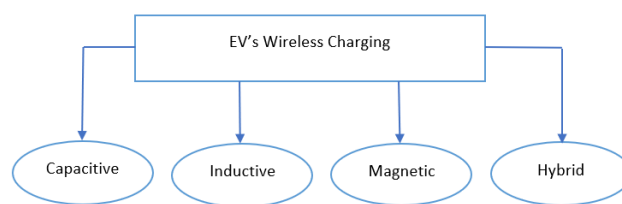
**Table 2: Comparing EV charging using dynamic and static wireless methods [18]**

	Static Wireless Charging	Dynamic Wireless Charging
Description	mandates that electric cars be parked on top of a stationary charging station or pad in order to be charged [18].	enables the recharging of electric vehicles while they are in motion; this is commonly employed for electric bus routes and electric roads [18].
Operating Principle	generates a magnetic field and wirelessly transfers energy between the underfloor coil of the car and a coil that matches the charging pad [18].	On-the-go charging is made possible by a continuous magnetic connection being formed between coils on the underside of the car and magnetic charging coils

		buried in the road surface [18].
Applications and Prevalence	-Houses, offices, and public charging locations [18]. -Common [18].	-Electric vehicle highways and bus lines [18]. -Anticipated to become more extensively used in the future [18].
Advantages and Disadvantages	Safe, simple to use, and appropriate for charging while parked. Several restrictions on usage and demands that cars be parked [18].	prevents energy depletion by enabling electric vehicles to charge while in motion. Complex infrastructure requirements are possible [18].

## 2.7 Different Methods of Wireless Power transfer

There are several methods that could make wireless charging feasible. Figure 2-4 depicts these various kinds. While there may be other approaches or technologies available, these four are the ones that are highlighted in this research.



**Figure 2-4: Different technologies for wireless charging system [23]**

Since the creation of electric vehicle wireless charging systems, four distinct WEVCS design techniques have been employed. Magnetic gear wireless power transmission (MGWPT), resonant inductive power transfer (RIPT), capacitive wireless power transfer (CWPT), and traditional inductive power transfer (IPT). A summary of the wireless power transfer options for battery-powered electric vehicles (BEVs) is shown in Table 3 [26] [27] [28].

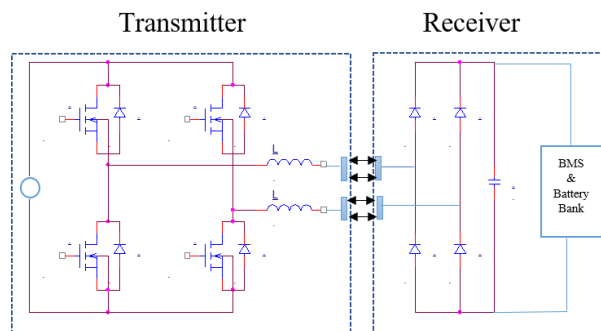
**Table 3: Overview of different methods of WPT for EV's [23]**

WPT Methods	Efficiency	EMI	Frequency Range(kHz)
Inductive	Medium/High	Medium	10-50
Capacitive	Low/Medium	Medium	100-150
Permanent magnet	Low/Medium	High	0.05-0.500

WPT Methods	Price	Size/Volume	Design	Power level
Inductive	Medium/High	Medium	Medium	Medium/high
Capacitive	Low	Low	Medium	Low
Permanent magnet	High	High	High	Medium/Low

### 2.7.1 Capacitive Charging

For low-power applications, such as portable electronics, the cheap cost and simplicity of CWPT technology which makes use of improved geometric and mechanical coupling capacitor topologies [29] are especially advantageous [30]. A typical schematic illustration of a CPWT based on a series resonant circuit is shown in Figure 2-5. Coupling capacitors are used in the CWPT to transfer power from the source to the receiver in place of coils or magnets [23]. An H-bridge converter receives the primary AC voltage through power factor adjustment circuitry. The H-bridge generates high-frequency AC, which is routed through coupling capacitors on the receiving end. Unlike the IPT, the CWPT is capable of handling both high voltage and low current [23].



**Figure 2-5: Diagram of Capacitive Wireless Power Transfer [23]**

To decrease the impedance between the transmitter and receiver sides at the resonant arrangement, more inductors are added in series with the coupling capacitors. This arrangement facilitates the incorporation of soft switching into the circuits as well. Similarly, the received

AC power is converted to DC for the battery bank or load using rectifier and filter circuits [19]. The power transmission level is directly influenced by the coupling capacitor's size and the separation between the two plates. For a tiny air gap, CWPT provides superior performance and enhanced field restrictions formed between the capacitor's two plates [31]. The application of CWPT in EVs has been restricted thus far because of large air gaps and high-power level requirements.

### 2.7.2 Inductive Charging

Figure 2-6 displays the fundamental block diagram of the classic IPT. It is predicated on several distinct electric vehicle charging schemes. IPT has been tested and applied in many milliwatt to kilowatt applications to transfer contactless power from the source to the receiver [32]. The magnet-charge's primary coil, also known as an inductive coupler or charging paddle, was inserted into the car's charging port. From there, electricity was transferred to the secondary coil, which enabled the EV to be charged [32]. A 6.6 kW Level 2 EV charger that could charge batteries between 200 and 400 V at an operating frequency of 77 kHz was on display at the University of Georgia. In this universal IPT, a 10 KVA coaxial winding transformed provides many benefits, such as an easily adjustable power range and flexible inductive coupling design [32].

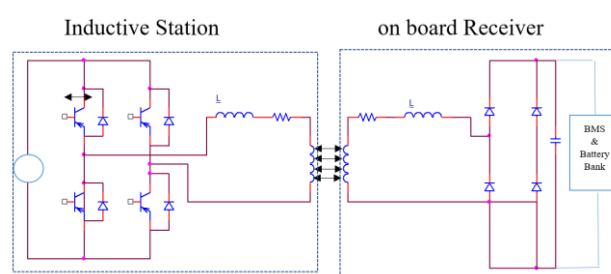
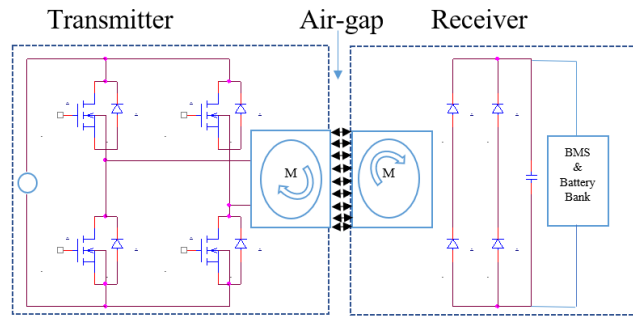


Figure 2-6:Diagram of Inductive Wireless Power Transfer [23]

### 2.7.3 Magnetic gear wireless power transfer

The magnetic gear WPT (MGWPT) is different from the CWPT and the IPT, as illustrated in Figure 2-7 [23].



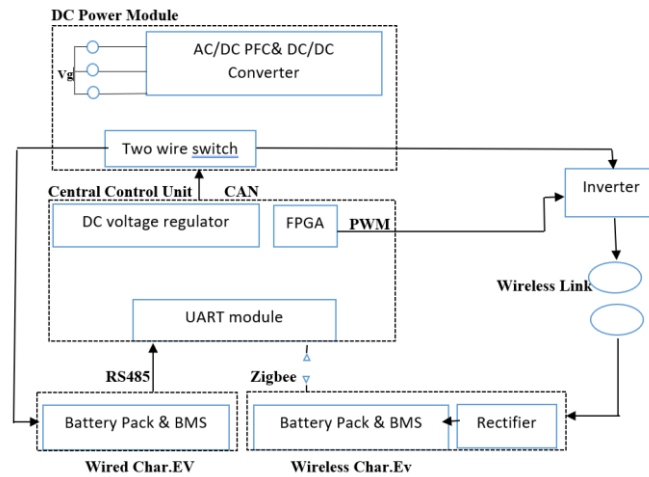
**Figure 2-7:Diagram of magnetic Gear based Wireless Power Transfer [23]**

Unlike other WEVC techniques that rely on coaxial wires, this method makes use of two permanent magnets (PM) that are synchronised and put side by side [19]. The primary PM experiences a mechanical torque as a result of the transmitter winding receiving the main power as the current source [19]. When the mechanical torque is applied, the primary PM rotates and exerts a torque on the secondary PM via mechanical interaction. When two synchronised PMs are used, the primary PM acts as a generator, and the secondary PM gathers energy and sends it to the battery through the power converter and BMS [19].

#### **2.7.4 Hybrid Charging System**

A block diagram of the hybrid wired/wireless charging system may be found in Figure 2-8. The power supply side, which powers the EV that is being charged wirelessly or through wired connections, is made up of the central control unit and the DC power module [2]. The DC/DC converter, which provides galvanic isolation between the input utility grid and the output, and the input power factor correction (PFC) make up the majority of the DC power module [2]. It should be noted that the commercial DC/DC module is quite inexpensive because it is widely used for wired EV charging [2]. It is consequently more economical to use a commercial DC/DC power module rather than to construct one that is integrated with the inverter. The power source for the wired or wireless mode is a two-wire switch. A command from the CAN bus of the central control unit can modify the DC power module's output voltage [2].





**Figure 2-8:Diagram of Hybrid Charging System [23]**

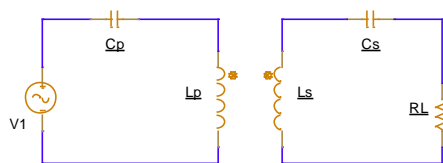
The DC voltage regulator, the inverter, and the universal asynchronous transmitter-receiver (UART) module are the main parts of the central control unit [2]. The battery management system (BMS) data is gathered and serial communication is managed by the UART module. There are two varieties of serial communication methods available: wireless and cable. Wired connection uses RS485; wireless communication uses Zigbee [2]. The DC voltage regulator is based on a PI controller, which outputs the DC module output voltage in response to real-time battery charging voltage and current. Furthermore, the inverter converts DC current to AC for wireless communication when the wireless charging mode is turned on [2]. Actually, there is a parking area dedicated to each hybrid charging system. Therefore, the hybrid system can only charge one charged object at a time—either the EV with cable charging or the EV with wireless charging [2]. It is not feasible to charge two or more electric vehicles at once. As a result, the central control unit can function in wireless or wired mode [2]. The hybrid charging system's overall cost is reduced because, as Figure 2-8 illustrates, the DC power module and the central control unit aside from the inverter are shared across the two charging modes. The DC power module's price is directly related to its rated power, which is the result of multiplying its maximum output voltage by the required current [2]. From a financial standpoint, it's critical to create a hybrid charging system that can accommodate both wired and wireless charging modes for a specific battery charging profile, in addition to meeting the DC module's minimum rated power need [2].

## 2.8 Compensation topologies

There are the four basic compensations: SS, SP, PS, and PP. The first S or P stands for series (S) or parallel (P) compensation from the primary side, and the second S or P stands for series (S) or parallel (P) compensation from the secondary side [33]. Because the air gap between the vehicle and the ground causes a large leakage inductance that limits power transfer, a compensation circuit is also required. One advantage of LC resonators is that they are easier to manage while designing. The LC resonator's compensator capacitors may be connected to the coil in series or parallel. The compensation network's four topologies are summarised in Tables 1 and 2 [34]. Because of the shifting load and varying coupling coefficient during the EV charging process, the Series-Series topology is recommended for EV applications. The Series-Series (SS) and Series-Parallel (SP) topologies provide superior performance when it comes to constant frequency WPT battery charging [35]. Furthermore, SS topology is more efficient than SP topology and functions over a larger range of load resistance.

### 2.8.1 Series-Series Compensation

Several key criteria are discovered for series-series compensation topologies as shown in Figure 2-9, each of which is crucial to their performance and appropriateness, especially in Electric Vehicle (EV) applications.



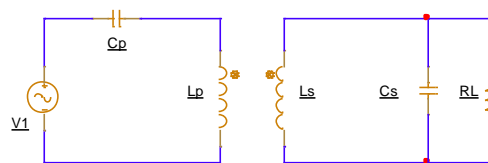
**Figure 2-9:Series-Series Compensation Circuit**

It provides for high input Volt-Ampere (VA) rating that ensures that there is enough power available for transfer. These are characterized by the transfer of high power in long distances and therefore ensuring the effective delivery of energy to its destination, even if the gap between the transmitter and the receiver is quite huge but in limited range. Further, a large tolerance of alignment is realized, which promotes effective power transmission even under slightly misaligned coils [36]. There is low impedance found at the resonant state, hence promoting effective power transfer. This is deemed in terms of how efficiency is affected when

the operating frequencies are outside the best range due to having limited tolerance for frequency changes. All these features taken together certainly underscore the efficiency and flexibility of the series-series compensation topology, making it especially appropriate for the cases needing reliable power transfer under various circumstances, such as those typical of EV charging scenarios [36].

### 2.8.2 Series-Parallel Compensation

A set of unique properties, present in series-parallel compensation topologies of Figure 2-10 is identified, which makes their use applicable, especially in the context of EV charging systems.



**Figure 2-10:Series-Parallel Compensation Circuit**

The high amount of power is ensured for the wireless transmission purpose by the high Volt-Ampere (VA) rating available at input. The different EV charging applications are satisfied with high output voltages by the topologies and meet all the requirements due to their special design. A remarkable property in them is high-power transfer capability across long distance within range this allows for efficient distribution of energy over airgaps. [36] Besides, high alignment tolerance is preserved where the effect of misalignments in alignment between the transmitting and receiving coils is voided in the power transfer process. Impedance is kept low at the resonant state, a factor that is very critical in the process of power transfer. However, the same study noted that the effect of poor frequency tolerance was also poor in tolerance of deviations from the mean frequency to suggest larger deviations from the mean frequency could result in poor efficiency. All these features represent how well the series-parallel compensation architecture is feasible for electric vehicle (EV) applications, with a positive answer towards high-voltage demand and effective power transmission in distant lands with great flexibility and promise by the alignment reasons described [36].

### 2.8.3 Parallel-Series Compensation

A particular set of properties are seen in parallel-series compensation topologies which is shown in Figure 2-11 which influence their performance and usefulness in a range of applications, albeit they have drawbacks when it comes to charging electric vehicles (EVs).

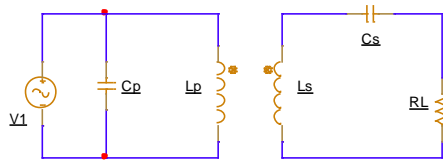


Figure 2-11: Parallel-Series Compensation Circuit

There is a low Volt-Ampere (VA) rating at the input, which means that there isn't much power transferred. These topologies match applications that demand lower power levels since they are designed for low output voltages. However, because of their poor long-distance power transfer capacity, they are deemed unsuitable for EV applications [36]. A modest alignment tolerance is offered, indicating that although a certain amount of coil misalignment is allowed, the alignment flexibility is not as high as in other topologies. High impedance is experienced at the resonant state, which adversely affects power transfer efficiency. Furthermore, a limited tolerance to frequency changes is noted, suggesting that departures from the ideal frequency might have a substantial impact on efficiency. Taken together, these features characterise the parallel-series compensation topologies as more limited in their use, especially inappropriate for high power requirements and the particular needs of EV charging systems [36].

### 2.8.4 Parallel-Parallel Compensation

Parallel-series compensation topologies which is shown in Figure 2-12 exhibit a unique set of properties that characterise their suitability and performance constraints, especially when used outside of EV charging systems.

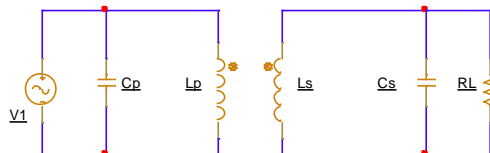


Figure 2-12: Parallel-Parallel Compensation Circuit

Its low Volt-Ampere (VA) input rating means that there isn't much power available for wireless transmission, which naturally reduces their usefulness for high-demand applications [36]. These topologies are recognised as unsuitable for EV applications even though they are

intended for high output voltages, mainly because of their limited ability to transfer power over long distances [36]. Their versatility is further limited by a low alignment tolerance, which means that accurate alignment of the transmitting and receiving coils is required for efficient power transfer. Furthermore, a high impedance at the resonant state is noted, which naturally reduces the energy transfer process's efficiency. These topologies' low tolerance for frequency deviations means that even little departures from the ideal operating frequency have a substantial effect on their efficiency. These characteristics taken together highlight the shortcomings of parallel-series compensation topologies in applications that demand strong power transfer capabilities, especially those that demand great efficiency and flexibility like EV charging systems [36].

## **2.9 Summary**

Chapter 2 featured a comprehensive review of the literature that covered a wide range of topics, including charging methodologies (e.g., plug-in and wireless), hybrid techniques, inductive, capacitive, magnetic gear, and hybrid techniques, as well as static and dynamic charging modes. This extensive examination, which highlighted the benefits and drawbacks of each technique and mode, set the foundation for understanding the state of electric vehicle (EV) charging technology today. Chapter 3 is devoted to the design of a variable capacitor technique for a series-series compensation circuit, with the goal of adjusting the resonance frequency.

## Chapter 3: Design of variable capacitor

### 3.1 Introduction

As the extensive literature analysis in Chapter 2 reviews, maintaining appropriate resonance frequency in the face of external environment variability or inductor-related issues has been critical to the development of wireless power transfer (WPT) devices. It has been found that fixed capacitors, which are typically employed in series-series compensation circuits, have a limited capacity to adjust to resonance frequency variations brought on by either internal or external disturbances. The incorporation of variable capacitors in replacement of fixed capacitors has become a crucial design concern in response to these difficulties.

### 3.2 Function of Variable Capacitor

In Figure 3-1 basic design of variable capacitor is shown. The value of the capacitor can be controlled by adjusting the duty cycle of the switches. The main idea in this proposed wireless charging design is to control the duty cycle of one of the two semiconductor switches (the switching function of the other switch is a complement of the first switch). By doing so the effective value of the capacitor can be controlled in order to control the resonant frequency without changing the physical value of the capacitor. The switching frequency of the two switches is high enough to produce stepless variation of the effective capacitance but not that high in order to minimise any switching losses. It should be noted that the switching frequency has nothing to do with the resonant frequency. The effective value of the capacitor is the one which will determine the resonant frequency.

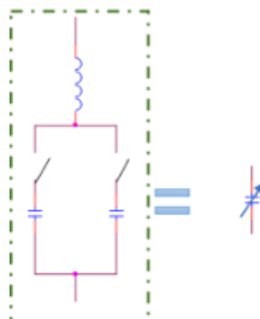


Figure 3-1: Basic diagram of Variable Capacitor

### 3.3 Proposed variable Capacitor

In Figure 3-2 proposed variable capacitor design is shown. The details of C-effective equations and values calculated in details sec 3.3.1

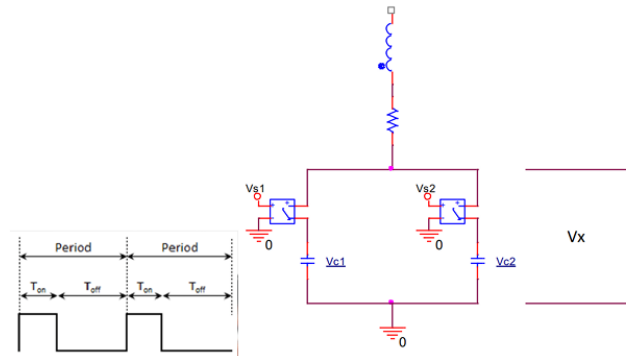


Figure 3-2:Diagram of Proposed Variable Capacitor

#### 3.3.1 C-effective Calculation

To calculate the effective value of the capacitor by adjusting the duty cycle of the switches in order to get the required resonance frequency required mathematical design. There are two ways by which value of effective capacitor get either to control the duty cycle of switch 1 or switch 2. In this proposed design both ways are derived.

By applying the Kirchoff voltage Law (KVL) on the left side of the circuit through switch 1 then the voltage across capacitor  $c_1$ , will be  $Vs_1(t)$  can be calculated by equation (3.1).

$$Vs_1(t) = i(t) + L di(t)/dt + Vc_1(t) \quad (3.1)$$

Similarly, by applying the Kirchoff voltage Law (KVL) on the right side of the circuit through switch 2 then the voltage across capacitor  $c_2$ , will be  $Vc_2(t)$  can be calculated by equation (3.2).

$$Vs_2(t) = i(t) + L di(t)/dt + Vc_2(t) \quad (3.2)$$

Current through capacitor  $c_1$  can be calculated by deriving the voltage across capacitor  $c_1$  with respect to time can be shown in equation (3.3).

$$i(t) = c \frac{dV_{c_1}(t)}{dt} \quad (3.3)$$

Likewise, current through capacitor  $c_2$  can be calculated by deriving the voltage across capacitor  $c_2$  with respect to time can be shown in equation (3.4).

$$i(t) = c \frac{dV_{c_2}(t)}{dt} \quad (3.4)$$

Maximum voltage ( $V_{max}$ ) produced in the system can be calculated by multiply the capacitance reactance of  $c_1$  which is  $X_{c_1}$  with square of duty cycle of switch 1 plus whole square of remaining duty cycle of the switch 2 multiply by capacitance reactance of  $c_2$ . After all this calculation is multiply by the maximum current of the proposed system can be shown in equation (3.5).

$$V_{max} = [d^2X_{c_1} + (1 - d)^2X_{c_2}]I_{max} \quad (3.5)$$

Likewise,  $V_{max}$  can also be calculated by multiply the capacitance reactance of  $c_2$  which is  $X_{c_2}$  with square of duty cycle of switch 2 plus whole square of remaining duty cycle of the switch 1 multiply by capacitance reactance of  $c_1$ . After all this calculation is multiply by the maximum current of the proposed system can be shown in equation (3.6)



$$V_{max} = [d^2 X_{c_2} + (1 - d)^2 X_{c_1}] I_{max} \quad (3.6)$$

Capacitance reactance of the effective value of the capacitance can be calculated  $V_{max}$  divided by  $I_{max}$  which is shown in equation (3.7).

$$X_{eff} = \frac{V_{max}}{I_{max}} \quad (3.7)$$

$N$  is the ratio of two capacitor  $c_2$  by  $c_1$  which is multiplied by duty cycle to get the effective value of the capacitor. Ratio is mentioned in equation (3.8).

$$N = \frac{X_{c_1}}{X_{c_2}} = \frac{c_2}{c_1} \quad (3.8)$$

Effective value of the capacitor can be calculated by equation (3.9) if considering switch 2.

$$C_{eff} = \frac{c_2}{d^2 N + (1-d)^2} \quad (3.9)$$

Effective value of the capacitor can be calculated by equation (3.10) if considering switch 1.

$$C_{eff} = \frac{c_1}{d^2 + (1-d)^2 N} \quad (3.10)$$

$d$  assigned to  $s_1$  or  $s_2$  can be calculated by using equation (3.11)

$$d = \frac{c_1}{c_1+c_2} \text{ or } d = \frac{c_2}{c_1+c_2} \quad (3.11)$$

The variable used in the all above equations (3.1) - (3.11) are explain in Table 4.

**Table 4: Variable used in the all above equations (3.1) - (3.11)**

<b>Notation</b>	<b>Description</b>
$V_{s_1}(t)$	Voltage across the first source as a function of time.
$V_{s_2}(t)$	Voltage across the second source as a function of time.
$i(t)$	Current through the system as a function of time.
$R$	Resistance in the circuit.
$L$	Inductance in the circuit.
$V_{c_1}(t)$	Voltage across the first capacitor $c_1$ as a function of time.
$V_{c_2}(t)$	Voltage across the second capacitor $c_2$ as a function of time.
$V_{max}$	Maximum voltage produced in the system.
$X_{c_1}$	Variable associated with capacitor $c_1$ .
$X_{c_2}$	Variable associated with capacitor $c_2$ .
$I_{max}$	Maximum current produced in the system.

$N$	Ratio by $\frac{X_{c1}}{X_{c2}}$ which is equal to $\frac{c2}{c1}$ .
$c_{eff}$	Effective capacitance of the system.
$c_1$	First capacitor in the circuit.
$c_2$	Second capacitor in the circuit.
$s_1$	Switch 1 in the circuit.
$s_2$	Switch 2 in the circuit.

In the proposed design of variable capacitor, the calculation of effective capacitance is discussed above. In the design  $V_{s1}(t)$  and  $V_{s2}(t)$  are the voltage across two distinct capacitors their values can be calculated by the sum of product of instantaneous current,  $i(t)$  and resistance  $R$  added to the integral of the instantaneous current with respect to time and the corresponding voltage across the capacitors,  $V_{c1}(t)$  and  $V_{c2}(t)$  respectively.

The instantaneous current across the capacitors,  $i(t)$  is more expressed in term of the derivative of the voltage across these capacitors, scaled by the coefficient,  $c$  which is represents a capacitance.

Furthermore, the maximum voltage  $V_{max}$ , is defined for both capacitors in terms of a parameter  $d$ , which represents a duty cycle and maximum current  $I_{max}$ .

The effective reactance  $X_{eff}$  is obtained by the ration of  $V_{max}$  to  $I_{max}$ .  $N$  is the ratio of the product of the first capacitor's reactance and second capacitor to the product of the second capacitor's reactance and the first capacitor.

The outcome, the effective capacitance  $c_{eff}$ , is calculated as a function of  $N$  and parameter  $d$ .

The graph generated in Figure 3-3 and Figure 3-4 by using excel data which is shown in Appendix B. Graph shows that when the duty cycle is zero then the C-effective value is equal to the value of  $c_2$  or  $c_1$  based on the C-effective equation that is used.

Similarly, when duty cycle is 1 then value of C-effective is double of  $c_2$  or  $c_1$  depends which equation of C-effective is used. Value of  $N$  is got by using the equation (3.8) of this chapter.  $N$  value can be obtained either vary the value of  $c_2$  or  $c_1$  but in this design the value of  $c_1$  is fixed

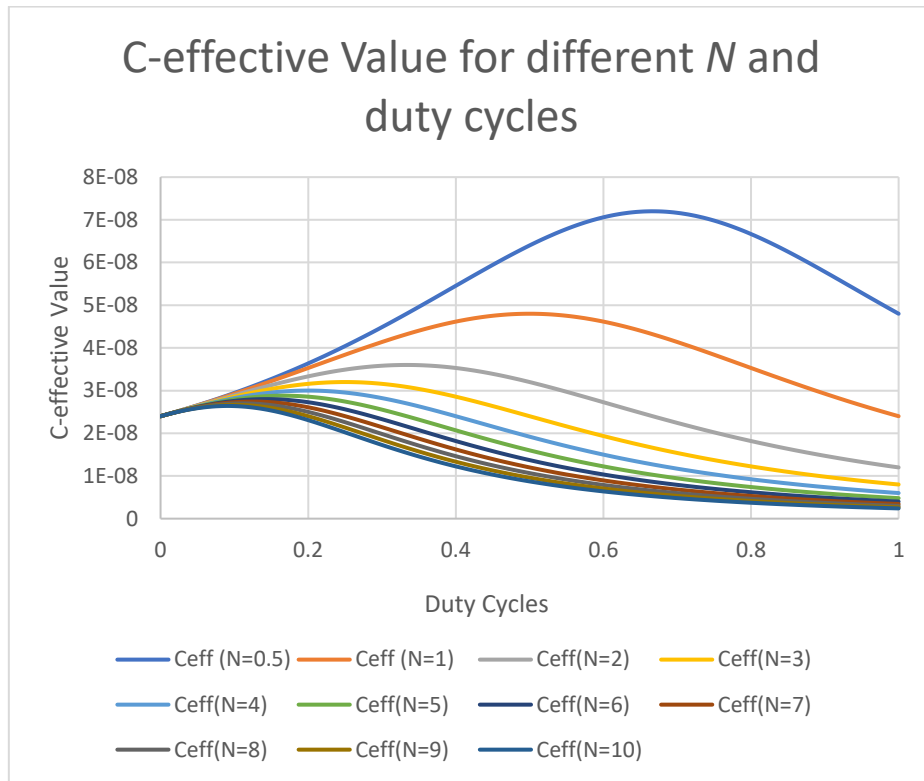
and changed the value of  $c_2$  to get the value of  $N$ . Complete calculation of  $N$  value is shown in Table 5 the value of C-effective is calculated by using equation (3.9).

**Table 5: Calculation of  $N$  value**

$c_1$	$c_2$	$N = c_2/c_1$
2	1	0.5
2	2	1
2	4	2
2	6	3
2	8	4
2	10	5
2	12	6
2	14	7
2	16	8
2	18	9
2	20	10

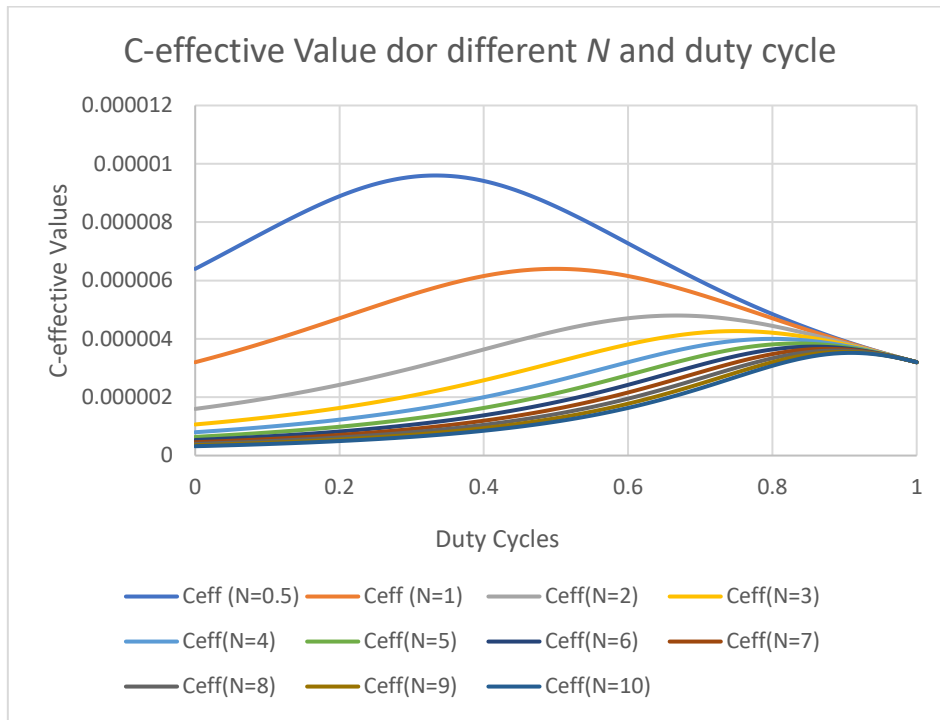
Figure 3-3 is shown the C-effective values for different  $N$  and duty cycle where X-axis is represented the duty cycle of the switches and Y-axis is represented the corresponding C-effective values. Furthermore, if  $N = 0.5$ , then  $c_1$ 's value is twice that of  $c_2$ , meaning that  $c_1$  needs a higher duty cycle than  $c_2$  in order to achieve the maximum value of C. This is seen in Figure 3-3 and the excel data in Appendix B1, where  $c_1$ 's duty cycle is roughly 0.65 and  $c_2$ 's duty cycle is 0.35.

At  $N=1$  both  $c_1$  and  $c_2$  are equal so it means both duty cycle is equal as well which is also shown in Figure 3-3 as well at 0.5 duty cycle maximum C-effective is achieved and so on. The graph shown in Figure 3-3 is generated according to the equation 3.9 used in this Chapter 3.



**Figure 3-3: C-effective values at different duty cycle and  $N$  by using other equation (3.9)**

There is another equation 3.10 also available where the value of C-effective can be achieved but for that need to Fix the value of  $c_2$  and vary the value of  $c_1$ . According to this calculation the graph is shown in Figure 3-4 and excel data is shown in Appendix B2. Figure 3-4 is shown the C-effective values for different  $N$  and duty cycle where X-axis is represented the duty cycle of the switches and Y-axis is represented the corresponding C-effective values.



**Figure 3-4: C-effective values at different duty cycle and N by using other equation (3.10)**

### 3.4 Summary

Chapter 3 provided an in-depth analysis of the design and intricate calculations pertaining to the operation of the variable capacitor, laying the groundwork for its crucial function in modifying the resonance frequency to achieve maximum efficiency in wireless power transfer (WPT) systems. This investigation prepared the ground for the implementation of these ideas to be further developed in Chapter 4, which focuses on the design and computation of a WPT system for electric vehicles (EVs) using series-series compensation.

The design and operational mechanics of a variable capacitor, which is essential for regulating the resonance frequency in wireless power transfer (WPT) systems, are the focus of Chapter 3. This chapter emphasises the importance of variable capacitors in attaining ideal resonance frequencies that account for operational and environmental variability and ensure effective energy transfer to electric vehicles (EVs). Building on the ideas presented in Chapter 3, Chapter 4 explores how these theories might be put into practice by concentrating on the design of the wireless charging infrastructure for electric vehicles. The concepts obtained from the variable capacitor design are expanded upon, emphasising how important they are to creating a reliable WPT system. Detailed explanations of how these capacitors are integrated into the system show

how they enable dynamic resonance frequency modifications, which are essential for optimising power transfer efficiency and dependability in real-world electric vehicle charging situations. This connection highlights how modifying resonance frequencies with varying capacitors can improve the efficiency and functionality of wireless EV charging systems, both theoretically and practically.

# Chapter 4: Design of Wireless charging System of Electric vehicle

## 4.1 Introduction

Chapter 4 delves deeply into the design and calculations related to Wireless Power Transfer (WPT) systems for Electric Vehicles (EVs). This builds on the fundamental ideas covered in Chapter 3 concerning the design of the variable capacitor and its critical function in resonance frequency adjustment. A thorough foundation for the electrical parts of the system was provided by the computations of primary and secondary capacitance as well as the use of inductor calculators. Calculations of reflective impedance and resonance frequency, which are essential for obtaining effective power transmission, highlight the significance of exact tuning for optimum system performance. In addition, mutual inductance and the quality factor were investigated, providing information about the effectiveness of energy transfer and the overall functioning of the system. Moreover, the coupling coefficient also calculated which is a crucial measure of how well the system transfers power between the primary and secondary coils.

## 4.2 Design of WPT System

The generic circuit diagram of WPT by using series-series compensation is shown in Figure 4-1. There are two sides of this whole circuit, one is primary side and the other one is secondary side. In primary side DC is applied as a source voltage and then H-bridge is connected to have a high frequency AC. Adding to this compensated circuit is connected in combination of capacitor and inductor to made the circuit resonance. Whereas, in secondary side rectifier is connected to convert AC to DC which is stored in battery. In Figure 4-1,  $R_0$  represented the equivalent resistance of the battery of the vehicle.

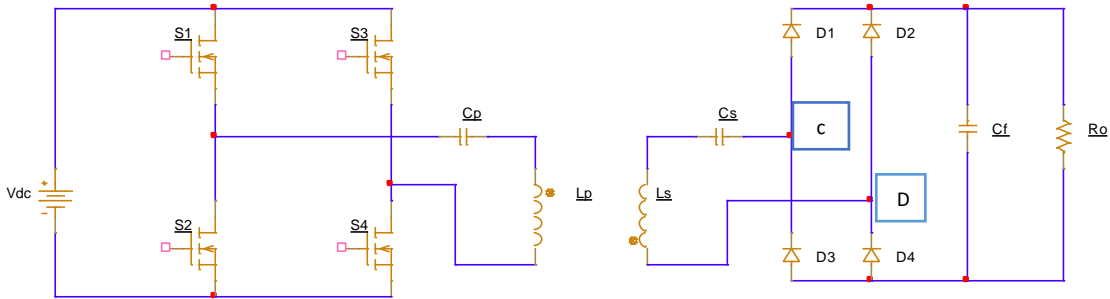


Figure 4-1: Circuit Diagram of wireless power transfer by using SS-Compensation topology



### 4.3 Equivalent Circuit and derivations

Design a wireless power system for electric vehicle included to find out the values of different components used in the system like primary and secondary side capacitor and inductor values. Adding to this, to find out the values of other parameters which is affected the efficiency of and performance of the system like mutual induction, quality factor and coupling co-efficient is also included in the design. Figure 4-2 shown the equivalent circuit diagram of wireless power transfer by using SS-compensation topology which is shown in Figure 4-1.

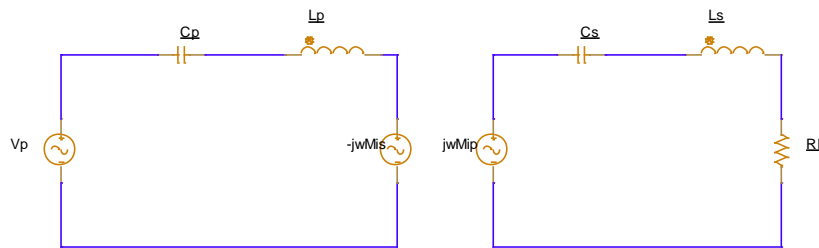


Figure 4-2:Equivalent Circuit Diagram of wireless power transfer by using SS-Compensation topology

In Figure 4-2  $V_p$  represented the voltage after inverted DC supply to get high frequency AC supply in the primary side.  $C_p$  and  $L_p$  are the primary side capacitance and inductance respectively.  $j\omega M Z_2 i_s$  is the mutual induced emf in the primary winding due to the current flowing in the secondary winding. Similarly,  $j\omega M i_p$  is the secondary induced emf in the secondary winding because of current flowed in the primary winding.  $R_L$  is the equivalent resistance as viewed from point C and D shown in Figure 4-1

By applying KVL on primary side will get equation.

$$Z_1 i_p - j\omega M i_p = V_p \quad (4.1)$$

Where as  $Z_1$  is the primary side impedance.

By applying KVL on secondary side will get equation.

$$Z_2 i_s = j\omega M i_p \quad (4.2)$$

Where as  $Z_2$  is the secondary side impedance.

The equivalent impedance of the primary and secondary side is shown in equations (4.3) and (4.4).

$$Z_1 = j\omega L_P - \frac{1}{j\omega C_P} \quad (4.3)$$

$$Z_2 = j\omega L_S - \frac{1}{j\omega C_S} + R_L \quad (4.4)$$

$R_L$  is equivalent resistance viewed from terminal CD. These points are at rectifier side.

By multiplying equation (4.1) with  $Z_2$  to have equation (4.5).

$$Z_1 Z_2 i_P - j\omega M Z_2 i_S = V_P Z_2 \quad (4.5)$$

By multiplying equation (4.2) with  $j\omega M$  to have equation (4.6).

$$j\omega M Z_2 i_S + \omega^2 M^2 i_P = 0 \quad (4.6)$$

By adding equation (4.5) and (4.6) to have equation (4.7).

$$Z_1 Z_2 i_P + \omega^2 M^2 i_P = V_P Z_2 \quad (4.7)$$

By dividing equation (4.7) by  $Z_2$  to have (4.8)

$$Z_1 i_P + \frac{\omega^2 M^2 i_P}{Z_2} = V_P \quad (4.8)$$

By dividing equation (4.8) by  $i_P$  to have (4.9)

$$Z_1 + \frac{\omega^2 M^2}{Z_2} = \frac{V_P}{i_P} \quad (4.9)$$

In equation (4.9),  $\frac{V_P}{i_P}$  is the impedance as viewed from primary side or it can be called as input impedance ( $Z_{in}$ ). However, it can be seen that there is also reflected impedance from secondary to primary side which is  $\frac{\omega^2 M^2}{Z_2}$ . So, reflected impedance ( $Z_r$ ). By put the value of  $Z_2$  in equation (4.9) will have equation (4.10).

$$Z_r = \frac{\omega^2 M^2}{j\omega L_S - \frac{1}{j\omega C_S} + R_L} \quad (4.10)$$

In these equations  $\omega$  is represented any frequency whereas  $\omega_o$  is represented the resonance frequency.

Reflected impedance  $Z_r$  at resonant frequency  $\omega_o$

$$Z_r = \frac{\omega_o^2 M^2}{j\omega_o L_S - \frac{1}{j\omega_o C_S} + R_L} \quad (4.11)$$

At resonance frequency the impedance became pure resistive, so term  $j\omega_o L_S - \frac{1}{j\omega_o C_S} = 0$ , and therefore the expression of secondary compensation capacitor shown in equation (4.12).

$$C_s = \frac{1}{L_s \omega_o^2} \quad (4.12)$$

Equation (4.12) is the for designing capacitor on the secondary side of the system.

So, the at resonate frequency the new expression of reflected impedance is

$$Z_r(\omega=\omega_o) = \frac{\omega M^2}{R_L} \quad (4.13)$$

The Input Impedance at resonant frequency is shown in equation (4.14)

$$Z_{in} = j\omega L_P - \frac{j}{\omega_o C_P} + \frac{\omega_o^2 M^2}{R_L} \quad (4.14)$$

It is noted that at resonance, the imaginary part of input impedance become zero, and from this we can get the value of the primary side compensation capacitor as

$$C_P = \frac{1}{L_P \omega_o^2} \quad (4.15)$$

In the resonance condition, the secondary side circuit become pure resistive because the reactance parameters cancel the effect of each other so by apply KVL in the secondary side at resonance condition will have equation (4.16)

$$|j\omega_o M i_{p_{rms}}| = i_{s_{rms}} * R_L \quad (4.16)$$

From equation (4.16), the expression for mutual inductance can be written as

$$M = i_{s_{rms}} * \frac{R_L}{i_{p_{rms}} * \omega_o} \quad (4.17)$$

Now, quality factor of secondary side can be expressed as

$$Q_s = \omega_o * \frac{L_S}{R_L} \quad (4.18)$$

From equation (4.18), design expression for secondary coil inductance as

$$L_S = Q_s * \frac{R_L}{\omega_o} \quad (4.19)$$

Additionally, coefficient of coupling factor K is expressed as

$$K = \frac{M}{\sqrt{L_p L_S}} \quad (4.20)$$

So, now from the equation (4.20), the primary coil inductance expression as

$$L_p = \frac{M^2}{K^2 * L_S} \quad (4.21)$$

In the design of wireless power transfer for electric vehicle the equations of primary side and secondary side capacitor and inductor has been derived. Now by using these equations the

actual values of the component are calculated to make the circuit resonant to have a required resonance frequency which is used in the chapter 4.

#### **4.4 Summary**

Wireless Power Transfer (WPT) systems were fully designed and calculated in this chapter, which laid the foundation for the next application and analysis. In the design of wireless power transfer for electric vehicle the equations of primary side and secondary side capacitor and inductor has been derived. Now by using these equations the actual values of the component are calculated which is used in the chapter 5.

As a basic element, the integration of variable capacitors to dynamically modify resonance frequencies was described in Chapter 3, which prepared the groundwork for a hands-on investigation in Chapter 5 which simulation part of this research.

Chapter 4 covers the design of a wireless charging system for electric vehicles, with a special emphasis on the integration of a variable capacitor to adjust the resonance frequency. In this chapter, the calculations of electrical components, which are crucial for maximizing the performance and power transfer efficiency of the system, are thoroughly detailed. These include calculations of primary and secondary capacitance, reflective impedance, resonance frequency, mutual inductance, quality factor, and coupling coefficient.

The concepts and designs introduced in Chapter 4 are further developed in Chapter 5. This involves the use of software such as PSPICE and MATLAB Simulink for the accurate simulation of the wireless power transfer system. The simulations are necessary to test the system's properties, including its efficiency, quality factor, mutual induction, compensation circuit, resonance frequency, and the behaviour of its variable capacitor in a controlled environment.

In summary, Chapter 4 establishes the theoretical groundwork and provides a detailed design for the wireless charging system, while Chapter 5 applies these designs in simulation, offering a practical evaluation of the system's functionality and validating the theoretical models established in Chapter 4.

# Chapter 5: Simulation of WPT with fixed and variable capacitor

## 5.1 Introduction

This chapter is implemented by using the concept discussed in chapter 3 which is about design and concept of variable capacitor and chapter 4 which is about concept and design of wireless power transfer for electric vehicles.

Simulation of the wireless power transfer including variable capacitor has been done in PSPICE in this chapter 5 and MATLAB SIMULINK design and results graphs are shown in Appendix C1 to Appendix C8. Lenovo laptop with processor of 11th Gen Intel(R) Core (TM) i7-1165G7 @ 2.80GHz 2.80 GHz and Installed RAM 8.00 GB and system type of 64-bit operating system, x64-based processor is used.

## 5.2 Simulation Design

Design shown in Figure 5-1. There are two side of this design primary side and secondary side respectively.

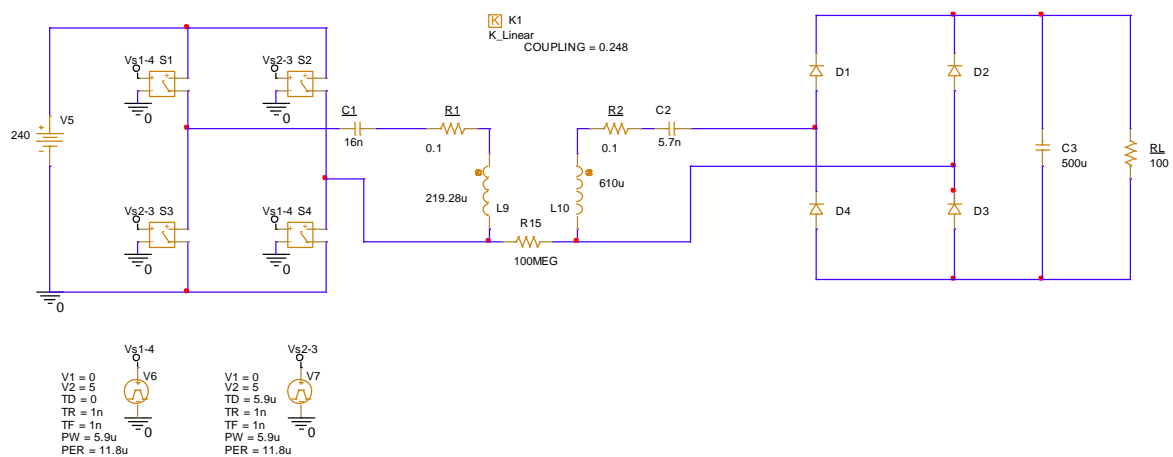


Figure 5-1: Wireless power transfer design with fixed capacitor

In the primary side, 240V DC voltage applied as a source and H-bridge inverter designed by using 4 ideal switches. An H-Bridge inverter is an essential part that transforms DC (direct current) power into AC (alternating current) power at a high frequency. This AC power is then

used to create an oscillating magnetic field that facilitates wireless power transfer. In order to achieve this, the four ideal switches in the H-Bridge are quickly switched into different states in a predetermined order. Switch S1 and S4 operate at same time and Switch S2 and S3 operate at same time. To operate these switches V-Pulse is used to control the switches. The specification of the V-Pulse is described in Table 6. Moreover, S-S compensated circuit has been designed in to the circuit to operate as a resonance circuit to achieve maximum flux passing through primary side to secondary side to get maximum power transfer. The resonant circuits on the primary and secondary sides of the system are made up of inductors and capacitors. The efficiency of power transfer across a distance is increased by tuning these circuits to resonate at the same frequency. In the secondary side, after received power from the primary side the high-frequency AC that is induced in the secondary coil is converted back into DC by the rectifier on the receiving side. Four ideal diodes are used for rectification. A DC filter capacitor is a crucial part that is positioned parallel between the rectifier and the battery in this design. Before the DC current reaches the battery for charging, it serves the primary purpose of smoothing it out.

In this design,  $K_{\text{linear}}$  for coupling is used. In this wireless power transfer (WPT) systems, particularly the coupling factor, generally represented by the symbol  $k$ , is a measurement of the efficiency with which two coils the primary coil and the secondary coil are magnetically connected. The number is dimensionless and has a range of 0 to 1, where 1 denotes perfect magnetic coupling and 0 denotes no magnetic coupling. The function of R15 which is 100MEG is just for the understanding of PSpice software to avoid open circuit. PSpice software think it is open circuit that why connected high resistance between primary and secondary coil but there is no current passed through this resistance because the value is so high.

Calculation of values for capacitors, primary side coil, secondary side coil, resonance frequency and  $K$  coupling are got by using equation from the equations discussed in chapter 4.

The values used for this design shown in Table 6. In literature review, it is concluded that for wireless power transfer high frequency is required. In this research 85kHz resonance frequency is used. By using this frequency time period is calculated which is inverse of frequency according to the formula. Time period is mentioned in Table 6 which is  $PER=11.8\mu s$ .

TD is the time delay of the switches of H-bridge which is 50% of each combination of switches.



As shown in Table 6, total time period is PER=11.8us so time delay is calculated TD=5.9us which is half of total time period. TR and TF are the time took to rise and fall of pulse respectively. Amplitude of the pulse is 5 which is shown in Table 6 as V2.

**Table 6: Value used in V-Pulse for H-Bridge**

<b>Vs (1-4), S1 and S4</b>	<b>Vs (2-3), S2 and S3</b>
V1=0	V1=0
V2=5	V2=5
TD=0	TD=5.9us
TR=1ns	TR=1ns
TF=1ns	TF=1ns
PW=5.9us	PW=5.9us
PER=11.8us	PER=11.8us

**Table 7: WPT design Components Values used**

<b>Terms</b>	<b>Value</b>
Source	240 DC
H-Bridge Inverter	Four Ideal Switches, S1, S2, S3, S4
Primary Coil	219.28u
Secondary Coil	610uH
C1 (Fixed)	16nF
C2	5.7nF
K_Linear	0.248
Rectifier	Four Ideal Diodes D1, D2, D3, D4
C3 DC filter	500uF
R Load	100ohm

Wireless power transfer design with fixed capacitor shown in Figure 5-1. By flipping the switches S1, S2, S3, and S4, the H-Bridge inverter transforms a DC voltage into an AC voltage. The voltage across the primary coil is positive when S1 and S4 are on and negative when S2 and S3 are on.

The resonant circuit created by L and C tends to smooth the square wave into a sinusoidal waveform when the square wave voltage from the H-bridge is supplied to it. This is because the resonant circuit will naturally oscillate at its resonant frequency, which should ideally coincide with the H-bridge switching frequency.

The diodes D1, D2, D3, and D4 rectify the sinusoidal voltage that is induced in the secondary coil. The AC voltage is changed back into a pulsing DC voltage through the rectification process. Producing a DC voltage that has significantly less ripple and can be utilised to power a load.

### 5.3 Results

An H-bridge inverter's output voltage is represented by the waveform in the Fig.20. The graphic displays a sequence of peaks and troughs that represent the usual switching movements in an H-bridge circuit to convert a direct current (DC) source into an alternating current (AC). The voltage levels alternate between high and low, indicating that the inverter is correctly transforming the DC input into a pulsed or modified square wave AC output.

The Figure 5-2 shows a series of positive and negative pulses of voltage. In this case, the voltage varies between a maximum of about +240V and a minimum of -240V. It actually tells that the x-axis of the graph represents time in milliseconds, and it is the speed at which the waveform is switching. On the y-axis, representing the potential difference applied across the load, the dependent variable under measurement would be voltage.

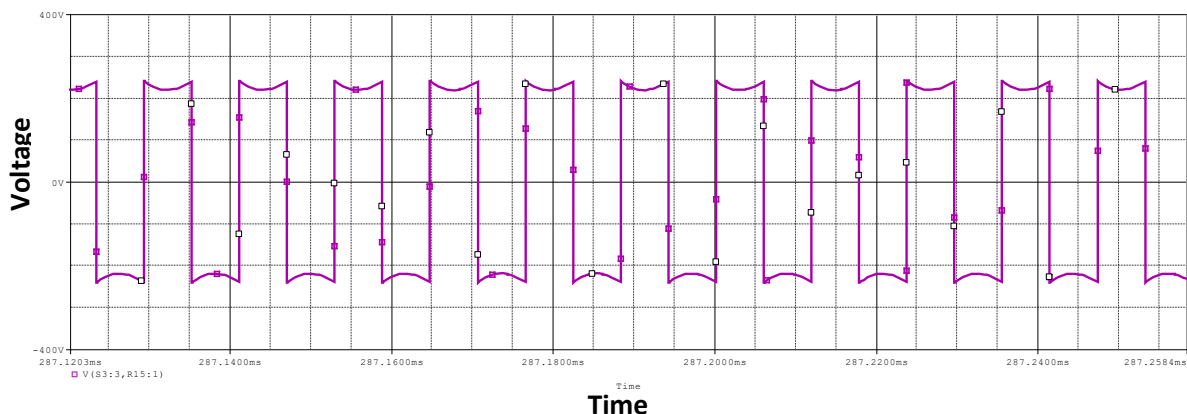
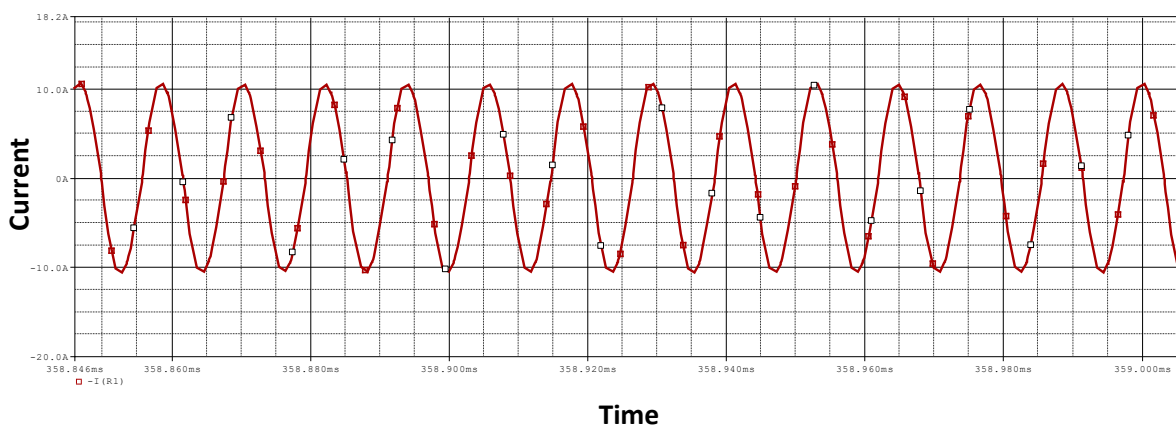


Figure 5-2:H-Bridge Output Voltage Waveform

The current flowing through a system's primary side is represented as a sinusoidal waveform, as seen in the Figure 5-3 plotting the waveform involves a red line, with white dots designating particular places along the curve that most likely correspond to sampled data points or significant characteristics of the current's behaviour over time.

The current waveform displayed in the figure is characterized by a sinusoidal shape, which is often observed in alternating current (AC) circuits. In the graph, the amplitude of the current oscillates between approximately -10 A and +10 A. This indicates that the peak current reaches these values in both the positive and negative directions. Time is plotted on the horizontal axis, with values indicated in milliseconds. A single cycle of the waveform is completed approximately every 35.8 to 35.9 milliseconds, suggesting a high frequency of oscillation. Each peak, whether positive or negative, is followed by a trough, forming a continuous wave pattern. The waveform's consistent pattern across the displayed time span suggests a stable AC supply with a fixed frequency and amplitude.

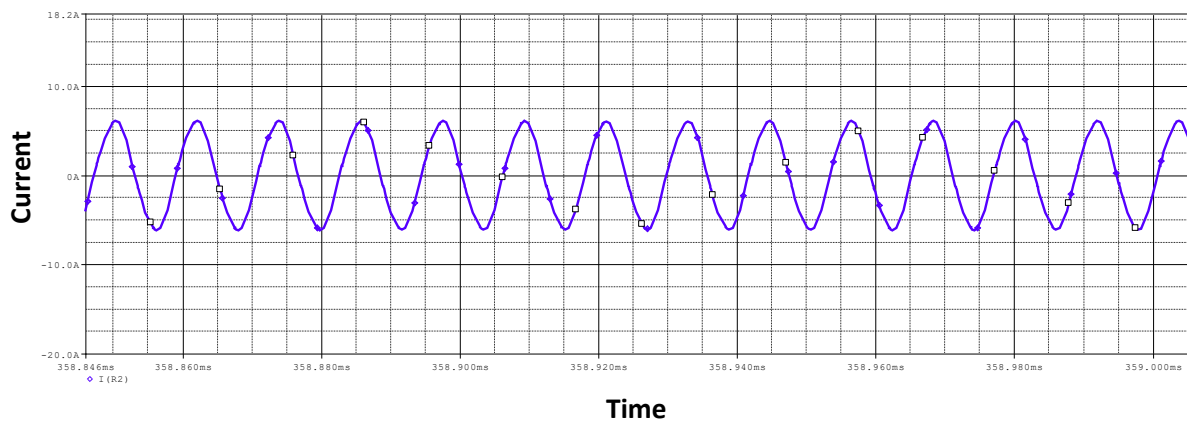


**Figure 5-3:Primary Side Current waveform**

The Figure 5-4 shows a blue waveform that represents the current flowing through a system's secondary side. One observes a sequence of peaks and troughs that correspond to the sinusoidal pattern that is characteristic of alternating current (AC). The waveform's constant amplitude and frequency indicate a steady AC current, which is necessary for the operation for wireless power transfer.

In the depicted waveform of Figure 5-4, the current on the secondary side is shown as oscillating in a sinusoidal pattern similar to that of the primary side, but with some notable differences. Here, the current is plotted against time, with the vertical axis representing current

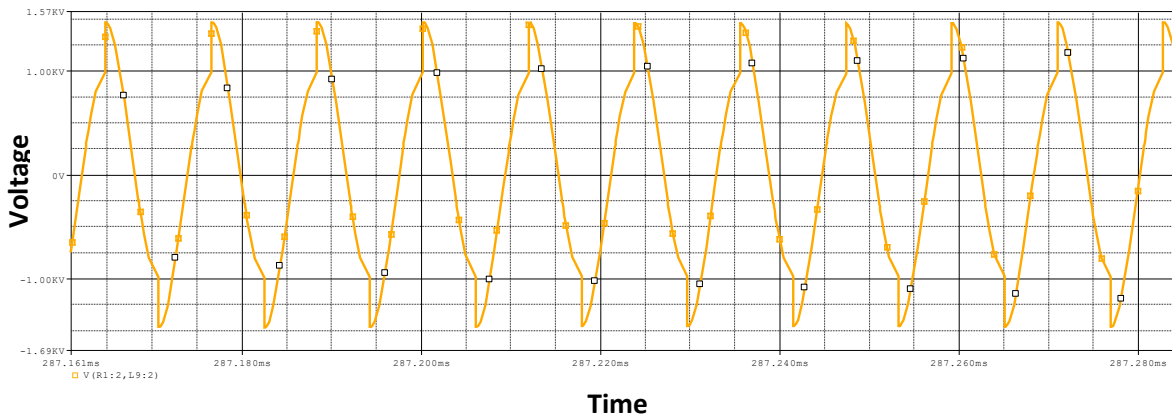
and the horizontal axis representing time, measured in milliseconds. The waveform is displayed with a peak amplitude oscillating between approximately -8.5 A and +8.5 A, which indicates a lower amplitude compared to the primary side waveform. The cycle frequency appears to match that of the primary side, suggesting that the frequency remains constant through the transformation process. Each cycle of the waveform is completed over a similar time interval as observed in the primary side, maintaining a consistent frequency across both sides of the system.



**Figure 5-4:Secondary Side Current waveform**

The Figure 5-5 is a golden coloured waveform that represents the voltage characteristic across the primary coil of the system. This is followed by a series of alternating peaks showing the sinusoidal voltage pattern that is characteristic operating in resonance behaviour. Periodicity and amplitude, as obvious from the regular time courses of the waveform, the period of stable voltage signal.

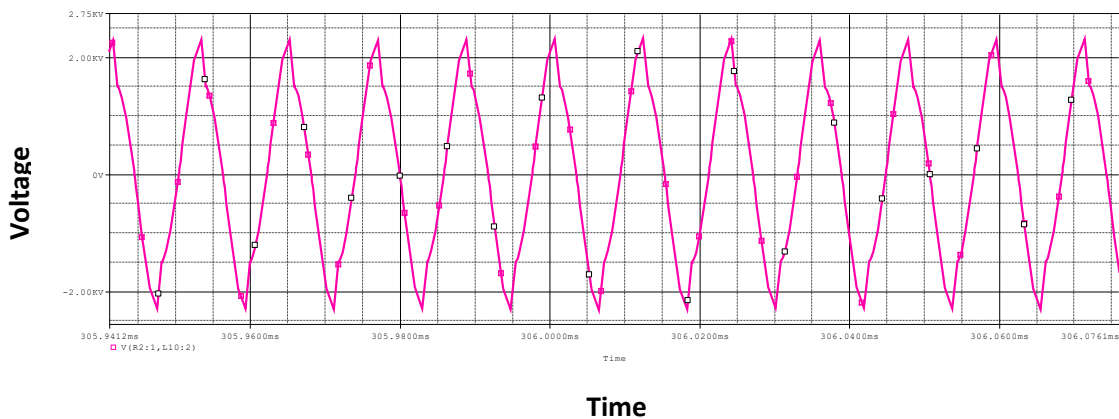
In Figure 5-5, the voltage waveform on the primary side is depicted as a series of oscillations, characterized by a sinusoidal pattern, similar to typical alternating current (AC) signals. The voltage is represented on the vertical axis, and it varies between approximately -1.5 kV and +1.5 kV, indicating a peak-to-peak voltage of about 3.0 kV. Time is shown on the horizontal axis, measured in milliseconds. The time scale extends over a short interval, suggesting the waveform's rapid oscillation, which is typical for high-frequency AC applications. Each cycle of the voltage waveform can be observed to complete in about 0.5 milliseconds, indicating a very high frequency. Sharp peaks are reached both in the positive and negative directions, which are mirrored about the horizontal axis, showing the alternating nature of the voltage.



**Figure 5-5: Primary Side Voltage Waveform**

The Figure 5-6 is a pink traced waveform that signifies the voltage that is produced by the secondary coil of a system. It represents a sinusoidal waveform with consistent oscillation; it has peaks and troughs representing an alternating voltage. The uniformity of the waveform is indicative of uniform or steady voltage output, which is periodic in nature, required by functioning of WPT system based on inductive coupling by the secondary coil.

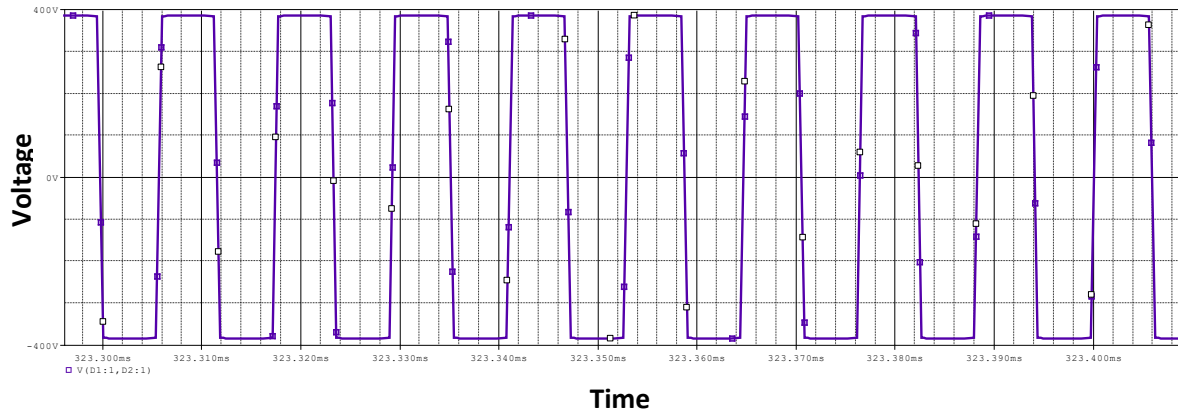
In Figure 5-6, the voltage waveform on the secondary side is depicted, where the voltage is shown oscillating between approximately -2.5 kV and +2.5 kV. This indicates a peak-to-peak voltage of about 5 kV. The sinusoidal pattern of the waveform is evident, typical of alternating current (AC) applications, but with a noticeable difference in amplitude compared to the primary side. Time, measured in milliseconds, is plotted along the horizontal axis, revealing the quick succession of voltage cycles. Each cycle of the voltage waveform appears to be completed in a short span of time, suggesting a high frequency, consistent with the primary side but adjusted in amplitude likely due to the transformation ratios involved in the system.



**Figure 5-6: Secondary Side Voltage Waveform**

The Figure 5-7 shows a purple waveform that represents a rectifier's input voltage. One notices a succession of consistent, vertical peaks and falls, which point to a full-wave rectified voltage pattern. The pattern exhibits the typical form of a DC signal that is pulsating after being corrected from an AC signal.

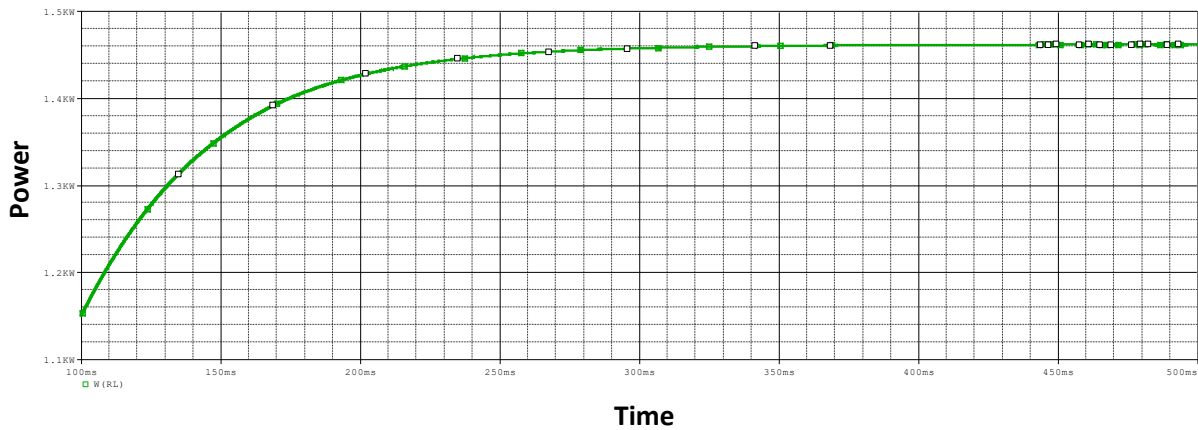
In Figure 5-7, the input voltage waveform for a secondary side rectifier is depicted. It is characterized by a series of alternating positive and negative pulses that form a full-wave rectified pattern. This waveform indicates that the voltage oscillates between approximately +400V and -400V, showing a peak-to-peak voltage of about 800V. The horizontal axis represents time, measured in milliseconds, showcasing the rapid changes in voltage that occur within a very short period. This rapid oscillation is typical of a full-wave rectified signal, where both halves of the AC waveform are used, but all in the same direction in terms of polarity. The presence of both positive and negative pulses in the waveform illustrates that the AC input is being converted effectively, with each half-cycle of the AC waveform being mirrored to maintain a constant polarity, which is typical in full-wave rectification.



**Figure 5-7:Secondary Side Rectifier Input Voltage waveform**

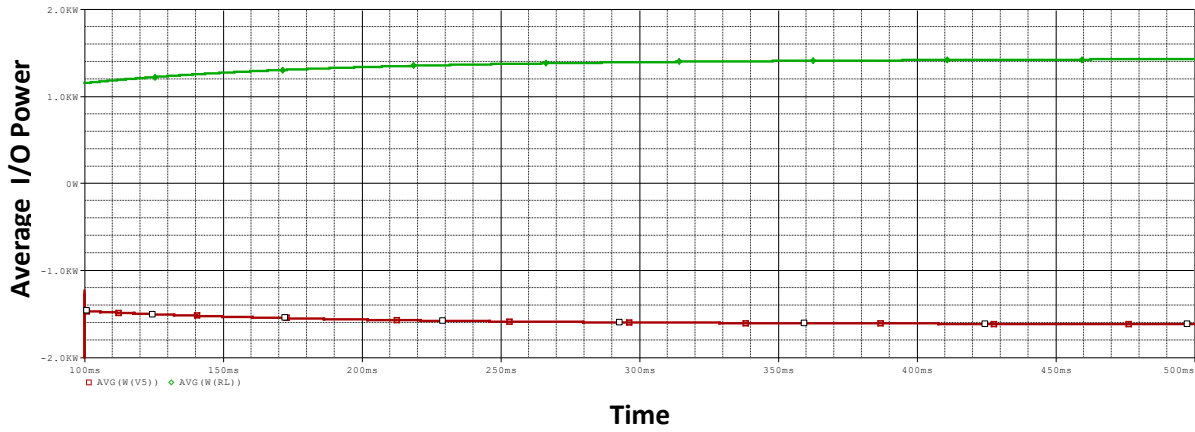
The Figure 5-8 shows a graph that shows a system's output power as a green curve. The curve starts out high on the left, indicating a high-power output, and then progressively levels off as it advances to the right, indicating a power output plateau. At regular intervals throughout the curve, there are little white markers that could indicate individual data points, sampling measurements over time, or another variable. The general curve shape indicates that the rate of growth in power output lowers until it stabilises as the variable on the x-axis increases.

In Figure 5-8, the output power at the load side, is presented over a time period. The curve displayed on the graph shows a gradual increase in power over time, starting from approximately 1.15 kW and reaching a plateau near 1.3 kW. The time is plotted on the horizontal axis, measured in milliseconds, and spans from 10 to 50 milliseconds. Initially, the power is observed to rise steeply, indicating a rapid increase in the power being delivered to the load. As time progresses, this increase in power levels off, and a steady state is reached where the power remains relatively constant at around 1.3 kW.



**Figure 5-8: Output Power at load Side RL**

In Figure 5-9, the average input and output powers are depicted over time, plotted to illustrate the dynamics between the power supplied to a system and the power delivered by it. The horizontal axis, representing time measured in milliseconds, spans from 10 to 50 milliseconds. Two distinct lines are observed on the graph. The green line, which is relatively constant throughout the period, represents the average input power maintained at approximately 1.2kW. This line indicates that the power input into the system remains stable over the time period displayed. Contrastingly, the red line, which indicates the average output power, is shown below zero.



**Figure 5-9: Average Input and Output Powers**

A resonant circuit, like an LC (inductor-capacitor) circuit, can be made to operate at a particular frequency by using fixed capacitors. This frequency can be calculated using the formula shown in equation 5.1.

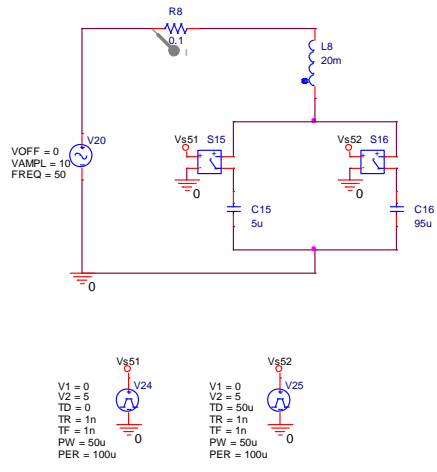
$$f = \frac{1}{2\pi\sqrt{LC}} \quad (5.1)$$

Since the capacitance of a fixed capacitor is constant, the resonance frequency is likewise fixed. A fixed capacitor will not provide the flexibility if needed to tune the circuit to different frequencies or if the operating frequency varies. To overcome this issue variable capacitor concept has been designed to get the desire resonance frequency.

## 5.4 Variable Capacitor Simulation

Circuit design of variable capacitor with different capacitor values is shown in Figure 5-10. 10V AC applied as source, small resistance and inductor is connected in series with source. Two switches S15 and S16 are connected with capacitor C15 and C16 in series respectively. V-Pulse is used for the input of the switches.





**Figure 5-10: Variable Capacitor Circuit Diagram**

The description of the V- in this circuit shown in Table 8 and other values and components used in this circuit shown in Table 9 and Table 10. Complete operation of this variable capacitor has been discussed in chapter 3 sec 3.3.1.

**Table 8: V-Pulse value used for variable capacitor design**

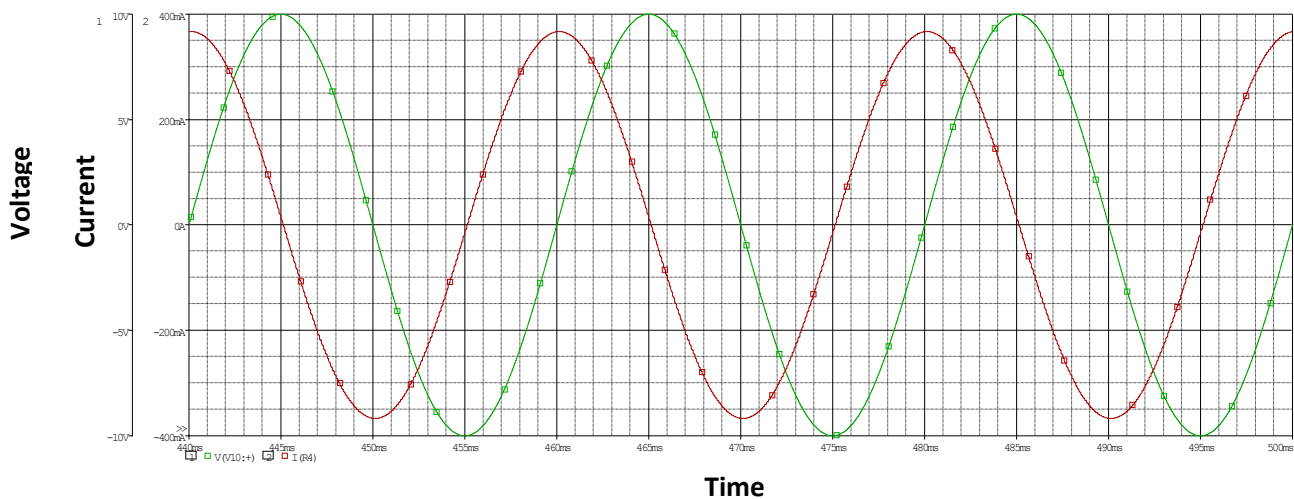
V-Pulse S5	V-Pulse S5
V1=0	V1=0
V2=5	V2=5
TD=0	TD=50us
TR=1ns	TR=1ns
TF=1ns	TF=1ns
PW=50us	PW=50us
PER=100us	PER=100us

**Table 9: Components and their values used in variable capacitor design with different C values**

Terms	Values
Source	10V AC
R	0.1 ohm
C15	5uF
C16	95uF
L	20mH

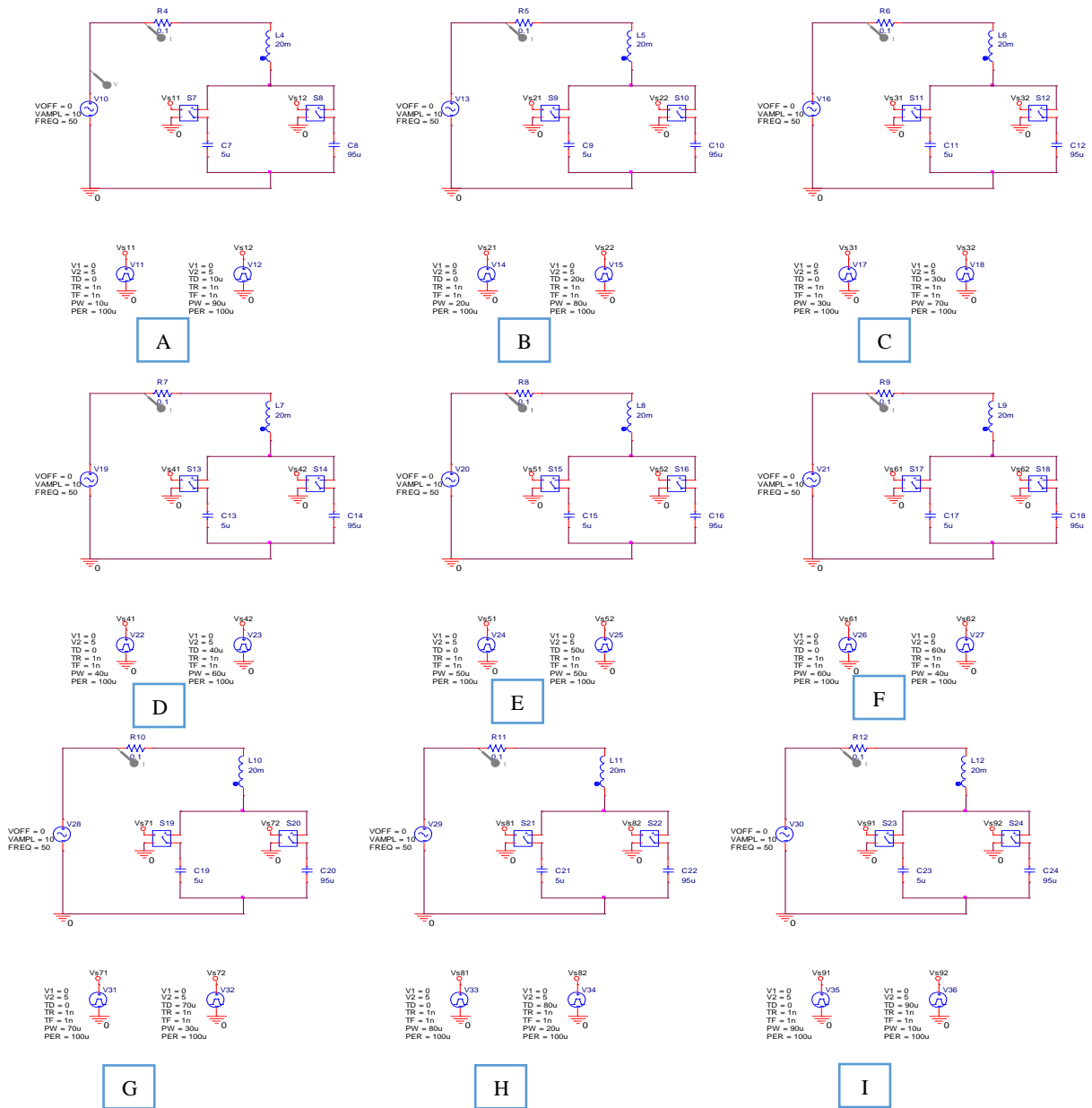
In Figure 5-11 is shown the capacitive effect of the design circuit. The current is leading the voltage which is the capacitive nature of the in case of capacitor. Green sinusoidal wave represented the voltage and red sinusoidal wave represented the current. The result is shown in Figure 5-11 by setting the duty cycle of the switches 50% each. The voltage waveform is seen

peaking before the current waveform at each cycle, indicating the characteristic phase shift observed in capacitive circuits where the current lags the voltage by 90 degrees. This phase difference is a typical property of capacitive components, reflecting the time delay required to charge the capacitor. The amplitude of the voltage waveform remains consistent throughout the displayed time span, oscillating between approximately +10 V and -10 V. Similarly, the current waveform maintains a consistent amplitude, oscillating between about +400 mA and -400 mA, albeit out of phase with the voltage. The capacitive effect is illustrated by the nature of the phase shift between voltage and current. This shift is key to understanding how capacitors influence in circuits, affecting the timing and magnitude of power delivered through the system.



**Figure 5-11:Result Graph for Variable Capacitor**

To verify the capacitive effect of the design circuit different duty cycle put for both switches. Circuits design with different duty cycle is shown in Figure 5-12.



**Figure 5-12: Variable Capacitor Circuits with different duty cycles**

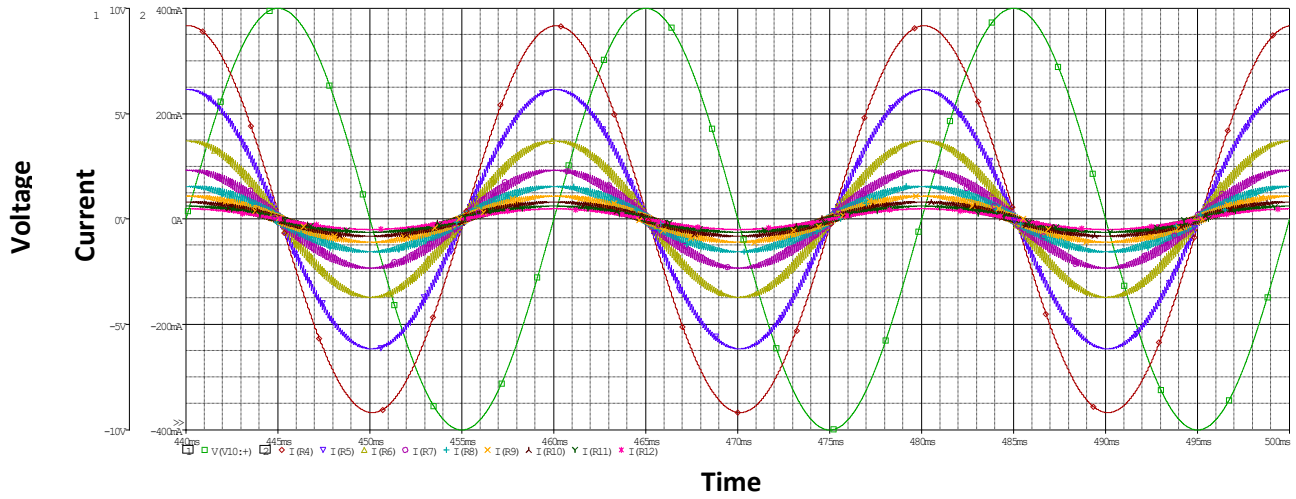
Different duty cycles of switches for Design A, B, C, D, E, F, G, H, and I of Figure 5-12 are shown in Table 10.

**Table 10:Duty cycle set for design A-I**

Design	Duty Cycles	
	S1	S2
A	10	90
B	20	80
C	30	70
D	40	60
E	50	50
F	60	40
G	70	30
H	80	20
I	90	10

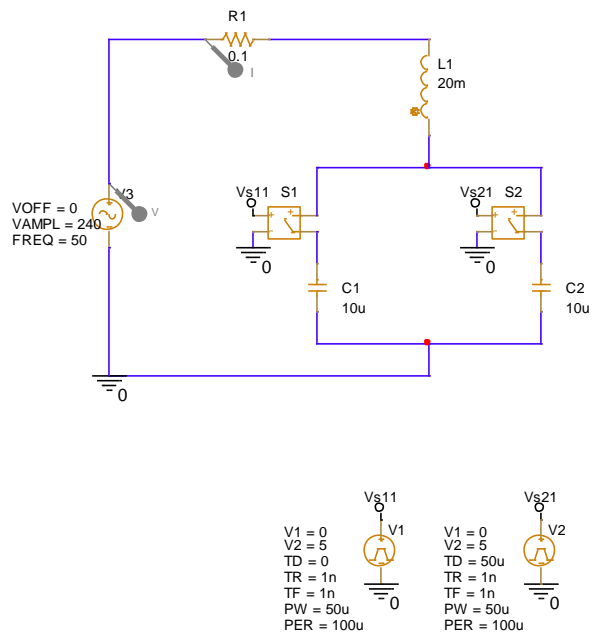
It can be seen in Figure 5-13 as a result that the circuit design is behaved as a capacitor in all combination of the duty cycle of switches. When the duty cycle combination in Table 10 is used, the current leads the voltage, indicating that the circuit design functions as a capacitor. In Figure 5-13, the results for a variable capacitor with different duty cycles are displayed, where multiple current wave forms and a voltage waveform in green are plotted over time. The green voltage waveform demonstrates oscillations influenced by the capacitive properties of the circuit, where phase shifts and voltage magnitudes are modified by different duty cycles. These duty cycles, ranging from 10% to 90% for S1 and inversely for S2, determine the duration for which each switch in the circuits is closed within one cycle. This timing directly impacts the charging and discharging dynamics of the capacitors.

For each of the designs labelled from A to I, the behaviour of the capacitor varies, which is depicted through the multiple current waveforms. These currents change in amplitude and phase in response to the voltage applied and the charge state of the capacitor, determined by the switches' duty cycles. When the duty cycle of S1 is low (and S2 is high), for example, capacitors charge more briefly and discharge more lengthily, resulting in more gradual current decreases as observed in the respective current waveforms.



**Figure 5-13:Results Graph of Variable capacitor with different duty cycles**

Variable capacitor design with same capacitors values is shown in Figure 5-14 and their component value is mentioned in Table 11. The complete design of this variable capacitor with same capacitor values is shown in Appendix D1.



**Figure 5-14:Variable Capacitor design with same C values**

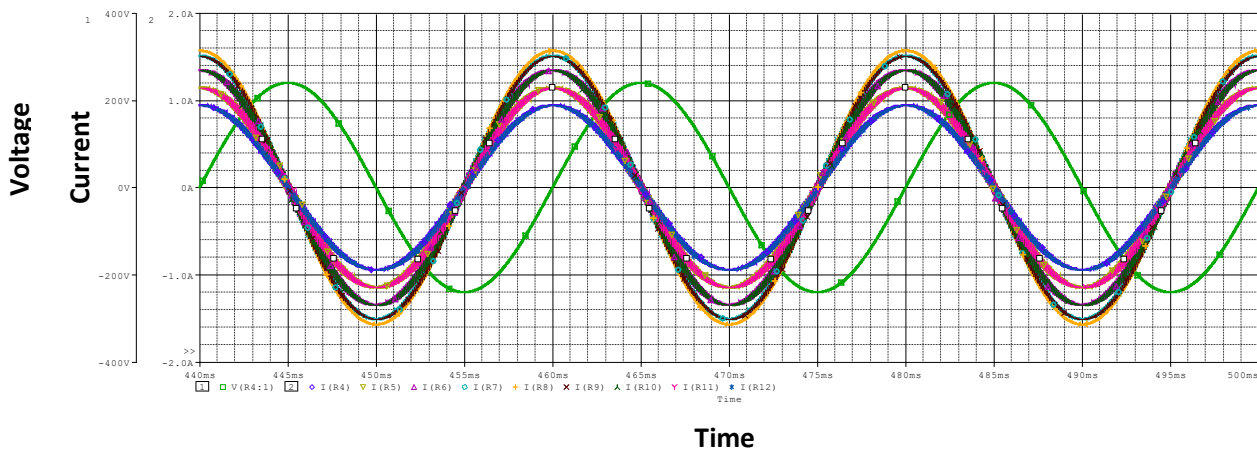
**Table 11:Components and their values used in variable capacitor design with equal C values**

Terms	Values
Source	240V AC
R	0.1 ohm
C4	10uF
C5	10uF
L	20mH

In Figure 5-15 is shown the capacitive effect of the design circuit results with same capacitor values. Because of the capacitor's capacitive nature, the current continues to lead the voltage.

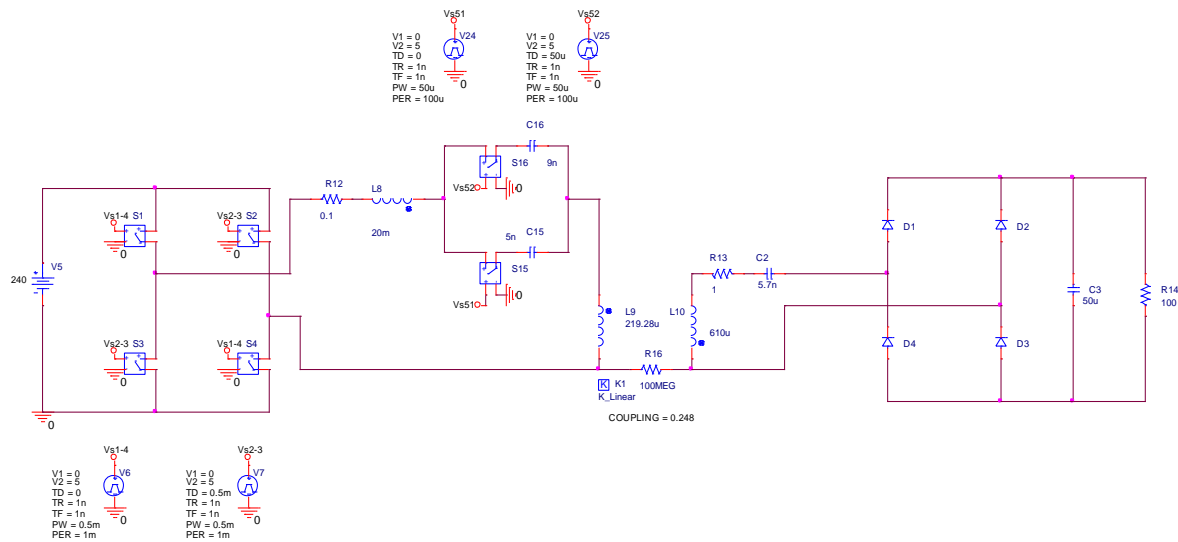
Green sinusoidal wave represented the voltage and other sinusoidal wave represented the current. The result is shown in Figure 5-15 by setting the duty cycle of the switches 50% each as well.

In Figure 5-15 it is clearly seen the behaviour is still capacitive. It is confirmed that by changing the values of these capacitor does not affect the nature of the designed variable capacitor. However, by changing the duty cycles of the switches new value of the capacitor can be obtained to get the new resonance frequency to operate the circuit in resonance which is the requirement of this design and research.



**Figure 5-15:Result Graph for Variable Capacitor with same capacitor values**

The circuit design of WPT with variable capacitor is shown in Figure 5-16. Fixed capacitor C1 value of 16nF is replaced by proposed variable capacitor. The function and values calculation of this design has been discussed in chapter 3 section 3.3.1.



**Figure 5-16: Circuit diagram of WPT with variable capacitor**

Different frequency range with their corresponding capacitor values are mentioned in Table 12. The value of fixed capacitor used was 16nF and its corresponding resonance frequency was 85kw which is mentioned in Table 12 as well.

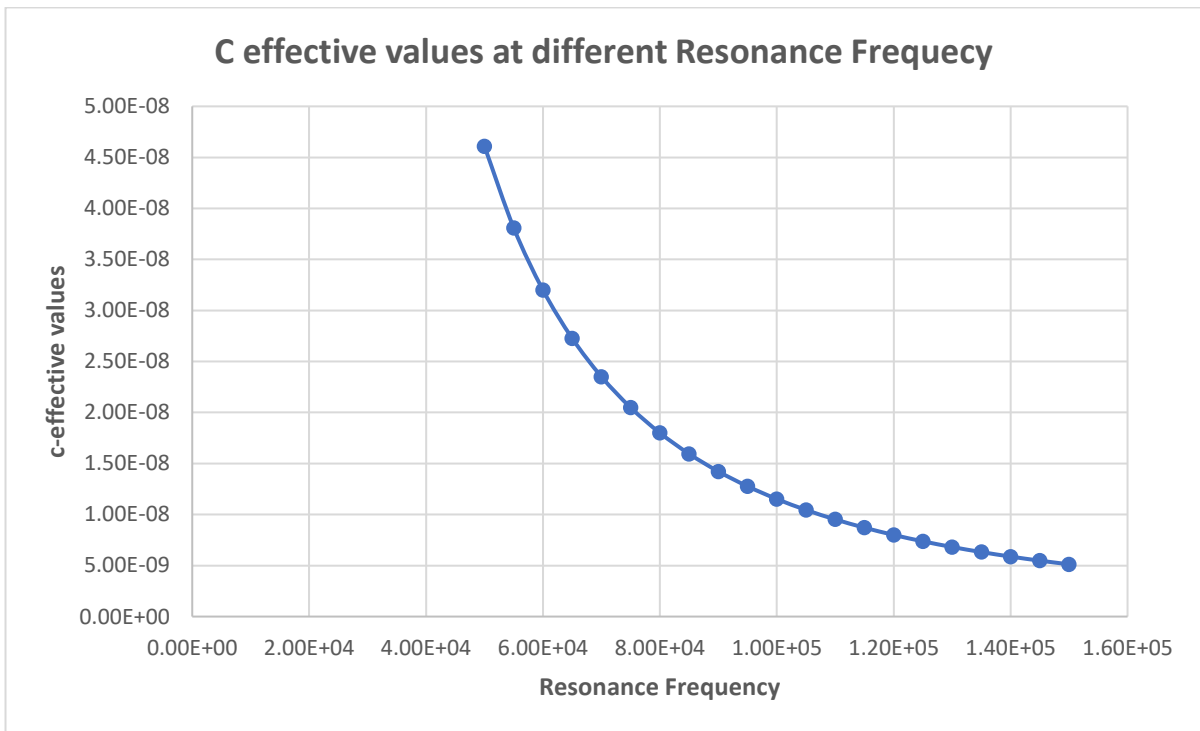
**Table 12: C-effective values for different resonance frequency**

Resonance Frequency	L	C
50kHz	220uH	46.1nF
55 kHz	220uH	38.1nF
60 kHz	220uH	32.0nF
65 kHz	220uH	27.3nF
70 kHz	220uH	23.5nF
75 kHz	220uH	20.5nF
80 kHz	220uH	18.0n
<b>85 kHz</b>	<b>220uH</b>	<b>15.9nF</b>
90 kHz	220uH	14.2nF
95 kHz	220uH	12.8nF
100 kHz	220uH	11.5nF
105 kHz	220uH	10.4nF
110 kHz	220uH	9.52nF
115 kHz	220uH	8.71nF
120 kHz	220uH	8.00nF
125 kHz	220uH	7.37nF

130 kHz	220uH	6.82nF
135 kHz	220uH	6.32nF
140 kHz	220uH	5.88nF
145 kHz	220uH	5.48nF
150 kHz	220uH	5.12nF

The graphical representation of Table 12 is shown in Figure 5-17. The graph shows the decreasing trend with increasing the resonance frequency which fulfil the condition of resonance frequency equation 5.1 where  $L$  is inductor,  $C$  is capacitor and  $f$  is the resonance frequency.

$$f = \frac{1}{2\pi\sqrt{LC}} \quad (5.1)$$



**Figure 5-17:Graph for C-effective values at more different resonance frequency**



## 5.5 Summary

Using the fundamental ideas and designs originally developed in Chapters 3 and 4, the simulation work for Wireless Power Transfer (WPT) systems customised for electric vehicles was carefully carried out in Chapter 5. Through simulations with the PSpice programme, this investigation offered a thorough examination of the system's overall performance and efficiency. Building on this important work, Chapter 6 explores in greater detail the particulars of inductor coil design with an emphasis on the simulation work required to optimise this important WPT system component.

Chapter 5 was implemented on all concepts that have been discussed earlier in Chapter 3 and 4, which deals with the design and concept of variable capacitors and the concept framework of WPT to the electric vehicle. For this chapter, a simulation of WPT with variable capacitor was done by using both PSPICE and MATLAB SIMULINK. Primary-Secondary side of various circuit designs was implemented using a Lenovo laptop, which has high specification designs. The DC voltage of 240V was applied on the primary side through a H-Bridge inverter to realise oscillating magnetic field to ensure effective power transfer. More importantly, the inductor capacitor (LC) resonance circuits were specifically tuned so that it could lead to high flux and power transfer efficiency. In this chapter, the performance of the circuit was thoroughly analysed and recorded as various graphs and tables which showed the current, voltage, and other properties in primary and secondary coils.

The following Chapter 6 is well guided by the simulations and basic knowledge presented in Chapter 5, articulating in detail the design and optimization of the inductor coils that are critical to improvement of the WPT systems. In general, the chapter was constructed upon a deeper, subsequent analysis of the work in Chapter 5, in the development of the framework and performance benchmarks required by the WPT system, which is of utmost importance to the advanced simulations and enhancements in the following chapter.

## **Chapter 6: Inductor coil design**

### **6.1 Introduction**

The design of inductor coils is well researched herein, based on the features in ANSYS Electronics in this chapter within the field of electromagnetic modelling. The following outlines this process briefly to show the meticulous and serious methodology that, with precise simulation and analysis, provides the maximum performance and effectiveness of the inductor coil. Creation of the geometric model of the inductor coil is the first step. The advanced ANSYS Electronics modelling tools help in more precisely developing the physical dimensions of coil and properties. Proper geometry representations ensure that simulation results are, in fact, a reflection of the real inductor's behaviour and represent solely their physical properties.

Once the geometric model has been established, material properties is defined. This is where materials with certain electromagnetic properties are chosen and added to the geometric model; this is an extremely important phase in simulating an inductor coil's actual operation.

Electrical conductivity and magnetic permeability, among other pertinent properties, are taken into consideration while choosing materials because they are essential to the simulation's accuracy.

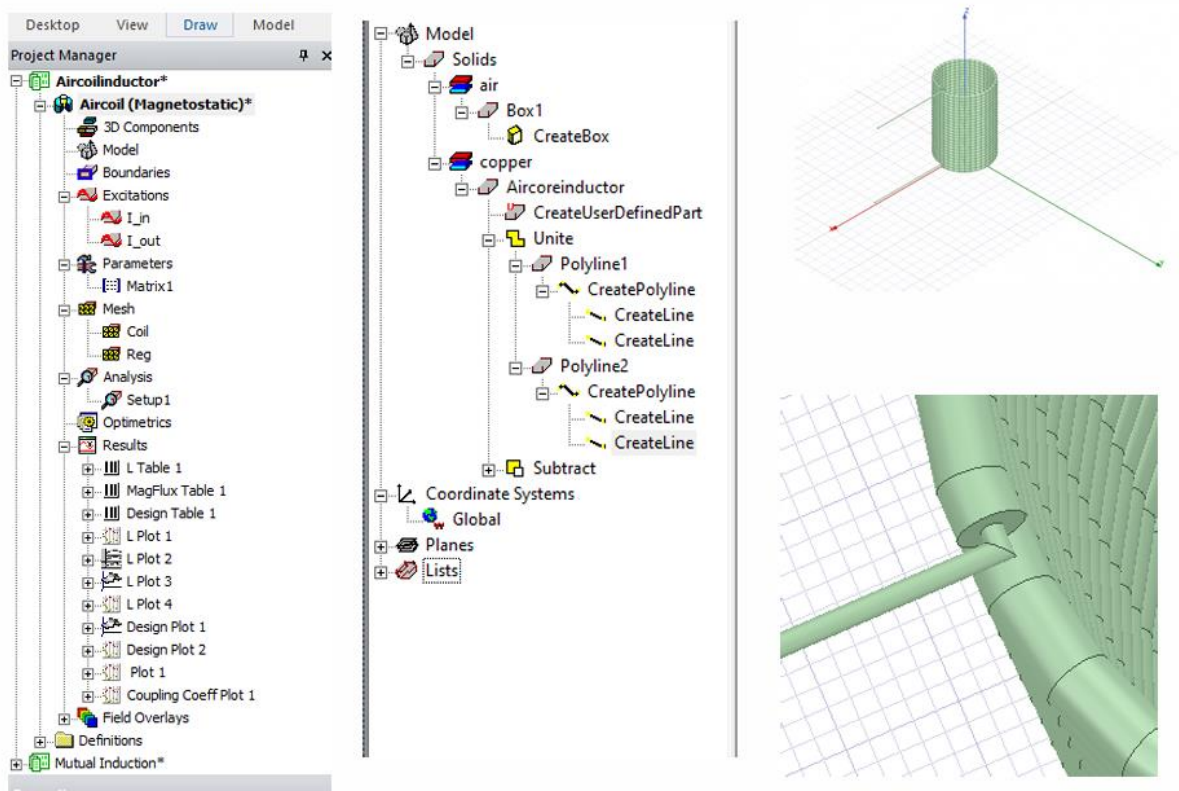
The simulation is run, and the electromagnetic field equations are solved by ANSYS Electronics using finite element analysis (FEA). In order to provide comprehensive insights into the performance characteristics of the inductor coil, the programme carefully computes the electromagnetic fields, currents, and forces within and around it during this period.

### **6.2 Single Inductor Coil Design Simulation**

Ansys software interference is depicted in Figure 6-1. Figure 6-1 illustrates how the coil appears once its characteristics, such as pitch, inner and outer radius, quantity of turn, and shape, have been adjusted. However, this coil is not excitable; current must excite through this coil in order to observe the coil's properties, such as inductance. Figure 6-2 shows the excitation of the current both in and out of the coil. The coil is operated in a laboratory setting, where the air may be the surrounding environment.

To observe the coil's proper response in simulation, this environment boundary must also be placed around the coil. Before the simulation runs, a number of parameters must be configured.

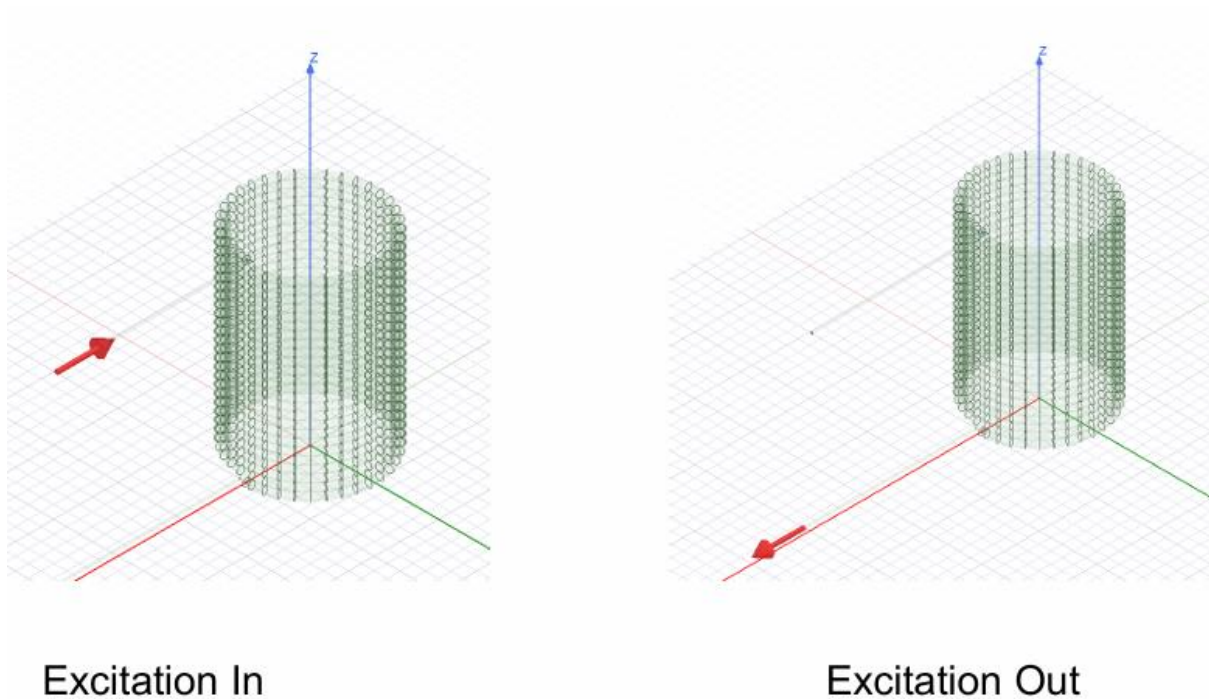
In Figure 6-1 simulation software package's graphical user interface (GUI), Ansys, is seen in the image that has been provided. The graphical user interface appears to be divided into multiple panels. The left panel shows a project hierarchy with the label "Project AircoilInductor," indicating that the simulation of an air coil inductor is the main emphasis of this project. The project's observable components include models, materials, and analyses, all of which point to a methodical approach to the simulation process.



**Figure 6-1: Graphical User Interface of Ansys Software**

The GUI's central screen displays a 3D model workspace with a prominently displayed circular coil design. The hierarchy indicates that the design is a helical coil, potentially composed of copper, as "Copper" is classified under the "Solids" group. The multiturn coil, which is a common feature of an inductor used in electromagnetic applications, is displayed in the three-dimensional image. A close-up of the coil is shown in the lower right corner of the picture, showcasing the detailed layout of each turn and the spaces created by air between them. For evaluating the geometric characteristics, such as inductance, quality factor, and coupling coefficient, that impact the inductor's performance, this in-depth view is essential.

In Figure 6-2 excitation of current in an out the coil is shown. Two identical 3D models of a cylindrical inductor coil are shown side by side in the image, each positioned against a grid that acts as a guide for spatial orientation. The "Excitation In" on the left indicates that it's an introduction of some electrical current into the coil. This will usually be connected to the coil being energized at the beginning of a simulation. As the right model is labelled "Excitation Out," this is indicated that the simulation stops here or an instance is when the coil is not being energized by an outside current supply.



**Figure 6-2: Current Excitation (in and out)**

The red, green, and blue lines of the different axes orientations in the two models are indicative of the X, Y, and Z axes, respectively. In this case, the orientation of the coils with respect to the axes can be critical in the analysis of the distribution of the magnetic field and the other electromagnetic properties during simulation. Coils are evidently many turns that result from an electric current flowing through them and create a magnetic field. Understanding how the inductor behaves in response to electrical stimuli depends on seeing the coil in two distinct

states of excitation side by side. This is also a critical part of the analysis process in electromagnetic simulations. These models are frequently used to forecast the coil's performance in practical applications, like wireless power transfer systems.

Two graphical user interface (GUI) windows labelled "Design List" are shown in the Figure 6-3. The list in the left pane, labelled "Coil," has an entry called "AircoilInductor," which indicates that the design is about an inductor coil. The usage of copper as the material in this design and attributes like colour, model type, design variable, and so on.

Terms like "Type: Current, " on the right pane, which has the name "Current," suggest that it shows information about the electrical current flowing through the coil.

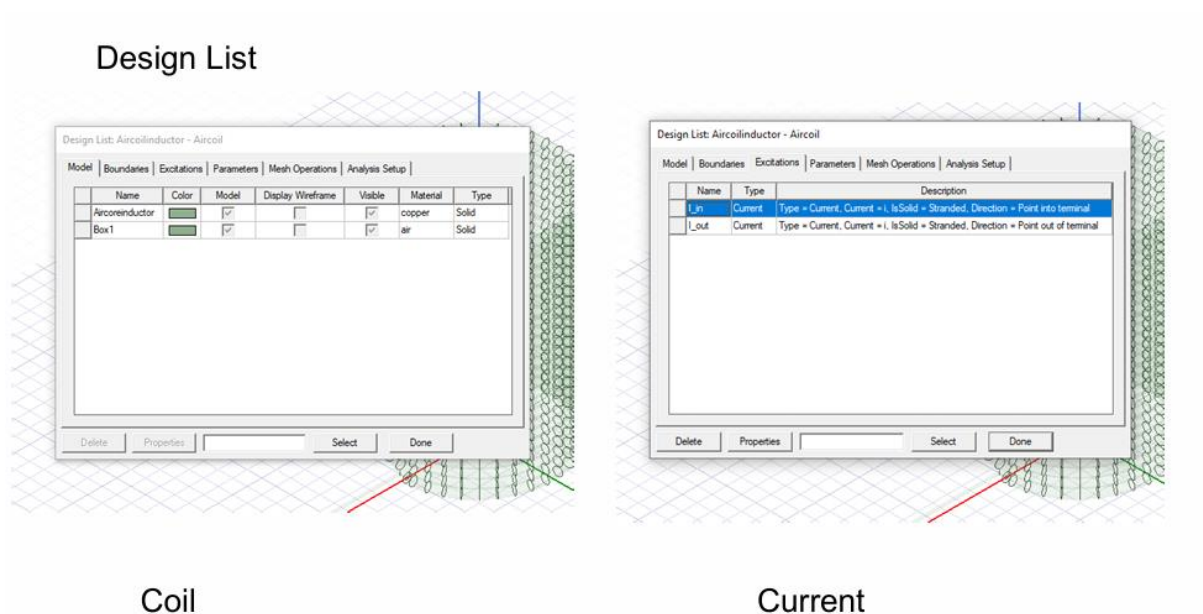
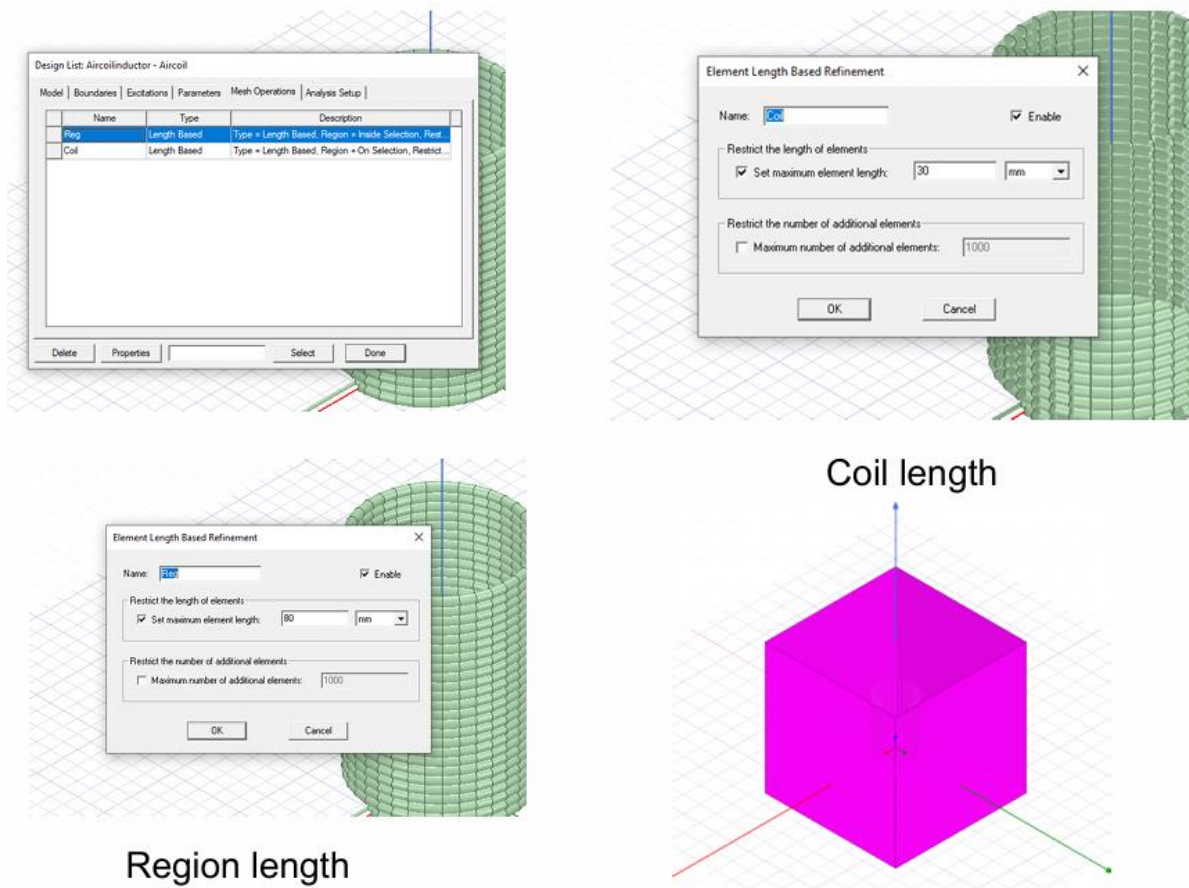


Figure 6-3: Design List dialog box

Two dialogue boxes related to coil and region length specification are displayed in the Figure 6-4, which shows a user interface from a simulation or design programme. An entry for "Coil Length" can be seen in the top dialogue box, which is labelled "Design List AircoilInductor - Axial," and it indicates where the coil's length parameter is defined. Beneath it, another dialogue box with the title "Element Length Based Refinement" offers options suggesting that the mesh can be refined according to the length of the elements; checkboxes allow you to specify minimum and maximum lengths and estimate the number of extra elements.



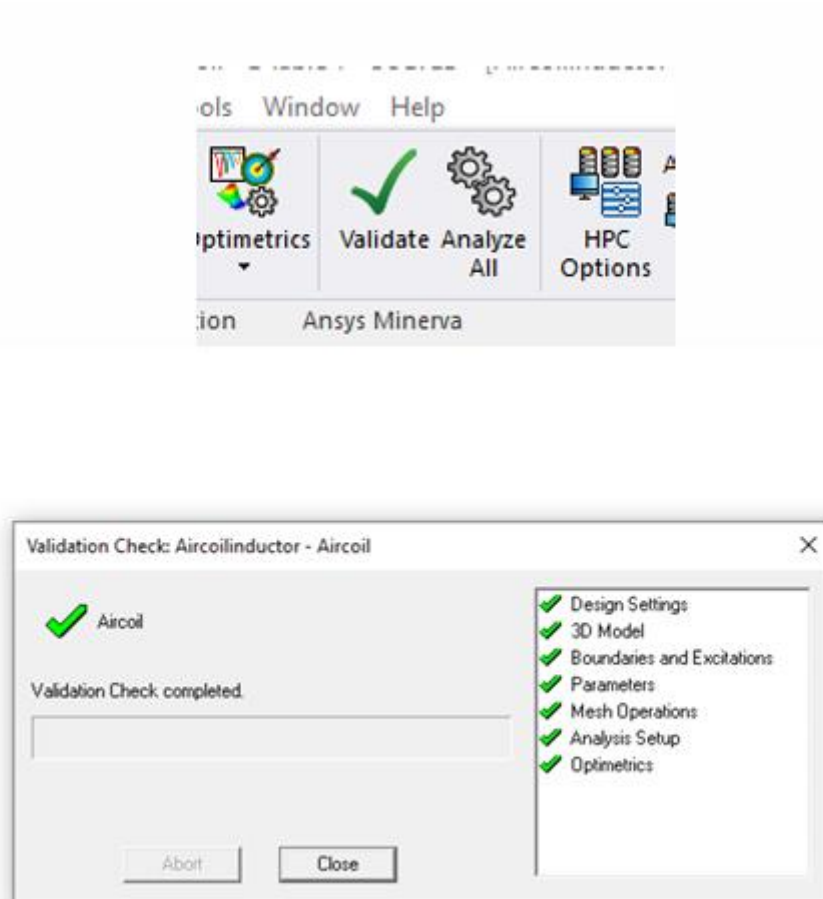
**Figure 6-4: Different Parameter setting dialog box (Length)**

A third "Element Length Based Refinement" dialogue box, labelled "Region Length," appears on the lower left. This suggests adjusting the simulation mesh refinement in a particular area, most likely the area surrounding the coil. The designer has the ability to adjust the refinement details, including the quantity of extra elements, which have an impact on the simulation's resolution and accuracy in that area.

At last, a 3D representation of a coil is shown on the lower right, surrounded by a cube of magenta colour that bears the label "Coil length." Next to it, there's a reference to another cube that's not shown but looks similar and is labelled "Region length," which suggests that these visual aids are a representation of the actual dimensions that are being set in the dialogue boxes. These cubes are served as a clear and understandable visual aid for the regions of interest or spatial limitations in the simulation, showing where the mesh refinement parameters will be applied. The general arrangement conveys how intricate and adaptable the simulation

environment is, giving exact control over the model's dimensions and meshing to enable precise analysis.

The "Validation Check shown in Figure 6-5, AircoilInductor - Aircoil" validation. The word "Aircoil" has a green checkmark in this window, indicating that the validation check was successful.

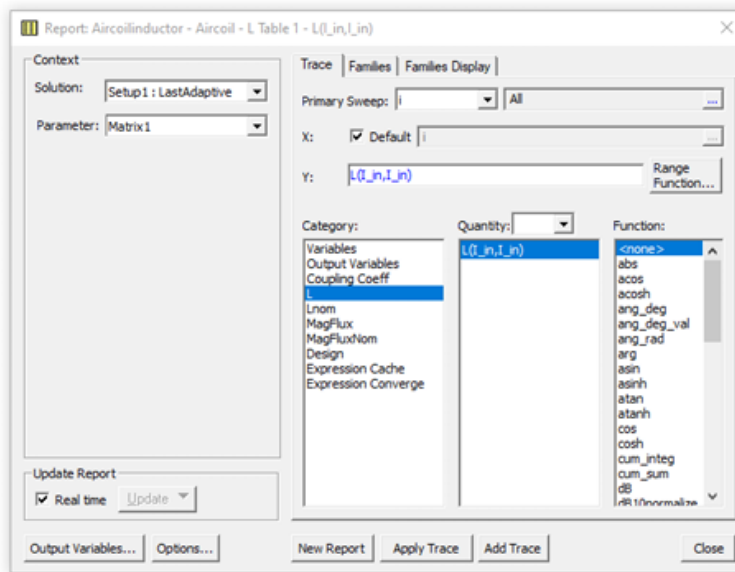


**Figure 6-5:Simulation Validation dialog box**

The list on the right side of the window, which contains items like Design Settings, 3D Model, Boundaries and Excitations, Parameters and Mesh Operations, suggests that this check appears to cover a number of simulation model characteristics. It is implied by the list that every one of these components has been examined and verified inside the simulation environment.

Report dialog box of a simulation program is shown in Figure 6-6 and then software interface that is connected to electromagnetic design or analysis. In order to establish the customization of the report, inside the menu is being displayed a dialog box entitled "Report: AircoilInductor

- Aircoil - L Table 1 -  $[L(A)]-L(A)$ ". The dialog box portrays categories and functions which in essence is implied that the user has been permitted to make selection concerning some forms of characteristics and features. Alongside a variety of functions like "avg," "sum," and "rms," categories like "Intrinsic Variables" and "Global Variables" are visible, demonstrating the software's capacity to perform and report on a variety of statistical and mathematical operations on the simulation data.



L Table 1

	i [A]	L(l_in,l_in) [uH] Setup1 : LastAdaptive
1	5.000000	29.806958

**Figure 6-6: Measurement report of designed coil**

Under the conversation box, Figure 6-6 displayed two numerical entries for the values of current and inductance. This coil design and specification yield an inductor with a resultant value of 29.806958uH.



### 6.3 Two Coil design Primary and Secondary

The single coil that was used earlier is comparable to the primary and secondary coils, which have the same design. These both coils with air boundary is shown in Figure 6-7 and their current excitation can be seen in Figure 6-8. In this design, to check the effects of airgap between the both coil different distance set between both coils.

A multi-view depiction of a simulation environment of Ansys most likely of two coils primary and secondary respectively is shown in Figure 6-7. There are four views displayed, each providing a distinct viewpoint on the central coil item. A three-dimensional image is presented in the top-left view. It depicts a translucent box enclosing the coil, and coloured lines clearly indicate the coil's axis, indicating a spatial orientation within the simulation environment. The top-right view appears to be a top-down viewpoint that highlights the coil's location in relation to the vertical axis.

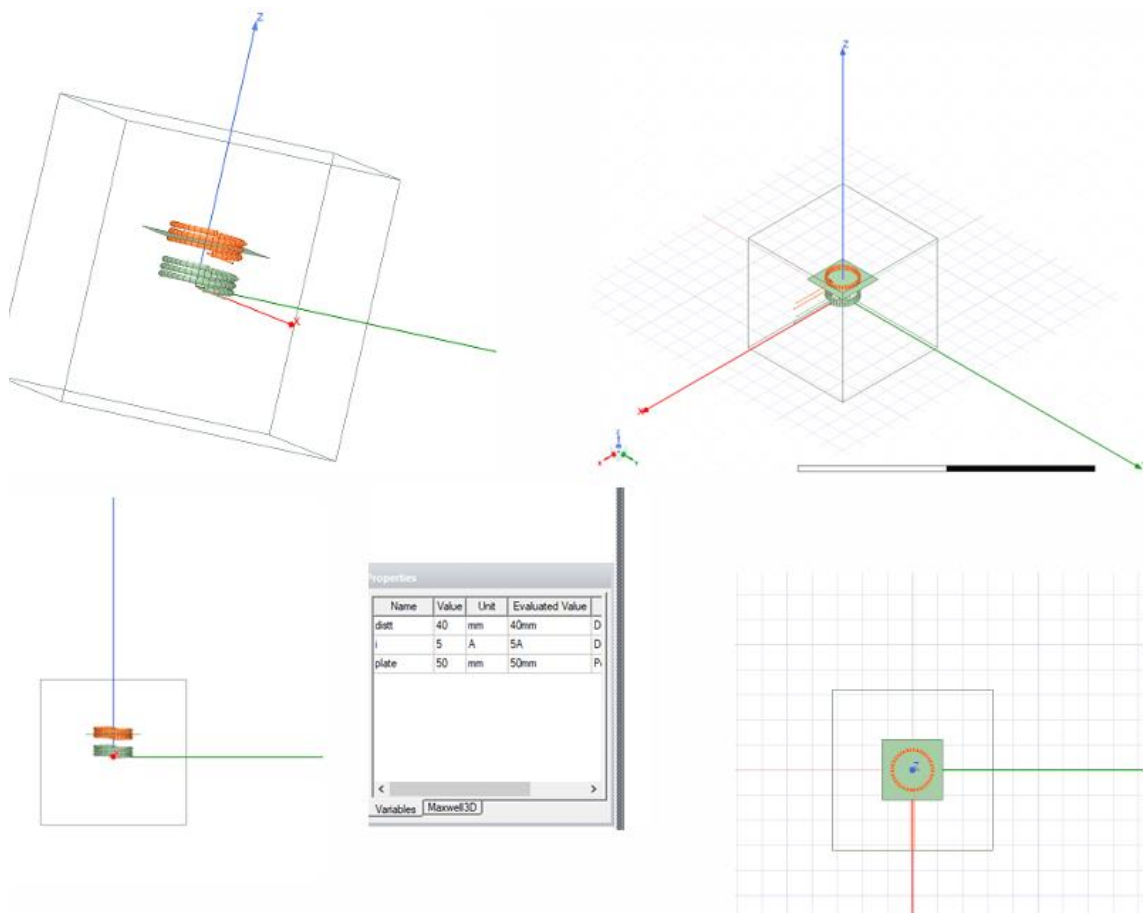
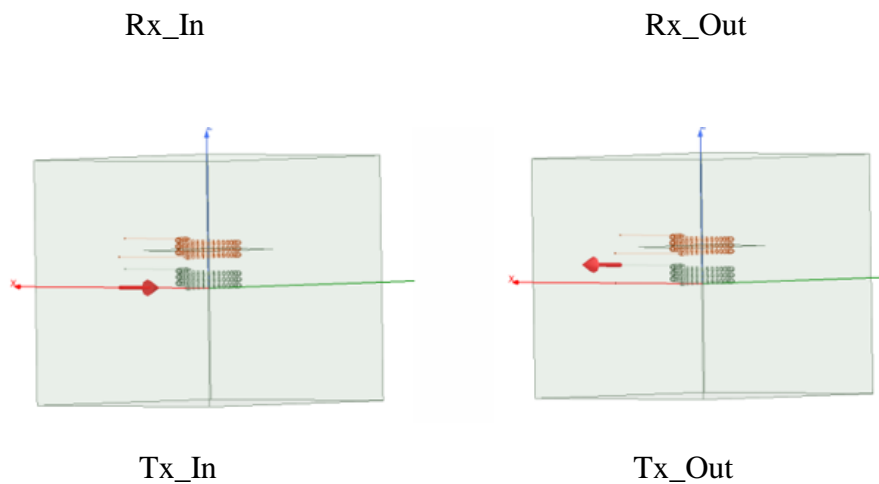


Figure 6-7: Simulation environment of Primary and secondary coil

A side view is shown in the bottom-left picture, which makes it easy to see how tall the coil is in relation to the horizontal plane. This view is accompanied by a "Variables" dialogue box that lists many parameters with numerical values, representing the coil's or the region of interest's dimensions, such as "Width," "Height," and "Depth." Finally, a frontal projection is displayed in the bottom-right view, which enables a close-up look at the coil's structure. any view's background grid serves as a point of reference for measurements, making it possible to precisely determine the coil's size and location from any viewpoint. In the middle of Figure 6-7 size of plate and the distance between two coils are mentioned which are 50mm and 40mm respectively.

The Figure 6-8 is presented four schematics, each having coils within a simulation setup that was meant to be used for examining current flow in a Wireless Power Transfer (WPT) system. Excitation arrow is also red, the red ones are for exciting the direction of the current: for "Rx\_In" and "Tx\_In" it shows that the direction of the current goes into the coils, and for "Rx\_Out" and "Tx\_Out," it shows which direction is going out.

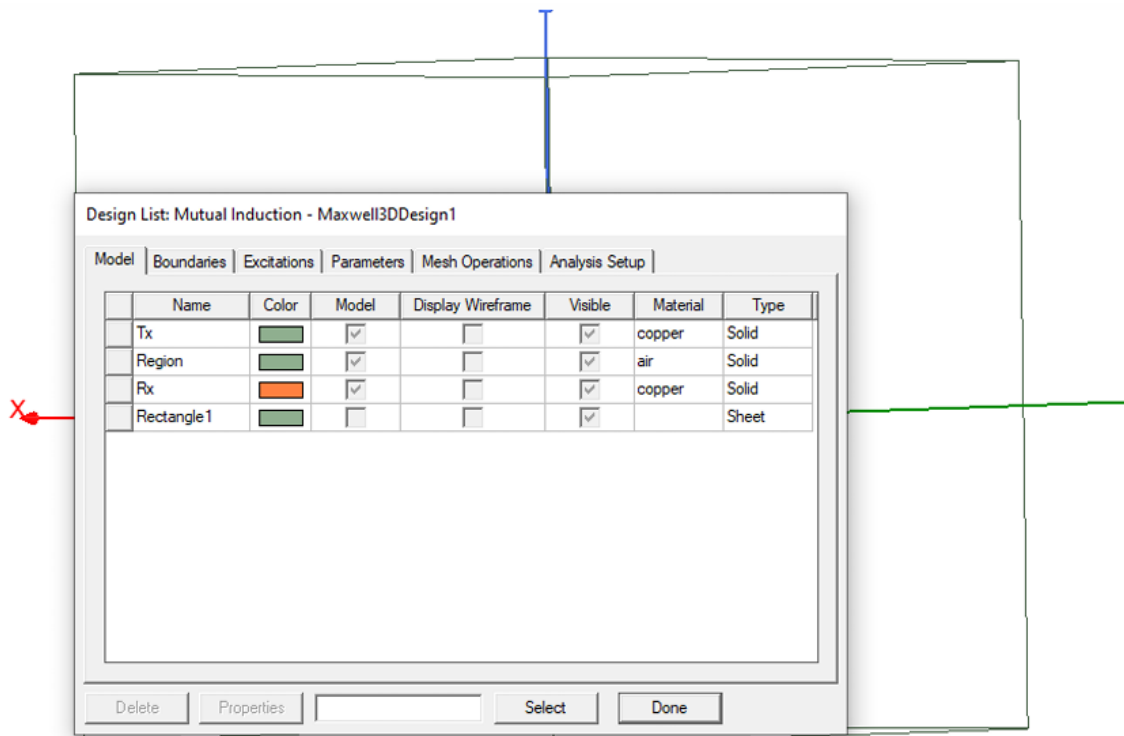


**Figure 6-8:Current Excitation diagram (In and out)**

The orange coloured coils are the primary coils, which are usually responsible for the generation of the magnetic field in the WPT system. Green shows the secondary coils, which are intended to absorb the magnetic field and set up a current in order to transfer power. The

coil placement and the direction of the current excitation are to be such that both the primary and the secondary components of the WPT system interact in a desired manner. The red, green, and blue lines represent the orthogonal axes, and the consistency of coil orientation with respect to these lines points to a regulated environment where characteristics like alignment and positioning are meticulously controlled within the simulation settings.

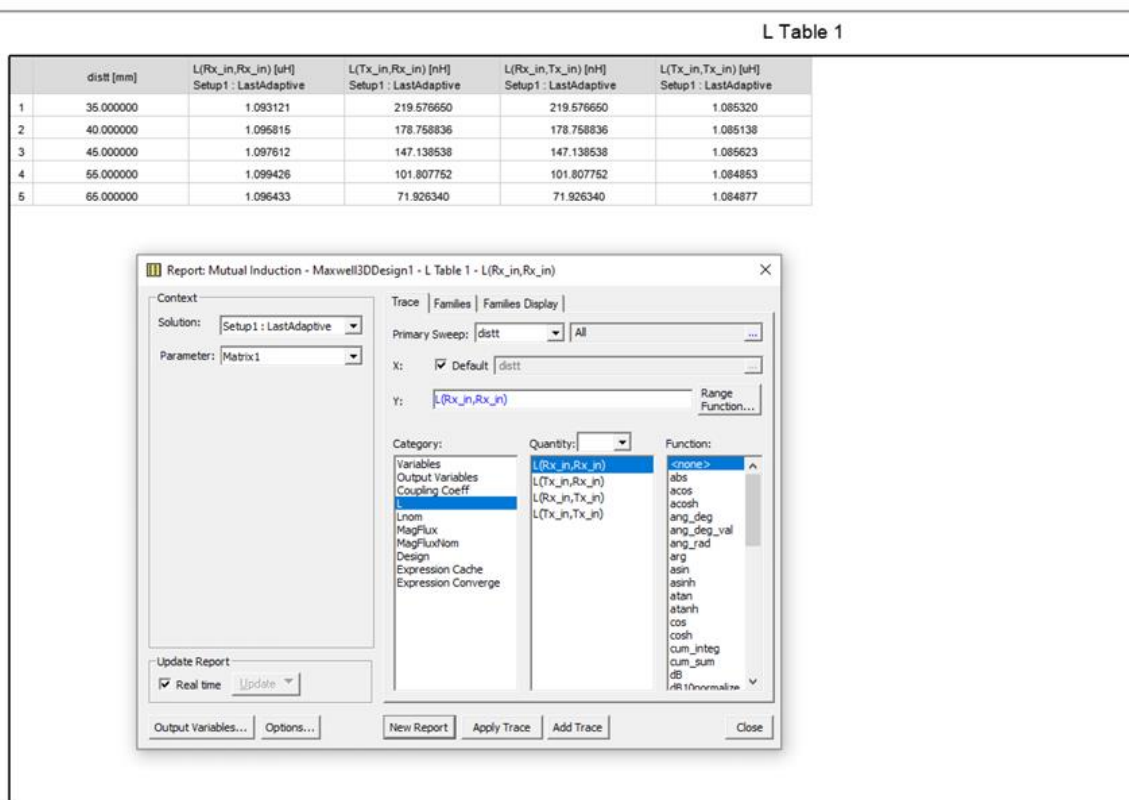
A dialogue window labelled "Design List Mutual Induction - Maxwell3DDesign1" from a Ansys software is shown in the Figure 6-9. The dialogue box has a list with a variety of things in it, including "Region," "Tx," "Rx," and "Rectangle1." Specific parameters such as model, name, colour, and visibility of the display wireframe are linked to each entry in the list. The items in the simulation environment is made visible or concealed, as indicated by the "Visible" checkboxes. The items "Tx" and "Rx" have materials listed as copper and are classified as "Solid," however the item "Region" does not have a material stated and is also classified as "Solid."



**Figure 6-9:Design List for Mutual Induction**

The Figure 6-10 show a detailed analysis gap between the primary and secondary coil and their effect on the inductance values. Many numbers are included in Figure 6-7 and it appears that

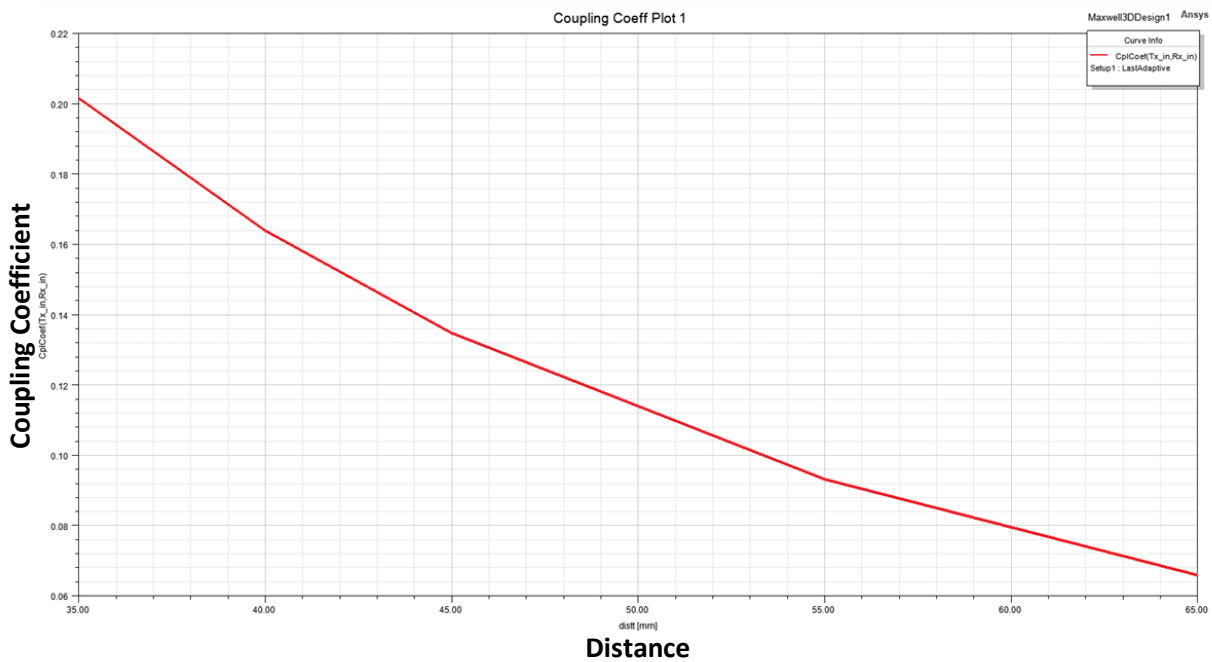
these values represent the variations in inductance in a Wireless Power Transfer (WPT) system as a function of the spacing between the primary and secondary coils. A thorough examination of the relationship between the inductance and the distance between coils is provided by the columns that display various factors, such as gap sizes and the related inductance values. The Figure 6-10 data displayed show that the connection between a WPT system's coil gap and consequent inductance. Due to the extreme sensitivity of the inductive coupling between coils to the physical separation of the components, this type of analysis is crucial for optimising the performance and efficiency of WPT systems.



**Figure 6-10: Measurements results of Designed Coils**

Figure 6-11 showed the relationship between coupling coefficient vs distance, It can be clearly seen that with increasing the distance between both coil value of this coeffect decreases which meant to be more losses or less flux is passed through these coils. The relationship between the coupling coefficient on the y-axis and the gap distance (in mm) on the x-axis is plotted as

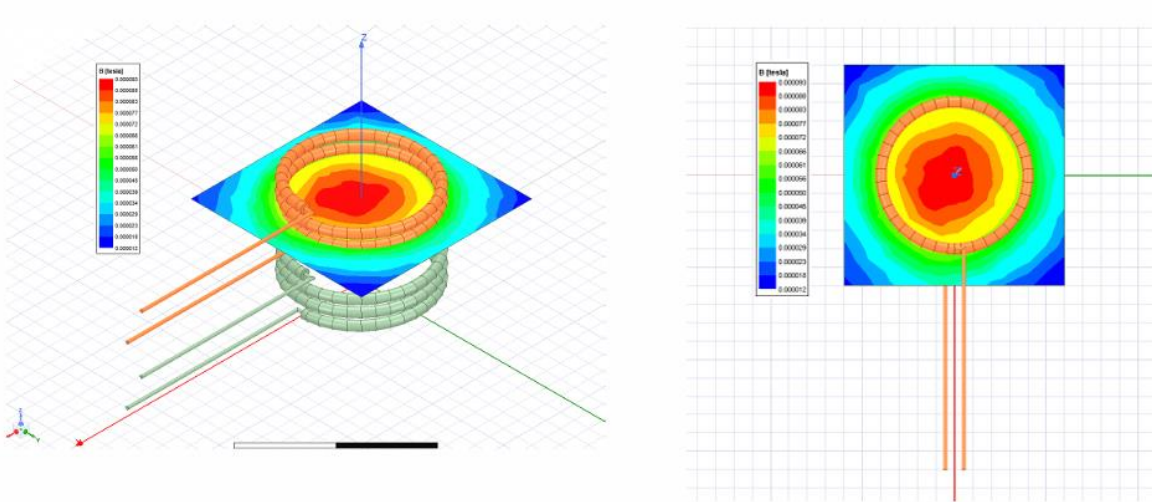
a curve on the graph. The curve shows a decreasing trend, meaning that the coupling coefficient decreases with increasing distance between the coils.



**Figure 6-11: Graphical representation results of designed coil**

This suggests that a direct correlation—wherein the inductive connection between two coils decreases with increasing distance—is a critical component in the design and optimisation of Wireless Power Transfer (WPT) systems.

Two representations of magnetic field distributions, each representing a coil in a simulation environment, are shown in the Figure 6-12.

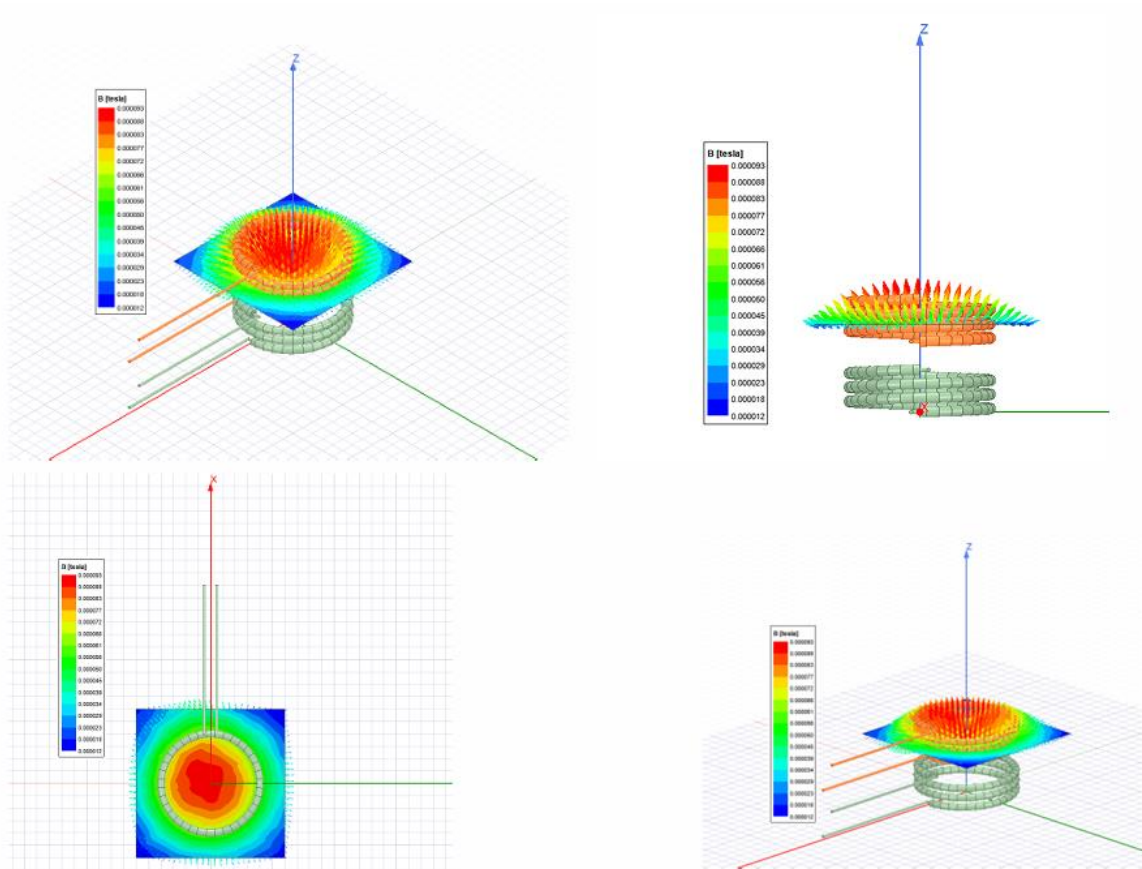


## Magnetic Fields

**Figure 6-12: Magnetic field distribution of designed coil**

The magnetic field intensity surrounding the coil is seen in a 3D perspective on the left, along with a colour gradient scale that indicates the field's strength at various spatial positions. With concentric colour bands showing the gradient of the magnetic field from the coil's centre outward, the right image offers a top-down, two-dimensional depiction of the magnetic field intensity.

The Figure 6-13 is displayed four comparable visualisations, each of which depicts the dispersion of the magnetic field around a coil, most likely in the same simulation environment.



**Figure 6-13: Different views of magnetic field representation**

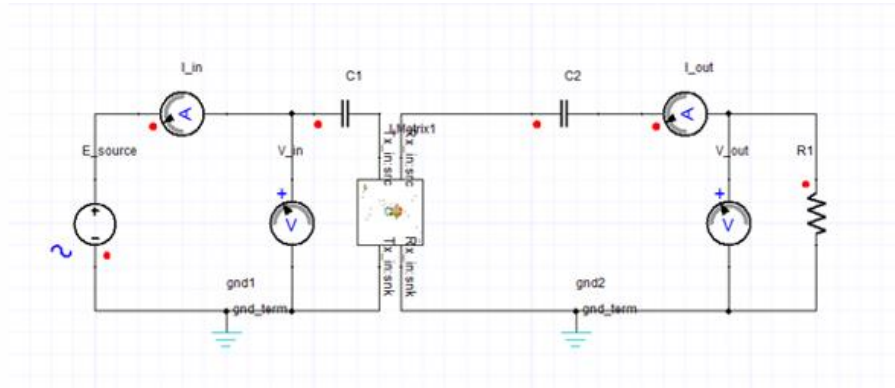
The visualisation on top left presents a three-dimensional view to the previous Figure 6-9, however the visualisations on top right and bottom left present top-down and side views, respectively, and use colour gradients to represent the field intensity. A thorough three-dimensional view of the magnetic fields is provided by the bottom right visualisation, which has returned to a three-dimensional viewpoint.

## 6.4 Simplorer/ Twin builder Design

In the Ansys software option to simulate the design coil in the circuit. The primary and secondary coils design is tested in the Simplorer to check the efficiency of the transfer power.

The Figure 6-14 showed a circuit schematic with the label "Simplorer / Twin Builder Circuit of WPT indicating that simulation software that is build and analyse electrical systems was used to produce the design. An AC voltage source, denoted by the sinusoidal symbol in the circuit diagram, is linked to an inductor. The designed primary and secondary coils in the

previous section are used in this design for wireless power transfer. Primary coil is connected in series with capacitor C1 to create a resonant circuit. The secondary side is linked to an additional resonant circuit that comprises a capacitor C2. This secondary resonant circuit's output is linked to a load resistor, R1.

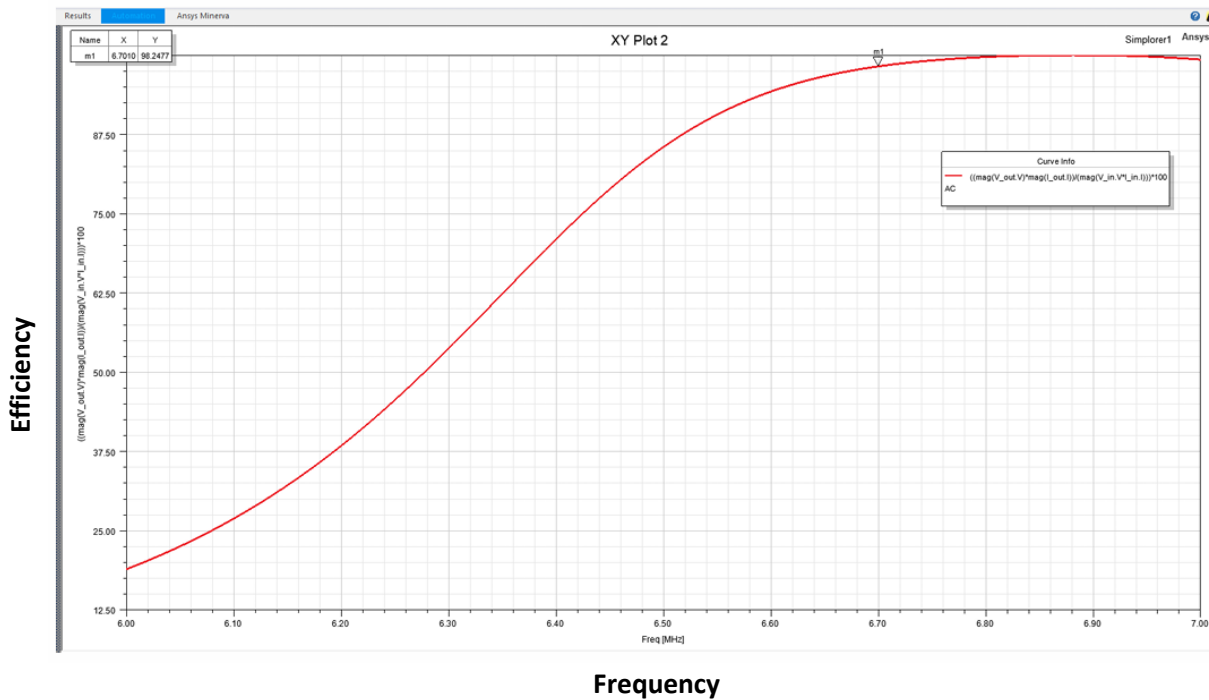


**Figure 6-14: Simplerer/ Twin Builder circuit of WPT**

Ground symbols are positioned correctly to indicate the circuit's return routes, and voltage probes are positioned across the input and output sections to monitor voltage levels. The design allows for the examination of voltage, current, and power across various components and acts as a template for simulating the behaviour of a resonant wireless power transfer system.

Figure 6-15 showed a graph that shows the analysis findings from a software interface, Simplerer. The graph, titled "XY Plot 2," shows a curve that illustrates the relationship between an output parameter efficiency (Y-axis) and frequency (on the x-axis)





**Figure 6-15:Result graph of Simplorer/ Twin builder design**

## 6.5 Summary

In this chapter the design of primary and secondary coils is presented. The Twin builder design (which is a part of Ansys software) is used to test the design of the coils. From the testing results it is found that the output parameter efficiency increases when the frequency reaches a specific point, as shown by a smooth, climbing graph.

Chapter 6 detailed work on the design of the inductor coils by simulating them in ANSYS Electronics, which places a major interest in the ability to represent properly various types of electromagnetic behaviours. The first was to construct a geometric model of the coil, and then implement the materials with accurate electromagnetic characteristics. The setup allowed making simulations as close as possible to the real conditions for coil operation.

The boundary conditions and simulation settings clearly stipulate the environment of the inductor coil and bring out the inductive operational atmosphere in the right manner. The electromagnetic field equations are solved by finite element analysis in determining the performance characteristics of the inductor coil. Several parameters were put into determination, adjusted to perfect the model and simulation results, and included the

determination of the inductance value, which is depicted in the detailed graphical user interface and diagrams.

The careful work of simulation in Chapter 6 provided a strong base for Chapter 7, where the focus turned to hardware prototyping. The elaborate simulations, most especially in dealing with different configurations of the capacitors, informed well on the detail and precision in making design decisions that are critical in the hardware phase. This capitalization of the simulations in Chapter 7 led to entry into the development of hardware, specifically in the development of coil design using Ansys software.

## **Chapter 7: Hardware Implementation**

### **7.1 Introduction**

The simulations based on the different capacitor configurations enabled to look at the performance of the system, and this informed how the subsequent decisions in the design have to be tackled with a lot of precision. The emphasis is shifted to hardware prototyping in Chapter 7, based on this analytical groundwork, with a special focus on coil designing using Ansys software. This stage is important in converting the theoretical and simulation-based findings in Chapter 6 into a workable prototype that could allow effectiveness and operational viability to be tested and validated in the realistic environment of the WPT system. The complete coil-design process of Ansys studies the impact of the simulation results to the definition of the coil characteristics, as material, size, and geometry, with target of the maximisation of the prototype's efficiency and the power transfer capability.

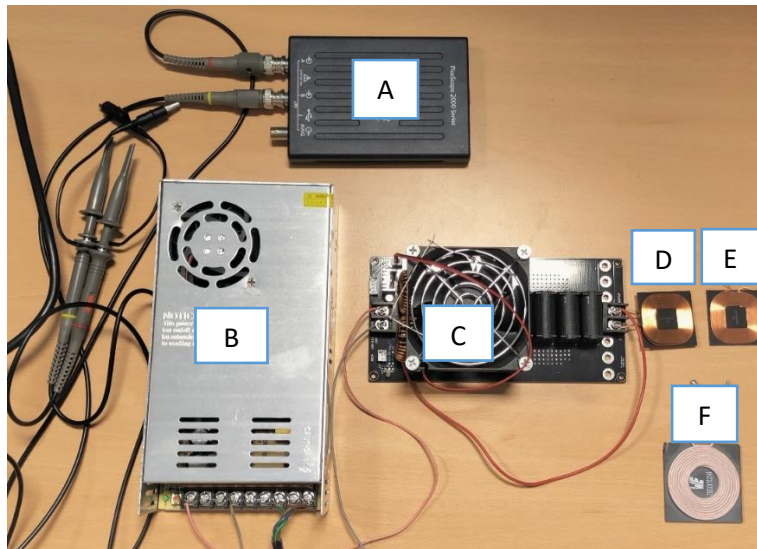
The iterative process of refining WPT system design from theoretical models and simulations to actual hardware realisation is demonstrated, bridging the gap between concept and application. This is accomplished by connecting the simulation insights from Chapter 6 with the practical hardware development efforts in Chapter 7. This results in a cohesive narrative.

### **7.2 Hardware Implementation**

Systems for wireless power transfer (WPT) allow energy to be transmitted without the need for physical connections, revolutionising the way that electrical power is distributed. The hardware elements of a WPT system, such as the power supply, inverter, primary and secondary coils, control circuitry, and measuring instruments, are covered in detail in this chapter. Hardware setup is shown in Figure 7-1. Hardware labelled is given in Table 13. Detailed description of the hardware is given in Appendix E1-E4.

**Table 13:Labelled hardware description**

A	Oscilloscope
B	Power Supply
C	High Frequency Inverter
D	Primary Coil
E	Secondary Coil with single layer
F	Secondary Coil with Double layer



**Figure 7-1:Hardware of WPT System**

### **7.3 Results**

As shown in Figure 7-1 two different configurations of coils have been used in secondary side of the system. One is 1 coil with single layer labelled E and second is 1 coil with double layers labelled F in Figure 7-1. The configuration of both coils can be seen data sheet in Appendix A1 and A2.

### 7.3.1 Test 1

In this test 1 coil with single layer is used. The value of this coil is 8uH this value of this coil is got from data sheet and can be seen in Appendix A1. The value of inverter total capacitance is 1.65uF. According to these inductor and capacitance value calculated resonance frequency is 43.805kHz which can be seen Figure 7-2 measured frequency value approximately 44.23kHz. The system is functioning at resonance frequency, as seen by the sine waves on the primary and secondary sides of the results.

The Figure 7-2 displayed the output from a PicoScope 7 T&M oscilloscope, where two sinusoidal waveforms, represented in red and blue, are captured. Time in microseconds ( $\mu\text{s}$ ) is represented on the x-axis, allowing detailed temporal analysis of the voltage oscillations, while voltage in volts (V) is shown on the y-axis, indicating the potential difference measured.

Similar characteristics are exhibited by both waveforms: they are sinusoidal with a frequency of approximately 44.23 kHz, indicating that they oscillate 44,230 times per second. An amplitude of about 50V is reached by each waveform, and they have a peak-to-peak voltage of around 100V. Notably, a peak-to-peak voltage of 131.8V is recorded by the red waveform (Channel A), an RMS (Root Mean Square) voltage of 47.48V, and voltages ranging from -69.2V to 33.07V are observed. Similarly, a peak-to-peak voltage of 131.8V is shown by the blue waveform (Channel B), but with a lower RMS voltage of 20.43V, ranging from -64.8V to 51.84V.

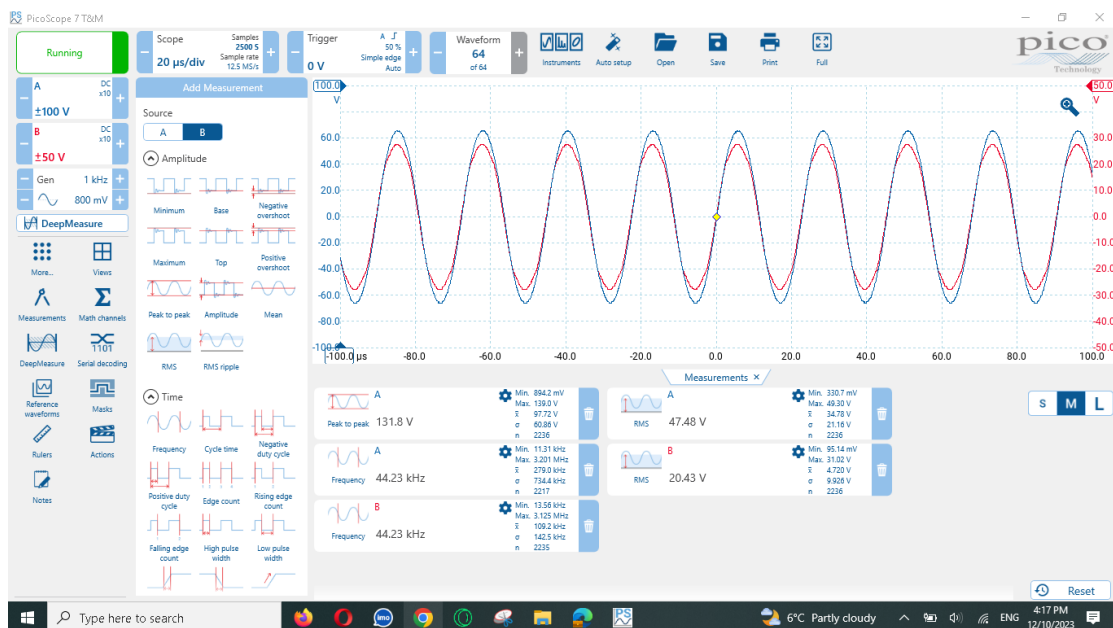


Figure 7-2: Result of Test

### 7.3.2: Test 2

In this test, 1 coil with double layer is used. The value of this coil is 19.5uH which is get from data sheet and can be seen in Appendix A2. The value of inverter total capacitance is 1.65uF. According to these inductor and capacitance value calculated resonance frequency is 28kHz which can be seen Figure 7-3 measured frequency value approximately 26.29kHz. The results demonstrate that the system is running at resonance frequency. The primary and secondary sides of the system exhibit sine waves, however the secondary side is out of phase as a result of the probe connections being inverted.

It is also noted that with increased the value of Inductor the value of resonance frequency is decreased which is correct according to the resonance equation (5.1) used in chapter 5.

The Figure 7-3 provided the output from a PicoScope 7 T&M oscilloscope, showing two sinusoidal waveforms in red and blue, captured over time and voltage on the x-axis and y-axis, respectively. These waveforms are characterized by their opposite polarity, indicating a phase relationship where each waveform is the inverse of the other, typical of systems where waveforms are phase-shifted by 180 degrees due to opposite polarity or connections. Measurements from Channel A reveal that the peak-to-peak voltage reaches up to 139.0V, and an RMS voltage of 47.90V is recorded, reflecting the power of the waveform oscillating at a frequency of 26.30 kHz. Channel B shows a similar peak-to-peak voltage of 139.0V, but with a slightly lower RMS voltage of 30.37V, and a frequency slightly below that of Channel A, at 26.29 kHz.

$$f = \frac{1}{2\pi\sqrt{LC}} \quad (5.1)$$

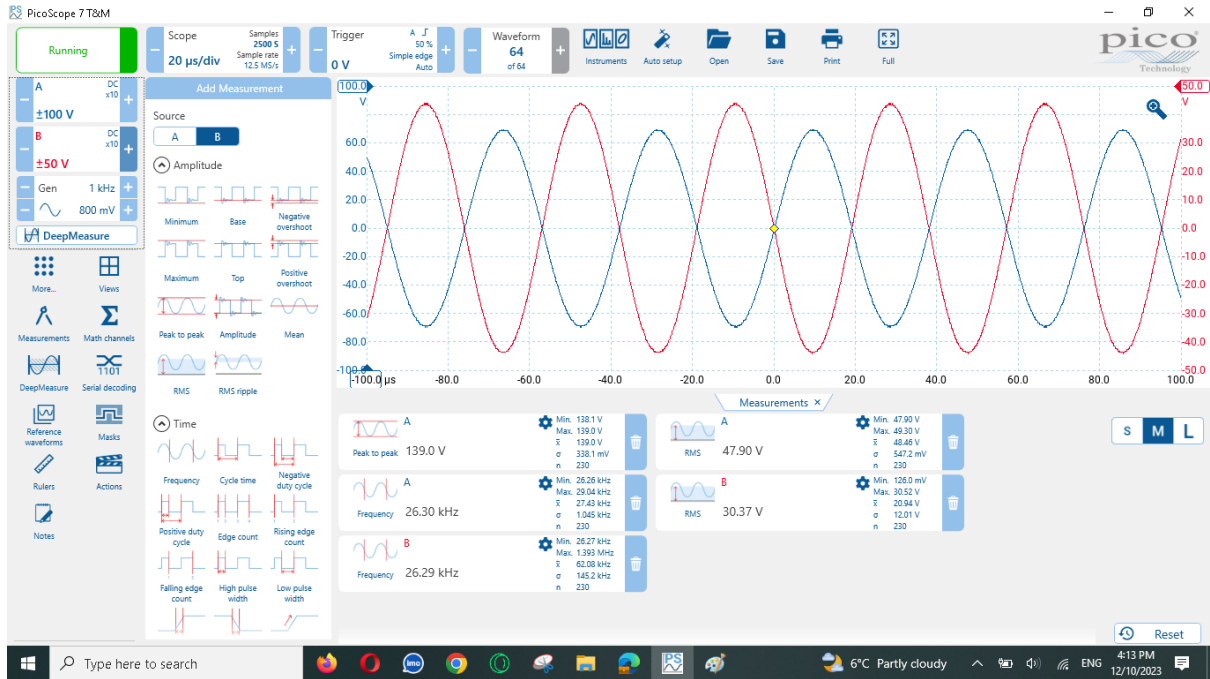


Figure 7-3:Result of Test 2

## 7.4 Comparison between Simulation and Hardware

In the simulation-based approach detailed in Chapter 5, variable and fixed capacitors were utilized to test their efficiency in a controlled environment using PSPICE and MATLAB SIMULINK. High levels of control over environmental variables and parameters were achieved, allowing for precise manipulation of the conditions under which the WPT system operated. The simulation primarily focused on optimizing the resonance frequency and coupling efficiency through variable capacitors, providing a theoretical foundation for efficient energy transfer.

Conversely, the hardware-based experiments described in Chapter 7 involved the physical construction of WPT systems using the design principles established in the simulations. The implementation in a realistic setting allowed for the observation of practical challenges, such as material imperfections and environmental interferences, which are often overlooked in simulations. This phase tested the viability of transferring theoretical knowledge into a tangible prototype, focusing particularly on coil design and the physical constraints affecting system performance.

The results from Chapter 7 showed that when applied in a real-world environment, the theoretical configurations might not perform with the same efficiency as predicted by simulations. For instance, variations in coil configurations, such as single versus double-layer coils, demonstrated different resonance frequencies and power transfer capabilities, emphasizing the complexities introduced by actual hardware implementation.

Both simulation and hardware indicated that achieving resonance frequency is critical for optimizing WPT system efficiency. However, chapter 7 provided insights into how actual hardware might slightly deviate from the expected performance due to practical limitations, like the alignment of coils and the quality of components used.

## **7.5 Summary**

In this chapter two different inductor design configuration is used. The first one is the single layer coil as the inductor value is low, a high resonant frequency is achieved. In the second design a double layer coil is used which has the opposite effect (high inductance value and low resonance frequency). Although the value of the inductance should be fixed where the capacitor is the one which will be tuned, but the reason of using the single- and double-layer inductor is to test the extreme variation required in the variable capacitor.

Moreover, this chapter mainly focuses on this important activity of converting results of a simulation into an actual physical prototype and testing it for the practicality and feasibility of the designed concept in an operational environment.



## Chapter 8: Conclusions and Future Work

### 8.1 Conclusions

In this thesis a comprehensive literature review on wireless EV charging topologies is presented. The literature review revealed some of the research gaps in this area. One of the research gaps is the need to improve the compensated circuits used in the wireless charging system. Existing compensated circuit rely on fixed LC values in order to transfer the required power from the charging station to the EV. A new variable capacitor technique is proposed so that a more flexible and more efficient compensation circuit is achieved. A detailed design is presented in chapter 3 to illustrate the visibility of this technique. The results showed that variable values of capacitance can be achieved through the control of the duty cycle of the variable capacitor semiconductor switches.

Chapter 4 shows the integration of the variable capacitor within the compensated circuit. In this chapter, a detailed design results are presented to work out the parameter values used in the WPT.

A detailed simulation work is presented in Chapter 5 where the variable capacitor is integrated in the compensation circuit. The key output from this chapter is the relationship between the resonance frequency as function of the effective capacitor value.

The design of the primary and secondary inductors is carried out using Ansys software. The effect of airgap between the coils is also investigated in chapter 6. In this chapter an efficiency of 98.2% is achieved at 6.7 MHz resonance frequency.

A hardware implementation is carried out in the lab and the results are presented in Chapter 7. Two coil configurations are used in the practical setup in order to demonstrate the possibility of the wide range capacitance variation which can be supplied by the variable capacitor circuit.

Electric vehicle (EV) wireless power transfer (WPT) system, implemented through the use of a variable capacitor technique, was used. The problems with fixed capacitors were totally developed under conventional schemes, and the possibility to tune resonance frequency on a dynamic basis had come forward, using variable capacitor technology. This modification proved to improve the performance and reliability of power transmission in an effective way. It has been shown conclusively that a laboratory setup was able to deliver 87.75% efficiency, which proves that the proposed system is practically feasible.

This is more important than the findings of the research study per se. The variable capacitor strategy is proposed as a strong solution for the long-present problem of disturbance in resonance frequency, which in most cases is caused by outer and inner interferences in classical WPT systems. The real-time tunability has drastically increased the robustness of EV charging technologies against changing operational conditions.

## **8.2 Future Recommendation Work**

The work presented in this thesis is mainly dealing with static wireless charging where the EV is charged while it is on the top of the charging unit. Dynamic wireless charging where the EV can be charged on the move needs to be investigated in more depth. There is some research work which dealt with dynamic wireless charging however the efficiency of such systems was not considered and this area needs to be investigated into more depth.

So far Lithium-Ion batteries are considered to be the main battery in EV. However, future research work is on progress on solid state batteries which offer much higher power density, safer operation, faster charging and longer life-time. A detailed study on how the wireless charging systems can be used in solid state batteries is another needed area of future research.

One of the limitations of the WPT is the airgap distance between the charging coil and the EV coil. Varying the resonant frequency in order to reduce the effective airgap has also some limitations. Research work could be carried out for different mechanism where the two coils can have dynamic adjustment in order to reduce the wasted energy during the charging process.

Another future work could be carried out on the alignment between the two coils particularly when a resonant technique is used in order to transfer the maximum energy to the EV. There are many studies on the alignment issue but they are mainly focused on the capacitive wireless charging.

## References

- [1] S. A. Q. Mohammed and J.-W. Jung, "A Comprehensive State-of-the-Art Review of Wired/Wireless Charging Technologies for Battery Electric Vehicles: Classification/Common Topologies/Future Research Issues," *IEEE Access*, vol. 9, pp. 19572–19585, 2021, doi: <https://doi.org/10.1109/access.2021.3055027>.
- [2] Q. Deng *et al.*, "Wired/Wireless Hybrid Charging System for Electrical Vehicles With Minimum Rated Power Requirement for DC Module," *IEEE Transactions on Vehicular Technology*, vol. 69, no. 10, pp. 10889–10898, Oct. 2020, doi: <https://doi.org/10.1109/TVT.2020.3019787>.
- [3] S. S. G. Acharige, M. E. Haque, M. T. Arif, N. Hosseinzadeh, K. N. Hasan and A. M. T. Oo, "Review of electric vehicle charging technologies standards architectures and converter configurations," *IEEE Access*, vol. 11, 2023.
- [4] O. US EPA, "Why We Need to Decarbonize Transportation," [www.epa.gov](http://www.epa.gov), Feb. 09, 2023. <https://www.epa.gov/greenvehicles/why-we-need-decarbonize-transportation> (accessed Jan. 18, 2024).
- [5] X. Feng, Y. Pan, X. He, L. Wang, and M. Ouyang, "Detecting the internal short circuit in large-format lithium-ion battery using model-based fault-diagnosis algorithm," *Journal of Energy Storage*, vol. 18, pp. 26–39, Aug. 2018, doi: <https://doi.org/10.1016/j.est.2018.04.020>.
- [6] B. Mao, C. Zhao, H. Chen, Q. Wang, and J. Sun, "Experimental and modeling analysis of jet flow and fire dynamics of 18650-type lithium-ion battery," *Applied Energy*, vol. 281, p. 116054, Jan. 2021, doi: <https://doi.org/10.1016/j.apenergy.2020.116054>.
- [7] X. Feng *et al.*, "Investigating the thermal runaway mechanisms of lithium-ion batteries based on thermal analysis database," *Applied Energy*, vol. 246, pp. 53–64, Jul. 2019, doi: <https://doi.org/10.1016/j.apenergy.2019.04.009>.
- [8] G. Zhang, X. Wei, X. Tang, J. Zhu, S. Chen, and H. Dai, "Internal short circuit

mechanisms, experimental approaches and detection methods of lithium-ion batteries for electric vehicles: A review,” *Renewable and Sustainable Energy Reviews*, vol. 141, p. 110790, May 2021, doi: <https://doi.org/10.1016/j.rser.2021.110790>.

[9] T. Yuvaraj, “A Comprehensive Review and Analysis of the Allocation of Electric Vehicle Charging Stations in Distribution Networks | IEEE Journals & Magazine | IEEE Xplore,” *ieeexplore.ieee.org*, Jan. 03, 2024. <https://ieeexplore.ieee.org/document/10380227>

[10] X. Zhu *et al.*, “Overcharge investigation of large format lithium-ion pouch cells with Li(Ni<sub>0.6</sub>Co<sub>0.2</sub>Mn<sub>0.2</sub>)O<sub>2</sub> cathode for electric vehicles: Thermal runaway features and safety management method,” vol. 169, pp. 868–880, Feb. 2019, doi: <https://doi.org/10.1016/j.energy.2018.12.041>.

[11] Zhenpo Wang, “Intelligent decision support platform of new energy vehicles | BIAI Journals & Magazine | IEEE Xplore,” *ieeexplore.ieee.org*, Aug. 22, 2022. <https://ieeexplore.ieee.org/document/9883004>

[12] Y. Chen, H. Zhang, S.-J. Park, and D.-H. Kim, “A Switching Hybrid LCC-S Compensation Topology for Constant Current/Voltage EV Wireless Charging,” *IEEE Access*, vol. 7, pp. 133924–133935, 2019, doi: <https://doi.org/10.1109/ACCESS.2019.2941652>.

[13] X. Mou, D. T. Gladwin, R. Zhao, H. Sun, and Z. Yang, “Coil Design for Wireless Vehicle-to-Vehicle Charging Systems,” *IEEE Access*, vol. 8, pp. 172723–172733, 2020, doi: <https://doi.org/10.1109/ACCESS.2020.3025787>.

[14] S. Sharma, A. K. Panwar, and M. M. Tripathi, “Storage technologies for electric vehicles,” *Journal of Traffic and Transportation Engineering (English Edition)*, vol. 7, no. 3, Jun. 2020, doi: <https://doi.org/10.1016/j.jtte.2020.04.004>.

[15] Alperen Mustafa Colak and Erdal Irmak, “Electric Vehicle Advancements, Barriers, and Potential: A Comprehensive Review,” *Electric Power Components and Systems*, pp. 1–33, Jul. 2023, doi: <https://doi.org/10.1080/15325008.2023.2239238>.

- [16] A. Ahmad, Z. A. Khan, M. Saad Alam, and S. Khateeb, "A Review of the Electric Vehicle Charging Techniques, Standards, Progression and Evolution of EV Technologies in Germany," *Smart Science*, vol. 6, no. 1, pp. 36–53, Dec. 2017, doi: <https://doi.org/10.1080/23080477.2017.1420132>.
- [17] M. Ashfaq, O. Butt, J. Selvaraj, and N. Rahim, "Assessment of electric vehicle charging infrastructure and its impact on the electric grid: A review," *International Journal of Green Energy*, vol. 18, no. 7, pp. 657–686, Mar. 2021, doi: <https://doi.org/10.1080/15435075.2021.1875471>.
- [18] Ilhami Colak, "A Brief Overview and Key Points in Electric Vehicle Charging Systems | IEEE Conference Publication | IEEE Xplore," *ieeexplore.ieee.org*, Dec. 15, 2023. <https://ieeexplore.ieee.org/document/10349473>
- [19] C. Panchal, S. Stegen, and J. Lu, "Review of static and dynamic wireless electric vehicle charging system," *Engineering Science and Technology, an International Journal*, vol. 21, no. 5, pp. 922–937, Oct. 2018, doi: <https://doi.org/10.1016/j.jestch.2018.06.015>.
- [20] S. Lukic and Z. Pantic, "Cutting the Cord: Static and Dynamic Inductive Wireless Charging of Electric Vehicles," *IEEE Electrification Magazine*, vol. 1, no. 1, pp. 57–64, Sep. 2013, doi: <https://doi.org/10.1109/mele.2013.2273228>.
- [21] S. Moon, B.-C. Kim, S.-Y. Cho, C.-H. Ahn, and G.-W. Moon, "Analysis and Design of a Wireless Power Transfer System With an Intermediate Coil for High Efficiency," *IEEE Transactions on Industrial Electronics*, vol. 61, no. 11, pp. 5861–5870, Nov. 2014, doi: <https://doi.org/10.1109/tie.2014.2301762>.
- [22] F. van der Pijl, P. Bauer, and M. Castilla, "Control Method for Wireless Inductive Energy Transfer Systems With Relatively Large Air Gap," *IEEE Transactions on Industrial Electronics*, vol. 60, no. 1, pp. 382–390, Jan. 2013, doi: <https://doi.org/10.1109/TIE.2011.2163917>.
- [23] MS SIKANDAR, "Review of Wireless Charging of EV | IEEE Conference

Publication | IEEE Xplore,” *ieeexplore.ieee.org*, Oct. 18, 2022.

<https://ieeexplore.ieee.org/document/9917793> (accessed Feb. 11, 2024).

[24] J. L. Villa, J. Sallan, J. F. Sanz Osorio, and A. Llombart, “High-Misalignment Tolerant Compensation Topology For ICPT Systems,” *IEEE Transactions on Industrial Electronics*, vol. 59, no. 2, pp. 945–951, Feb. 2012, doi: <https://doi.org/10.1109/tie.2011.2161055>.

[25] K. Kalwar, S. Mekhilef, M. Seyedmahmoudian, and B. Horan, “Coil Design for High Misalignment Tolerant Inductive Power Transfer System for EV Charging,” *Energies*, vol. 9, no. 11, p. 937, Nov. 2016, doi: <https://doi.org/10.3390/en9110937>.

[26] K. A. Kalwar, M. Aamir, and S. Mekhilef, “Inductively coupled power transfer (ICPT) for electric vehicle charging – A review,” *Renewable and Sustainable Energy Reviews*, vol. 47, pp. 462–475, Jul. 2015, doi: <https://doi.org/10.1016/j.rser.2015.03.040>.

[27] S. Y. R. Hui, W. Zhong, and C. K. Lee, “A Critical Review of Recent Progress in Mid-Range Wireless Power Transfer,” *IEEE Transactions on Power Electronics*, vol. 29, no. 9, pp. 4500–4511, Sep. 2014, doi: <https://doi.org/10.1109/TPEL.2013.2249670>.

[28] T. W. Ching and Y. S. Wong, “Review of wireless charging technologies for electric vehicles,” *IEEE Xplore*, Dec. 01, 2013. <https://ieeexplore.ieee.org/document/6828235> (accessed Jul. 05, 2021).

[29] C. Liu, A. P. Hu, B. Wang, and N.-K. C. Nair, “A Capacitively Coupled Contactless Matrix Charging Platform With Soft Switched Transformer Control,” *IEEE Transactions on Industrial Electronics*, vol. 60, no. 1, pp. 249–260, Jan. 2013, doi: <https://doi.org/10.1109/TIE.2011.2172174>.

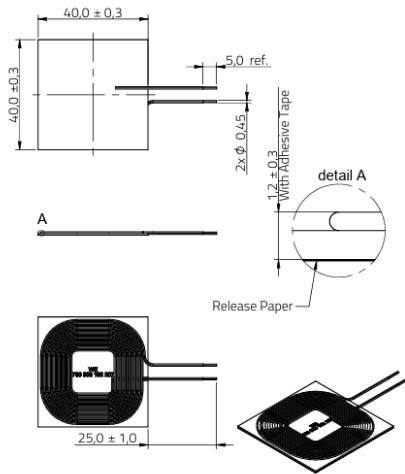
[30] A. Hu, L. Xiang, and G. Tang, “Vibration Signal Analysis Based on Hilbert-Huang Transform,” *IEEE Xplore*, Oct. 01, 2008. <https://ieeexplore.ieee.org/document/4667516> (accessed Jul. 05, 2021).

- [31] J. Kim and F. Bien, “Electric field coupling technique of wireless power transfer for electric vehicles,” *IEEE Xplore*, Apr. 01, 2013. <https://ieeexplore.ieee.org/document/6584453> (accessed Jul. 05, 2021).
- [32] F. Musavi and W. Eberle, “Overview of wireless power transfer technologies for electric vehicle battery charging,” *IET Power Electronics*, vol. 7, no. 1, pp. 60–66, Jan. 2014, doi: <https://doi.org/10.1049/iet-pel.2013.0047>.
- [33] Masood Rehman, “A Review of Inductive Power Transfer: Emphasis on Performance Parameters, Compensation Topologies and Coil Design Aspects | IEEE Journals & Magazine | IEEE Xplore,” *ieeexplore.ieee.org*, Dec. 18, 2023. <https://ieeexplore.ieee.org/document/10363190> (accessed Feb. 06, 2024).
- [34] Siqi Li and C. C. Mi, “Wireless Power Transfer for Electric Vehicle Applications,” *IEEE Journal of Emerging and Selected Topics in Power Electronics*, vol. 3, no. 1, pp. 4–17, Mar. 2015, doi: <https://doi.org/10.1109/jestpe.2014.2319453>.
- [35] G. Buja, M. Bertoluzzo, and K. N. Mude, “Design and Experimentation of WPT Charger for Electric City Car,” *IEEE Transactions on Industrial Electronics*, vol. 62, no. 12, pp. 7436–7447, Dec. 2015, doi: <https://doi.org/10.1109/tie.2015.2455524>.
- [36] M. Zamani, M. Nagrial, J. Rizk, and A. Hellany, “A review of inductive power transfer for electric vehicles,” *IEEE Xplore*, Nov. 01, 2019. <https://ieeexplore.ieee.org/document/8956971>

# Appendixes

## Appendix A1: Data Sheets of Coil used In Primary and Secondary with Single layer.

Dimensions: [mm]



Scale - 1:1,5

Recommended Hole Pattern: [mm]



Scale - 2:1

Schematic:



Electrical Properties:

Properties	Test conditions	Value	Unit	Tol.
Inductance	L 125 kHz/ 10 mA	8	µH	±10%
Rated Current	I <sub>r</sub> ΔT = 40 K	5	A	max.
Q-Factor	Q 125 kHz/ 10 mA	30		typ.
Power Capability	P V <sub>DC</sub> = 20 V	80	W	typ.
DC Resistance	R <sub>DC</sub> @ 20 °C	60	mΩ	typ.
DC Resistance	R <sub>DC</sub> @ 20 °C	80	mΩ	max.
Self Resonant Frequency	f <sub>res</sub>	16	MHz	typ.

Certification:

RoHS Approval	Compliant [2011/65/EU&2015/863]
REACH Approval	Conform or declared [IEC1907/2006]
Halogen Free	Conform [JEDEC JS709B]
Halogen Free	Conform [IEC 61249-2-21]


General Information:

Operating Temperature	-20 up to +105 °C
Storage Conditions (in original packaging)	< 40 °C ; < 75 % RH
Moisture Sensitivity Level (MSL)	1
Test conditions of Electrical Properties: +20 °C, 33 % RH if not specified differently	

	ORDER CODE CMe 002.001	REVISION 002.001	DATE (YYYY-MM-DD) 2022-11-03	GENERAL DRAWING DIN ISO 2768-1m	REFLECTION SMT 100	
WURTH ELEKTRONIK MORE THAN YOU EXPECT	WE-WPCC Wireless Power Transfer Receiver Coil		ORDER CODE 760308102207			
WURTH Elektronik GmbH & Co. KG DMC & Inductive Solutions Max-Eyth-Str. 1 74638 Wismarburg Germany Tel. +49 (0) 79 42 945 - 0 www.wer.com info@wer-online.com	DATE PUBLISHED 40 x 40 x 1.2 mm	BUSINESS UNIT eSOS	STATUS Valid	PAGE 1/6		

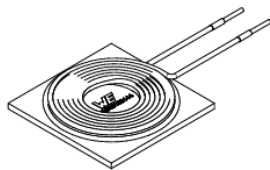
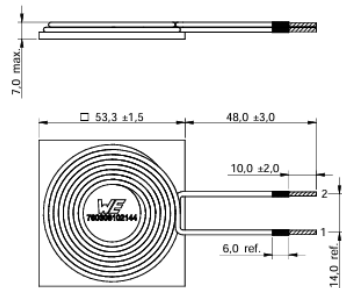


## Appendix A2: Specification of Coil used In Primary and Secondary with Single layer.

Specifications <span style="float: right;">^</span>		
Product Attribute	Attribute Value	Select Attribute
Manufacturer:	Würth Elektronik	<input type="checkbox"/>
Product Category:	Wireless Charging Coils	
RoHS:	 <a href="#">Details</a>	
Series:	<a href="#">WE-WPCC</a>	<input type="checkbox"/>
Inductance:	8 uH	<input type="checkbox"/>
Function:	Receiver	<input type="checkbox"/>
Maximum DC Resistance:	80 mOhms	<input type="checkbox"/>
Tolerance:	10 %	<input type="checkbox"/>
Minimum Operating Temperature:	- 20 C	<input type="checkbox"/>
Maximum Operating Temperature:	+ 105 C	<input type="checkbox"/>
Q Minimum:	30	<input type="checkbox"/>
Number of Coils:	1 Coil, 1 Layer	<input type="checkbox"/>
Length:	40 mm	<input type="checkbox"/>
Width:	40 mm	<input type="checkbox"/>
Height:	1.2 mm	<input type="checkbox"/>
Packaging:	Bulk	<input type="checkbox"/>
Brand:	Würth Elektronik	
Product Type:	Wireless Charging Coils	
Self Resonant Frequency:	16 MHz	
<a href="#">Factory Pack Quantity:</a>	56	
Subcategory:	Wireless Charging	
Unit Weight:	6 g	

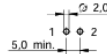
# Appendix A3: Data Sheets of Coil used In Primary and Secondary with Double layer.

## Dimensions: [mm]



Scale - 1:1.5

## Recommended Land Pattern: [mm]



Scale - 1:1.5

## Schematic:



## Electrical Properties:

Properties	Test conditions	Value	Unit	Tol.
Inductance	125 kHz/ 10 mA	L	19.5	μH ±10%
Q-Factor	125 kHz/ 10 mA	Q	220	typ.
Rated Current	ΔT = 40 K	I <sub>R</sub>	9.5	A max.
Saturation Current		I <sub>SAT</sub>	20	A typ.
DC Resistance	@ 20 °C	R <sub>DC</sub>	35	mΩ typ.
DC Resistance	@ 20 °C	R <sub>DC</sub>	45	mΩ max.
Self Resonant Frequency		f <sub>SRF</sub>	5	MHz

## General Information:

It is recommended that the temperature of the component does not exceed +105°C under worst case conditions

Operating Temperature	-20 °C up to +105 °C
Storage Temperature (in original packaging)	-20 °C up to +60 °C
Test conditions of Electrical Properties: +20°C, 33% RH if not specified differently	


Würth Elektronik eGos GmbH & Co. KG  
 EMC & Inductive Solutions  
 Max Eyth-Str. 1  
 74300 Heidenberg  
 Germany  
 Tel. +49 (0) 7142 945-0  
 www.we-online.com  
 eGos@we-online.com



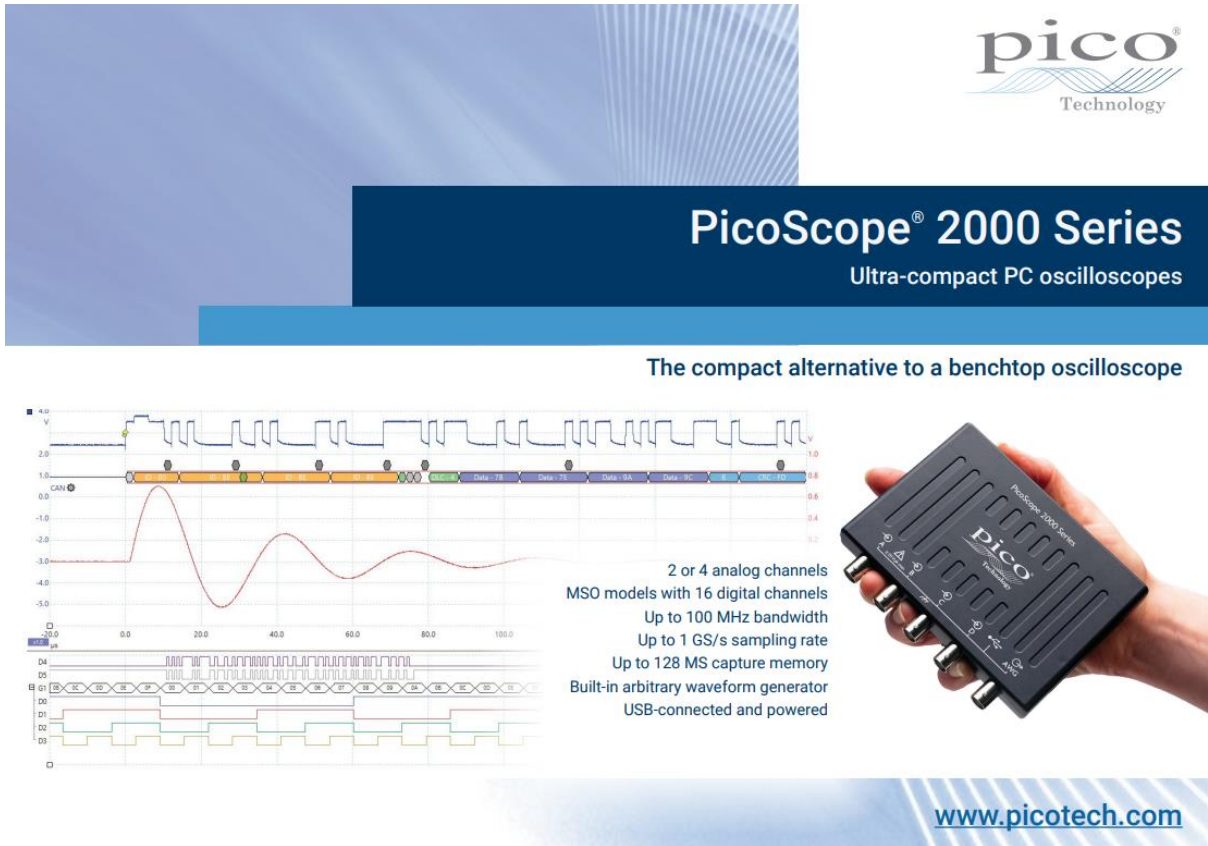
MARKET	INDIC	GENERAL STANDARDS	REVISION	
Ki68	CS2	DNV ISO 27001:18		
DESCRIPTION			ORDER CODE	
<b>WE-WPCC Wireless Power Charging Transmitter Coil</b>			<b>760308102144</b>	
ISS	REVISION	STATUS	DATE (YY-MM-DD)	CONTACT (NAME)
5353	001.001	Valid	2017-04-24	eGos
				FILE
				1/6

This electronic component has been designed and developed for usage in general electronic equipment only. This product is not authorized for use in equipment where a higher safety standard and reliability standard is especially required or where a failure of the product is reasonably expected to cause severe personal injury or death, unless the parties have concluded an agreement specifically governing such use. Moreover Würth Elektronik eGos GmbH & CoKG products are neither designed nor intended for use in areas such as military, aerospace, aviation, nuclear control, submarine, transportation, automotive control, train control, air-traffic control, telecommunication, disaster prevention, medical, public information network etc.. Würth Elektronik eGos GmbH & CoKG shall be informed about the extent of such usage before the device is placed in circulation, sufficient liability-responsible checks for safety.

## Appendix A4: Specification of Coil used In Primary and Secondary with Double layer.

Specifications <span style="float: right;">^</span>		
Product Attribute	Attribute Value	Select Attribute
Manufacturer:	Wurth Elektronik	<input type="checkbox"/>
Product Category:	Wireless Charging Coils	
RoHS:	 <a href="#">Details</a>	
Series:	<a href="#">WE-WPCC</a>	<input type="checkbox"/>
Inductance:	19.5 uH	<input type="checkbox"/>
Function:	Transmitter	<input type="checkbox"/>
Maximum DC Resistance:	45 mOhms	<input type="checkbox"/>
Tolerance:	10 %	<input type="checkbox"/>
Minimum Operating Temperature:	- 20 C	<input type="checkbox"/>
Maximum Operating Temperature:	+ 105 C	<input type="checkbox"/>
Number of Coils:	1 Coil, 2 Layer	<input type="checkbox"/>
Length:	53.3 mm	<input type="checkbox"/>
Width:	53.3 mm	<input type="checkbox"/>
Height:	7 mm	<input type="checkbox"/>
Packaging:	Bulk	<input type="checkbox"/>
Brand:	Wurth Elektronik	
Product Type:	Wireless Charging Coils	
Self Resonant Frequency:	5 MHz	
Factory Pack Quantity:	14	
Subcategory:	Wireless Charging	
Unit Weight:	60 g	

## Appendix A5: Data Sheets of Oscilloscope used in Hardware




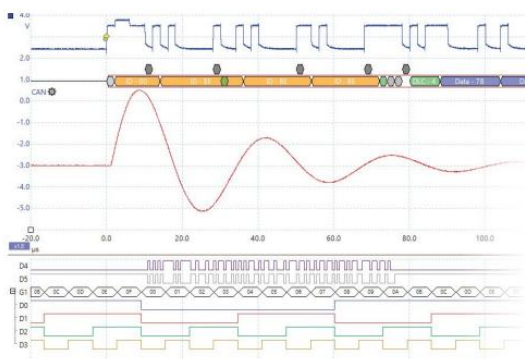
The advertisement features a blue gradient background. At the top right is the Pico Technology logo. Below it, a dark blue banner contains the text 'PicoScope® 2000 Series' and 'Ultra-compact PC oscilloscopes'. Underneath this is the tagline 'The compact alternative to a benchtop oscilloscope'. On the left, a screenshot of the PicoScope software interface shows multiple waveforms: a square wave at the top, a sine wave in the middle, and a digital bus waveform at the bottom. On the right, a hand holds the physical PicoScope 2000 Series device, which is a small, black, rectangular unit with several connectors on the front. A list of features is positioned between the software screenshot and the device. At the bottom right, the website 'www.picotech.com' is displayed.

**pico**  
Technology

### PicoScope® 2000 Series

Ultra-compact PC oscilloscopes

The compact alternative to a benchtop oscilloscope



- 2 or 4 analog channels
- MSO models with 16 digital channels
- Up to 100 MHz bandwidth
- Up to 1 GS/s sampling rate
- Up to 128 MS capture memory
- Built-in arbitrary waveform generator
- USB-connected and powered

[www.picotech.com](http://www.picotech.com)

## Quick product selector

### 2-channel oscilloscopes

Model
Bandwidth
Maximum sampling rate
Capture memory
AWG bandwidth

VIEW your waveform with a low-cost USB-powered and connected oscilloscope.

All standard PicoScope features are included: automatic measurements, serial decoding, persistence displays, mask limit testing, spectrum analysis, arbitrary waveform generator and more.

PicoScope 2204A	PicoScope 2205A
10 MHz	25 MHz
100 MS/s	200 MS/s
8 kS	16 kS
100 kHz	100 kHz

ANALYZE your waveform with a high-performance USB-powered and connected oscilloscope.

Deep memory allows you to capture over long time periods at high sampling rates. You can then zoom in on your data without having to recapture. This is essential when you need to analyze one-off events with detailed timing resolution.

The arbitrary waveform generator can store complex waveforms in its large memory buffer, allowing you to test your design with realistic inputs.

PicoScope 2206B	PicoScope 2207B	PicoScope 2208B
50 MHz	70 MHz	100 MHz
500 MS/s	1 GS/s	1 GS/s
32 MS	64 MS	128 MS
1 MHz	1 MHz	1 MHz

### 4-channel oscilloscopes

Model
Bandwidth
Maximum sampling rate
Capture memory
AWG bandwidth

PicoScope 2405A
25 MHz
500 MS/s
48 kS
1 MHz

PicoScope 2406B	PicoScope 2407B	PicoScope 2408B
50 MHz	70 MHz	100 MHz
1 GS/s	1 GS/s	1 GS/s
32 MS	64 MS	128 MS
1 MHz	1 MHz	1 MHz

### Mixed-signal oscilloscopes

2 analog + 16 digital inputs

Model
Bandwidth
Maximum sampling rate
Capture memory
AWG bandwidth

PicoScope 2205A MSO
25 MHz
500 MS/s
48 kS
1 MHz

PicoScope 2206B MSO	PicoScope 2207B MSO	PicoScope 2208B MSO
50 MHz	70 MHz	100 MHz
1 GS/s	1 GS/s	1 GS/s
32 MS	64 MS	128 MS
1 MHz	1 MHz	1 MHz

PicoScope 2000 Series oscilloscopes

# Appendix B1: Excel Data generated by using Variable capacitor equation 9 chapter 3.

B	C	D	E	F	G	H	I	J	K	L	M	N	O
d	C1	C2	Ceff(N=0.5)	Ceff(N=1)	Ceff(N=2)	Ceff(N=3)	Ceff(N=4)	Ceff(N=5)	Ceff(N=6)	Ceff(N=7)	Ceff(N=8)	Ceff(N=9)	Ceff(N=10)
0	3.20E-08	2.40E-08	2.4E-08	2.4E-08	2.4E-08	2.4E-08	0.000000024	2.4E-08	2.40E-08	2.40E-08	2.40E-08	2.40E-08	2.40E-08
0.01	3.20E-08	2.40E-08	2.4486E-08	2.4485E-08	2.4482E-08	2.448E-08	2.44773E-08	2.4475E-08	2.45E-08	2.45E-08	2.45E-08	2.45E-08	2.45E-08
0.02	3.20E-08	2.40E-08	2.4984E-08	2.4979E-08	2.4969E-08	2.4958E-08	2.4948E-08	2.4938E-08	2.49E-08	2.49E-08	2.49E-08	2.49E-08	2.49E-08
0.03	3.20E-08	2.40E-08	2.5495E-08	2.5483E-08	2.5459E-08	2.5435E-08	2.54103E-08	2.5386E-08	2.54E-08	2.53E-08	2.53E-08	2.53E-08	2.53E-08
0.04	3.20E-08	2.40E-08	2.6019E-08	2.5997E-08	2.5952E-08	2.5907E-08	2.58621E-08	2.5818E-08	2.58E-08	2.57E-08	2.57E-08	2.56E-08	2.56E-08
0.05	3.20E-08	2.40E-08	2.6556E-08	2.6519E-08	2.6446E-08	2.6374E-08	2.63014E-08	2.623E-08	2.62E-08	2.61E-08	2.60E-08	2.59E-08	2.59E-08
0.06	3.20E-08	2.40E-08	2.7106E-08	2.7051E-08	2.6942E-08	2.6834E-08	2.67261E-08	2.6619E-08	2.65E-08	2.64E-08	2.63E-08	2.62E-08	2.61E-08
0.07	3.20E-08	2.40E-08	2.767E-08	2.7593E-08	2.7438E-08	2.7285E-08	2.7134E-08	2.6984E-08	2.68E-08	2.67E-08	2.65E-08	2.64E-08	2.63E-08
0.08	3.20E-08	2.40E-08	2.8249E-08	2.8143E-08	2.7933E-08	2.7726E-08	2.75229E-08	2.7322E-08	2.71E-08	2.69E-08	2.67E-08	2.65E-08	2.64E-08
0.09	3.20E-08	2.40E-08	2.8841E-08	2.8701E-08	2.8426E-08	2.8156E-08	2.78908E-08	2.7631E-08	2.74E-08	2.71E-08	2.69E-08	2.66E-08	2.64E-08
0.1	3.20E-08	2.40E-08	2.9448E-08	2.9268E-08	2.8916E-08	2.8571E-08	2.82353E-08	2.7907E-08	2.76E-08	2.73E-08	2.70E-08	2.67E-08	2.64E-08
0.11	3.20E-08	2.40E-08	3.007E-08	2.9843E-08	2.9401E-08	2.8972E-08	2.85544E-08	2.8149E-08	2.78E-08	2.74E-08	2.70E-08	2.66E-08	2.63E-08
0.12	3.20E-08	2.40E-08	3.0706E-08	3.0426E-08	2.988E-08	2.9354E-08	2.88462E-08	2.8355E-08	2.79E-08	2.74E-08	2.70E-08	2.65E-08	2.61E-08
0.13	3.20E-08	2.40E-08	3.1358E-08	3.1016E-08	3.0353E-08	2.9718E-08	2.91086E-08	2.8524E-08	2.80E-08	2.74E-08	2.69E-08	2.64E-08	2.59E-08
0.14	3.20E-08	2.40E-08	3.2026E-08	3.1612E-08	3.0817E-08	3.006E-08	2.93399E-08	2.8653E-08	2.80E-08	2.74E-08	2.68E-08	2.62E-08	2.57E-08
0.15	3.20E-08	2.40E-08	3.2709E-08	3.2215E-08	3.127E-08	3.038E-08	2.95385E-08	2.8743E-08	2.80E-08	2.73E-08	2.66E-08	2.59E-08	2.53E-08
0.16	3.20E-08	2.40E-08	3.3408E-08	3.2823E-08	3.1712E-08	3.0675E-08	2.9703E-08	2.8791E-08	2.79E-08	2.71E-08	2.64E-08	2.56E-08	2.50E-08
0.17	3.20E-08	2.40E-08	3.4122E-08	3.3435E-08	3.2141E-08	3.0944E-08	2.98322E-08	2.8798E-08	2.78E-08	2.69E-08	2.61E-08	2.53E-08	2.45E-08
0.18	3.20E-08	2.40E-08	3.4853E-08	3.4052E-08	3.2556E-08	3.1185E-08	2.99252E-08	2.8763E-08	2.77E-08	2.67E-08	2.58E-08	2.49E-08	2.41E-08
0.19	3.20E-08	2.40E-08	3.56E-08	3.4672E-08	3.2953E-08	3.1397E-08	2.99813E-08	2.8688E-08	2.75E-08	2.64E-08	2.54E-08	2.45E-08	2.36E-08
0.2	3.20E-08	2.40E-08	3.6364E-08	3.5294E-08	3.3333E-08	3.1579E-08	0.00000003	2.8571E-08	2.73E-08	2.61E-08	2.50E-08	2.40E-08	2.31E-08
0.21	3.20E-08	2.40E-08	3.7143E-08	3.5917E-08	3.3694E-08	3.1729E-08	2.99813E-08	2.8416E-08	2.70E-08	2.57E-08	2.46E-08	2.35E-08	2.25E-08
0.22	3.20E-08	2.40E-08	3.7939E-08	3.6541E-08	3.4033E-08	3.1847E-08	2.99252E-08	2.8222E-08	2.67E-08	2.53E-08	2.41E-08	2.30E-08	2.20E-08
0.23	3.20E-08	2.40E-08	3.875E-08	3.7163E-08	3.435E-08	3.1932E-08	2.98322E-08	2.7992E-08	2.64E-08	2.49E-08	2.36E-08	2.25E-08	2.14E-08
0.24	3.20E-08	2.40E-08	3.9578E-08	3.7783E-08	3.4642E-08	3.1983E-08	2.9703E-08	2.7726E-08	2.60E-08	2.45E-08	2.31E-08	2.19E-08	2.08E-08
0.25	3.20E-08	2.40E-08	4.0421E-08	3.84E-08	3.4909E-08	3.2E-08	2.95385E-08	2.7429E-08	2.56E-08	2.40E-08	2.26E-08	2.13E-08	2.02E-08
0.26	3.20E-08	2.40E-08	4.128E-08	3.9012E-08	3.5149E-08	3.1983E-08	2.93399E-08	2.71E-08	2.52E-08	2.35E-08	2.21E-08	2.08E-08	1.96E-08
0.27	3.20E-08	2.40E-08	4.2153E-08	3.9617E-08	3.5362E-08	3.1932E-08	2.91086E-08	2.6744E-08	2.47E-08	2.30E-08	2.15E-08	2.02E-08	1.90E-08
0.28	3.20E-08	2.40E-08	4.3042E-08	4.0214E-08	3.5545E-08	3.1847E-08	2.88462E-08	2.6362E-08	2.43E-08	2.25E-08	2.09E-08	1.96E-08	1.84E-08
0.29	3.20E-08	2.40E-08	4.3944E-08	4.0802E-08	3.5698E-08	3.1729E-08	2.85544E-08	2.5957E-08	2.38E-08	2.20E-08	2.04E-08	1.90E-08	1.78E-08
0.3	3.20E-08	2.40E-08	4.486E-08	4.1379E-08	3.5821E-08	3.1579E-08	2.82353E-08	2.5532E-08	2.33E-08	2.14E-08	1.98E-08	1.85E-08	1.73E-08
0.31	3.20E-08	2.40E-08	4.5788E-08	4.1943E-08	3.5912E-08	3.1397E-08	2.78908E-08	2.5089E-08	2.28E-08	2.09E-08	1.93E-08	1.79E-08	1.67E-08
0.32	3.20E-08	2.40E-08	4.6729E-08	4.2493E-08	3.5971E-08	3.1185E-08	2.75229E-08	2.4631E-08	2.23E-08	2.04E-08	1.87E-08	1.73E-08	1.61E-08
0.33	3.20E-08	2.40E-08	4.7681E-08	4.3026E-08	3.5998E-08	3.0944E-08	2.7134E-08	2.4159E-08	2.18E-08	1.98E-08	1.82E-08	1.68E-08	1.56E-08

0.34	3.20E-08	2.40E-08	4.8642E-08	4.3541E-08	3.5993E-08	3.0675E-08	2.67261E-08	2.3678E-08	2.13E-08	1.93E-08	1.76E-08	1.63E-08	1.51E-08
0.35	3.20E-08	2.40E-08	4.9612E-08	4.4037E-08	3.5955E-08	3.038E-08	2.63014E-08	2.3188E-08	2.07E-08	1.88E-08	1.71E-08	1.57E-08	1.46E-08
0.36	3.20E-08	2.40E-08	5.059E-08	4.451E-08	3.5885E-08	3.006E-08	2.58621E-08	2.2693E-08	2.02E-08	1.82E-08	1.66E-08	1.52E-08	1.41E-08
0.37	3.20E-08	2.40E-08	5.1574E-08	4.4961E-08	3.5784E-08	2.9718E-08	2.54103E-08	2.2193E-08	1.97E-08	1.77E-08	1.61E-08	1.47E-08	1.36E-08
0.38	3.20E-08	2.40E-08	5.2562E-08	4.5386E-08	3.5651E-08	2.9354E-08	2.4948E-08	2.1692E-08	1.92E-08	1.72E-08	1.56E-08	1.43E-08	1.31E-08
0.39	3.20E-08	2.40E-08	5.3553E-08	4.5784E-08	3.5487E-08	2.8972E-08	2.44773E-08	2.119E-08	1.87E-08	1.67E-08	1.51E-08	1.38E-08	1.27E-08
0.4	3.20E-08	2.40E-08	5.4545E-08	4.6154E-08	3.5294E-08	2.8571E-08	0.000000024	2.069E-08	1.82E-08	1.62E-08	1.46E-08	1.32E-08	1.22E-08
0.41	3.20E-08	2.40E-08	5.5336E-08	4.6494E-08	3.5072E-08	2.8156E-08	2.35179E-08	2.0192E-08	1.77E-08	1.57E-08	1.42E-08	1.29E-08	1.18E-08
0.42	3.20E-08	2.40E-08	5.6524E-08	4.6802E-08	3.4823E-08	2.7726E-08	2.30326E-08	1.9698E-08	1.72E-08	1.53E-08	1.37E-08	1.25E-08	1.14E-08
0.43	3.20E-08	2.40E-08	5.7506E-08	4.7077E-08	3.4547E-08	2.7285E-08	2.25458E-08	1.9209E-08	1.67E-08	1.48E-08	1.33E-08	1.21E-08	1.10E-08
0.44	3.20E-08	2.40E-08	5.848E-08	4.7319E-08	3.4247E-08	2.6834E-08	2.20588E-08	1.8727E-08	1.63E-08	1.44E-08	1.29E-08	1.17E-08	1.07E-08
0.45	3.20E-08	2.40E-08	5.9443E-08	4.7525E-08	3.3922E-08	2.6374E-08	2.1573E-08	1.8251E-08	1.58E-08	1.40E-08	1.25E-08	1.13E-08	1.03E-08
0.46	3.20E-08	2.40E-08	6.0393E-08	4.7695E-08	3.3576E-08	2.5907E-08	2.10896E-08	1.7783E-08	1.54E-08	1.35E-08	1.21E-08	1.09E-08	9.97E-09
0.47	3.20E-08	2.40E-08	6.1326E-08	4.7828E-08	3.3209E-08	2.5435E-08	2.06097E-08	1.7324E-08	1.49E-08	1.31E-08	1.17E-08	1.06E-08	9.64E-09
0.48	3.20E-08	2.40E-08	6.2241E-08	4.7923E-08	3.2823E-08	2.4958E-08	2.01342E-08	1.6873E-08	1.45E-08	1.27E-08	1.14E-08	1.02E-08	9.32E-09
0.49	3.20E-08	2.40E-08	6.3133E-08	4.7981E-08	3.2419E-08	2.448E-08	1.96641E-08	1.6432E-08	1.41E-08	1.24E-08	1.10E-08	9.91E-09	9.02E-09
0.5	3.20E-08	2.40E-08	6.4E-08	4.8E-08	3.2E-08	2.4E-08	1.92E-08	1.6E-08	1.37E-08	1.20E-08	1.07E-08	9.60E-09	8.73E-09
0.51	3.20E-08	2.40E-08	6.4839E-08	4.7981E-08	3.1566E-08	2.352E-08	1.87427E-08	1.5578E-08	1.33E-08	1.16E-08	1.03E-08	9.30E-09	8.45E-09
0.52	3.20E-08	2.40E-08	6.5646E-08	4.7923E-08	3.112E-08	2.3041E-08	1.82927E-08	1.5167E-08	1.30E-08	1.13E-08	1.00E-08	9.01E-09	8.18E-09
0.53	3.20E-08	2.40E-08	6.6418E-08	4.7828E-08	3.0663E-08	2.2565E-08	1.78505E-08	1.4766E-08	1.26E-08	1.10E-08	9.72E-09	8.73E-09	7.92E-09
0.54	3.20E-08	2.40E-08	6.7152E-08	4.7695E-08	3.0196E-08	2.2091E-08	1.74165E-08	1.4375E-08	1.22E-08	1.07E-08	9.43E-09	8.46E-09	7.67E-09
0.55	3.20E-08	2.40E-08	6.7845E-08	4.7525E-08	2.9721E-08	2.1622E-08	1.69912E-08	1.3994E-08	1.19E-08	1.03E-08	9.15E-09	8.21E-09	7.44E-09
0.56	3.20E-08	2.40E-08	6.8493E-08	4.7319E-08	2.924E-08	2.1157E-08	1.65746E-08	1.3624E-08	1.16E-08	1.00E-08	8.88E-09	7.96E-09	7.21E-09
0.57	3.20E-08	2.40E-08	6.9095E-08	4.7077E-08	2.8753E-08	2.0697E-08	1.61671E-08	1.3264E-08	1.12E-08	9.76E-09	8.62E-09	7.72E-09	6.99E-09
0.58	3.20E-08	2.40E-08	6.9646E-08	4.6802E-08	2.8262E-08	2.0243E-08	1.57687E-08	1.2914E-08	1.09E-08	9.48E-09	8.37E-09	7.49E-09	6.78E-09
0.59	3.20E-08	2.40E-08	7.0145E-08	4.6494E-08	2.7768E-08	1.9795E-08	1.53797E-08	1.2575E-08	1.06E-08	9.21E-09	8.13E-09	7.27E-09	6.58E-09
0.6	3.20E-08	2.40E-08	7.0588E-08	4.6154E-08	2.7273E-08	1.9355E-08	0.000000015	1.2245E-08	1.03E-08	8.96E-09	7.89E-09	7.06E-09	6.38E-09
0.61	3.20E-08	2.40E-08	7.0974E-08	4.5784E-08	2.6777E-08	1.8921E-08	1.46297E-08	1.1925E-08</					

0.71	3.20E-08	2.40E-08	7.1397E-08	4.0802E-08	2.1972E-08	1.5034E-08	1.14259E-08	9.2145E-09	7.72E-09	6.64E-09	5.83E-09	5.19E-09	4.68E-09
0.72	3.20E-08	2.40E-08	7.109E-08	4.0214E-08	2.1521E-08	1.4691E-08	1.11524E-08	8.9874E-09	7.53E-09	6.47E-09	5.68E-09	5.06E-09	4.56E-09
0.73	3.20E-08	2.40E-08	7.0723E-08	3.9617E-08	2.1077E-08	1.4358E-08	1.08868E-08	8.7674E-09	7.34E-09	6.31E-09	5.53E-09	4.93E-09	4.44E-09
0.74	3.20E-08	2.40E-08	7.0299E-08	3.9012E-08	2.064E-08	1.4032E-08	1.06289E-08	8.5543E-09	7.16E-09	6.15E-09	5.40E-09	4.80E-09	4.33E-09
0.75	3.20E-08	2.40E-08	6.9818E-08	3.84E-08	2.0211E-08	1.3714E-08	1.03784E-08	8.3478E-09	6.98E-09	6.00E-09	5.26E-09	4.68E-09	4.22E-09
0.76	3.20E-08	2.40E-08	6.9284E-08	3.7783E-08	1.9789E-08	1.3405E-08	1.01351E-08	8.1477E-09	6.81E-09	5.85E-09	5.13E-09	4.57E-09	4.11E-09
0.77	3.20E-08	2.40E-08	6.8699E-08	3.7163E-08	1.9375E-08	1.3103E-08	9.89895E-09	7.9539E-09	6.65E-09	5.71E-09	5.00E-09	4.45E-09	4.01E-09
0.78	3.20E-08	2.40E-08	6.8066E-08	3.6541E-08	1.8969E-08	1.281E-08	9.66962E-09	7.766E-09	6.49E-09	5.57E-09	4.88E-09	4.34E-09	3.91E-09
0.79	3.20E-08	2.40E-08	6.7387E-08	3.5917E-08	1.8572E-08	1.2523E-08	9.44696E-09	7.5839E-09	6.33E-09	5.44E-09	4.76E-09	4.24E-09	3.82E-09
0.8	3.20E-08	2.40E-08	6.6667E-08	3.5294E-08	1.8182E-08	1.2245E-08	9.23077E-09	7.4074E-09	6.19E-09	5.31E-09	4.65E-09	4.14E-09	3.73E-09
0.81	3.20E-08	2.40E-08	6.5907E-08	3.4672E-08	1.78E-08	1.1974E-08	9.02086E-09	7.2363E-09	6.04E-09	5.18E-09	4.54E-09	4.04E-09	3.64E-09
0.82	3.20E-08	2.40E-08	6.5111E-08	3.4052E-08	1.7427E-08	1.171E-08	8.81705E-09	7.0705E-09	5.90E-09	5.06E-09	4.43E-09	3.94E-09	3.55E-09
0.83	3.20E-08	2.40E-08	6.4283E-08	3.3435E-08	1.7061E-08	1.1453E-08	8.61914E-09	6.9097E-09	5.77E-09	4.95E-09	4.33E-09	3.85E-09	3.47E-09
0.84	3.20E-08	2.40E-08	6.3425E-08	3.2823E-08	1.6704E-08	1.1202E-08	8.42697E-09	6.7537E-09	5.63E-09	4.83E-09	4.23E-09	3.76E-09	3.39E-09
0.85	3.20E-08	2.40E-08	6.2541E-08	3.2215E-08	1.6354E-08	1.0959E-08	8.24034E-09	6.6025E-09	5.51E-09	4.72E-09	4.14E-09	3.68E-09	3.31E-09
0.86	3.20E-08	2.40E-08	6.1633E-08	3.1612E-08	1.6013E-08	1.0722E-08	8.0591E-09	6.4558E-09	5.38E-09	4.62E-09	4.04E-09	3.59E-09	3.24E-09
0.87	3.20E-08	2.40E-08	6.0706E-08	3.1016E-08	1.5679E-08	1.0491E-08	7.88307E-09	6.3135E-09	5.27E-09	4.52E-09	3.95E-09	3.51E-09	3.16E-09
0.88	3.20E-08	2.40E-08	5.9761E-08	3.0426E-08	1.5353E-08	1.0267E-08	7.71208E-09	6.1754E-09	5.15E-09	4.42E-09	3.86E-09	3.44E-09	3.09E-09
0.89	3.20E-08	2.40E-08	5.8802E-08	2.9843E-08	1.5035E-08	1.0049E-08	7.54598E-09	6.0414E-09	5.04E-09	4.32E-09	3.78E-09	3.36E-09	3.03E-09
0.9	3.20E-08	2.40E-08	5.7831E-08	2.9268E-08	1.4724E-08	9.8361E-09	7.38462E-09	5.9113E-09	4.93E-09	4.23E-09	3.70E-09	3.29E-09	2.96E-09
0.91	3.20E-08	2.40E-08	5.6852E-08	2.8701E-08	1.442E-08	9.6293E-09	7.22783E-09	5.7851E-09	4.82E-09	4.13E-09	3.62E-09	3.22E-09	2.90E-09
0.92	3.20E-08	2.40E-08	5.5866E-08	2.8143E-08	1.4124E-08	9.428E-09	7.07547E-09	5.6625E-09	4.72E-09	4.05E-09	3.54E-09	3.15E-09	2.83E-09
0.93	3.20E-08	2.40E-08	5.4876E-08	2.7593E-08	1.3835E-08	9.2322E-09	6.92741E-09	5.5435E-09	4.62E-09	3.96E-09	3.47E-09	3.08E-09	2.77E-09
0.94	3.20E-08	2.40E-08	5.3884E-08	2.7051E-08	1.3553E-08	9.0416E-09	6.78349E-09	5.4279E-09	4.52E-09	3.88E-09	3.39E-09	3.02E-09	2.72E-09
0.95	3.20E-08	2.40E-08	5.2893E-08	2.6519E-08	1.3278E-08	8.8561E-09	6.6436E-09	5.3156E-09	4.43E-09	3.80E-09	3.32E-09	2.95E-09	2.66E-09
0.96	3.20E-08	2.40E-08	5.1903E-08	2.5997E-08	1.301E-08	8.6755E-09	6.50759E-09	5.2065E-09	4.34E-09	3.72E-09	3.25E-09	2.89E-09	2.60E-09
0.97	3.20E-08	2.40E-08	5.0918E-08	2.5483E-08	1.2748E-08	8.4998E-09	6.37635E-09	5.1005E-09	4.25E-09	3.64E-09	3.19E-09	2.83E-09	2.55E-09
0.98	3.20E-08	2.40E-08	4.9938E-08	2.4979E-08	1.2492E-08	8.3287E-09	6.24675E-09	4.9975E-09	4.16E-09	3.57E-09	3.12E-09	2.78E-09	2.50E-09
0.99	3.20E-08	2.40E-08	4.8965E-08	2.4485E-08	1.2243E-08	8.1622E-09	6.12167E-09	4.8974E-09	4.08E-09	3.50E-09	3.06E-09	2.72E-09	2.45E-09
1	3.20E-08	2.40E-08	4.8E-08	2.4E-08	1.2E-08	8E-09	6E-09	4.8E-09	4.00E-09	3.43E-09	3.00E-09	2.67E-09	2.40E-09

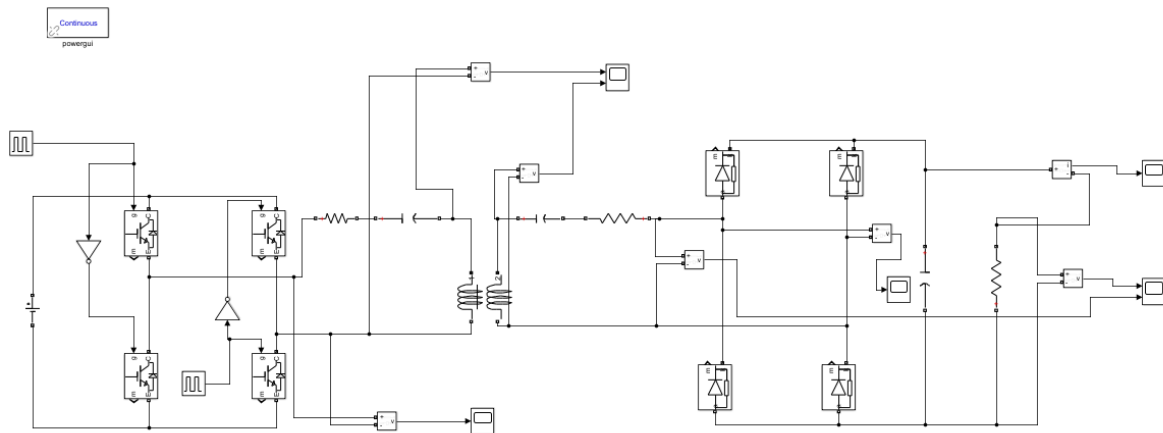
Appendix B2: Excel Data generated by using Variable capacitor equation 10 chapter 3.

B	C	D	E	F	G	H	I	J	K	L	M	N	O
d	C1	C2	Ceff (N=0.5)	Ceff (N=1)	Ceff(N=2)	Ceff(N=3)	Ceff(N=4)	Ceff(N=5)	Ceff(N=6)	Ceff(N=7)	Ceff(N=8)	Ceff(N=9)	Ceff(N=10)
0	3.20E-06	6.40E-05	0.0000064	0.0000032	0.0000016	1.0667E-06	0.0000008	0.00000064	5.33E-07	4.57E-07	4.00E-07	3.56E-07	3.20E-07
0.01	3.20E-06	6.40E-05	6.5286E-06	3.2646E-06	1.6324E-06	1.0883E-06	8.16222E-07	6.5298E-07	5.44E-07	4.66E-07	4.08E-07	3.63E-07	3.26E-07
0.02	3.20E-06	6.40E-05	6.6583E-06	3.3306E-06	1.6656E-06	1.1105E-06	8.329E-07	6.6633E-07	5.55E-07	4.76E-07	4.16E-07	3.70E-07	3.33E-07
0.03	3.20E-06	6.40E-05	6.789E-06	3.3977E-06	1.6997E-06	1.1333E-06	8.50046E-07	6.8007E-07	5.67E-07	4.86E-07	4.25E-07	3.78E-07	3.40E-07
0.04	3.20E-06	6.40E-05	6.9204E-06	3.4662E-06	1.7346E-06	1.1567E-06	8.67679E-07	6.942E-07	5.79E-07	4.96E-07	4.34E-07	3.86E-07	3.47E-07
0.05	3.20E-06	6.40E-05	7.0523E-06	3.5359E-06	1.7704E-06	1.1808E-06	8.85813E-07	7.0875E-07	5.91E-07	5.06E-07	4.43E-07	3.94E-07	3.54E-07
0.06	3.20E-06	6.40E-05	7.1846E-06	3.6069E-06	1.8071E-06	1.2055E-06	9.04466E-07	7.2372E-07	6.03E-07	5.17E-07	4.52E-07	4.02E-07	3.62E-07
0.07	3.20E-06	6.40E-05	7.3168E-06	3.679E-06	1.8447E-06	1.231E-06	9.23654E-07	7.3913E-07	6.16E-07	5.28E-07	4.62E-07	4.11E-07	3.70E-07
0.08	3.20E-06	6.40E-05	7.4488E-06	3.7523E-06	1.8832E-06	1.2571E-06	9.43396E-07	7.55E-07	6.29E-07	5.40E-07	4.72E-07	4.20E-07	3.78E-07
0.09	3.20E-06	6.40E-05	7.5802E-06	3.8268E-06	1.9227E-06	1.2839E-06	9.6371E-07	7.7134E-07	6.43E-07	5.51E-07	4.82E-07	4.29E-07	3.86E-07
0.1	3.20E-06	6.40E-05	7.7108E-06	3.9024E-06	1.9632E-06	1.3115E-06	9.84615E-07	7.8818E-07	6.57E-07	5.63E-07	4.93E-07	4.38E-07	3.95E-07
0.11	3.20E-06	6.40E-05	7.8403E-06	3.9791E-06	2.0046E-06	1.3398E-06	1.00613E-06	8.0552E-07	6.72E-07	5.76E-07	5.04E-07	4.48E-07	4.03E-07
0.12	3.20E-06	6.40E-05	7.9681E-06	4.0568E-06	2.0471E-06	1.3689E-06	1.02828E-06	8.2338E-07	6.87E-07	5.89E-07	5.15E-07	4.58E-07	4.12E-07
0.13	3.20E-06	6.40E-05	8.0941E-06	4.1354E-06	2.0905E-06	1.3988E-06	1.05108E-06	8.418E-07	7.02E-07	6.02E-07	5.27E-07	4.69E-07	4.22E-07
0.14	3.20E-06	6.40E-05	8.2178E-06	4.215E-06	2.135E-06	1.4296E-06	1.07455E-06	8.6077E-07	7.18E-07	6.16E-07	5.39E-07	4.79E-07	4.32E-07
0.15	3.20E-06	6.40E-05	8.3388E-06	4.2953E-06	2.1806E-06	1.4612E-06	1.09871E-06	8.8033E-07	7.34E-07	6.30E-07	5.51E-07	4.90E-07	4.42E-07
0.16	3.20E-06	6.40E-05	8.4567E-06	4.3764E-06	2.2272E-06	1.4937E-06	1.1236E-06	9.005E-07	7.51E-07	6.45E-07	5.64E-07	5.02E-07	4.52E-07
0.17	3.20E-06	6.40E-05	8.571E-06	4.4581E-06	2.2748E-06	1.527E-06	1.14922E-06	9.2129E-07	7.69E-07	6.60E-07	5.78E-07	5.14E-07	4.63E-07
0.18	3.20E-06	6.40E-05	8.6815E-06	4.5403E-06	2.3236E-06	1.5613E-06	1.17561E-06	9.4273E-07	7.87E-07	6.75E-07	5.91E-07	5.26E-07	4.74E-07
0.19	3.20E-06	6.40E-05	8.7876E-06	4.6229E-06	2.3734E-06	1.5965E-06	1.20278E-06	9.6484E-07	8.05E-07	6.91E-07	6.05E-07	5.39E-07	4.85E-07
0.2	3.20E-06	6.40E-05	8.8889E-06	4.7059E-06	2.4242E-06	1.6327E-06	1.23077E-06	9.8765E-07	8.25E-07	7.08E-07	6.20E-07	5.52E-07	4.97E-07
0.21	3.20E-06	6.40E-05	8.985E-06	4.789E-06	2.4762E-06	1.6698E-06	1.25959E-06	1.0112E-06	8.45E-07	7.25E-07	6.35E-07	5.65E-07	5.09E-07
0.22	3.20E-06	6.40E-05	9.0754E-06	4.8721E-06	2.5292E-06	1.7079E-06	1.28928E-06	1.0355E-06	8.65E-07	7.43E-07	6.51E-07	5.79E-07	5.22E-07
0.23	3.20E-06	6.40E-05	9.1599E-06	4.9551E-06	2.5834E-06	1.7471E-06	1.31986E-06	1.0605E-06	8.86E-07	7.61E-07	6.67E-07	5.94E-07	5.35E-07
0.24	3.20E-06	6.40E-05	9.2379E-06	5.0378E-06	2.6385E-06	1.7873E-06	1.35135E-06	1.0864E-06	9.08E-07	7.80E-07	6.84E-07	6.09E-07	5.49E-07
0.25	3.20E-06	6.40E-05	9.3091E-06	5.1215E-06	2.6947E-06	1.8286E-06	1.38378E-06	1.113E-06	9.31E-07	8.00E-07	7.01E-07	6.24E-07	5.63E-07
0.26	3.20E-06	6.40E-05	9.3732E-06	5.2016E-06	2.752E-06	1.8709E-06	1.41718E-06	1.1406E-06	9.54E-07	8.20E-07	7.19E-07	6.41E-07	5.77E-07
0.27	3.20E-06	6.40E-05	9.4298E-06	5.2823E-06	2.8102E-06	1.9143E-06	1.45158E-06	1.169E-06	9.79E-07	8.41E-07	7.38E-07	6.57E-07	5.92E-07
0.28	3.20E-06	6.40E-05	9.4787E-06	5.3619E-06	2.8694E-06	1.9589E-06	1.48699E-06	1.1983E-06	1.00E-06	8.63E-07	7.57E-07	6.75E-07	6.08E-07
0.29	3.20E-06	6.40E-05	9.5196E-06	5.4403E-06	2.9296E-06	2.0045E-06	1.52345E-06	1.2286E-06	1.03E-06	8.86E-07	7.77E-07	6.92E-07	6.24E-07
0.3	3.20E-06	6.40E-05	9.5522E-06	5.5172E-06	2.9907E-06	2.0513E-06	1.56098E-06	1.2598E-06	1.06E-06	9.09E-07	7.98E-07	7.11E-07	6.41E-07
0.31	3.20E-06	6.40E-05	9.5765E-06	5.5925E-06	3.0526E-06	2.0992E-06	1.5996E-06	1.					

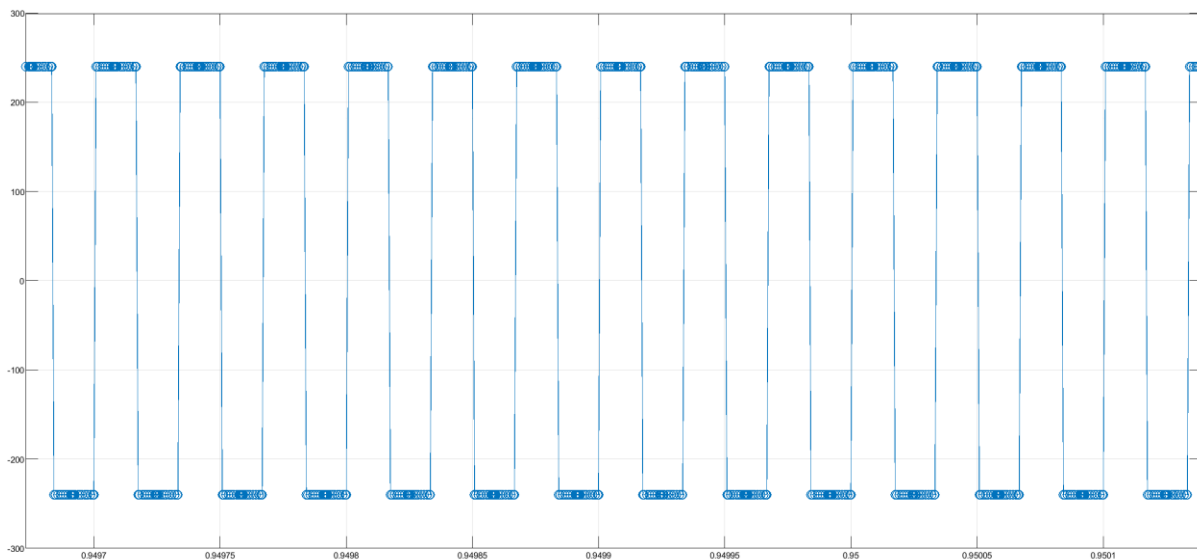
0.34	3.20E-06	6.40E-05	9.5981E-06	5.8055E-06	3.2428E-06	2.2497E-06	1.72228E-06	1.3952E-06	1.17E-06	1.01E-06	8.89E-07	7.93E-07	7.16E-07
0.35	3.20E-06	6.40E-05	9.588E-06	5.8716E-06	3.3075E-06	2.3022E-06	1.76552E-06	1.4318E-06	1.20E-06	1.04E-06	9.14E-07	8.15E-07	7.36E-07
0.36	3.20E-06	6.40E-05	9.5694E-06	5.9347E-06	3.3727E-06	2.3557E-06	1.80995E-06	1.4695E-06	1.24E-06	1.07E-06	9.39E-07	8.39E-07	7.57E-07
0.37	3.20E-06	6.40E-05	9.5423E-06	5.9948E-06	3.4383E-06	2.4104E-06	1.85561E-06	1.5084E-06	1.27E-06	1.10E-06	9.66E-07	8.63E-07	7.79E-07
0.38	3.20E-06	6.40E-05	9.5068E-06	6.0514E-06	3.5042E-06	2.4661E-06	1.9025E-06	1.5486E-06	1.31E-06	1.13E-06	9.94E-07	8.88E-07	8.02E-07
0.39	3.20E-06	6.40E-05	9.4633E-06	6.1045E-06	3.5702E-06	2.5229E-06	1.95062E-06	1.59E-06	1.34E-06	1.16E-06	1.02E-06	9.14E-07	8.26E-07
0.4	3.20E-06	6.40E-05	9.4118E-06	6.1538E-06	3.6364E-06	2.5806E-06	0.000002	1.6327E-06	1.38E-06	1.19E-06	1.05E-06	9.41E-07	8.51E-07
0.41	3.20E-06	6.40E-05	9.3526E-06	6.1991E-06	3.7024E-06	2.6394E-06	2.05062E-06	1.6766E-06	1.42E-06	1.23E-06	1.08E-06	9.69E-07	8.77E-07
0.42	3.20E-06	6.40E-05	9.2861E-06	6.2402E-06	3.7683E-06	2.6991E-06	2.1025E-06	1.7219E-06	1.46E-06	1.26E-06	1.12E-06	9.99E-07	9.04E-07
0.43	3.20E-06	6.40E-05	9.2126E-06	6.277E-06	3.8337E-06	2.7596E-06	2.15561E-06	1.7685E-06	1.50E-06	1.30E-06	1.15E-06	1.03E-06	9.32E-07
0.44	3.20E-06	6.40E-05	9.1324E-06	6.3091E-06	3.8986E-06	2.8209E-06	2.20994E-06	1.8165E-06	1.54E-06	1.34E-06	1.18E-06	1.06E-06	9.61E-07
0.45	3.20E-06	6.40E-05	9.0459E-06	6.3366E-06	3.9628E-06	2.8829E-06	2.26549E-06	1.8659E-06	1.59E-06	1.38E-06	1.22E-06	1.09E-06	9.91E-07
0.46	3.20E-06	6.40E-05	8.9536E-06	6.3593E-06	4.0262E-06	2.9455E-06	2.32221E-06	1.9166E-06	1.63E-06	1.42E-06	1.26E-06	1.13E-06	1.02E-06
0.47	3.20E-06	6.40E-05	8.8557E-06	6.377E-06	4.0884E-06	3.0086E-06	2.38007E-06	1.9687E-06	1.68E-06	1.46E-06	1.30E-06	1.16E-06	1.06E-06
0.48	3.20E-06	6.40E-05	8.7527E-06	6.3898E-06	4.1494E-06	3.0722E-06	2.43902E-06	2.0222E-06	1.73E-06	1.51E-06	1.34E-06	1.20E-06	1.09E-06
0.49	3.20E-06	6.40E-05	8.6451E-06	6.3974E-06	4.2089E-06	3.136E-06	2.49902E-06	2.0771E-06	1.78E-06	1.55E-06	1.38E-06	1.24E-06	1.13E-06
0.5	3.20E-06	6.40E-05	8.5333E-06	0.0000064	4.2667E-06	0.0000032	0.00000256	2.1333E-06	1.83E-06	1.60E-06	1.42E-06	1.28E-06	1.16E-06
0.51	3.20E-06	6.40E-05	8.4177E-06	6.3974E-06	4.3226E-06	3.264E-06	2.62188E-06	2.1909E-06	1.88E-06	1.65E-06	1.47E-06	1.32E-06	1.20E-06
0.52	3.20E-06	6.40E-05	8.2988E-06	6.3898E-06	4.3764E-06	3.3278E-06	2.68456E-06	2.2497E-06	1.94E-06	1.70E-06	1.51E-06	1.37E-06	1.24E-06
0.53	3.20E-06	6.40E-05	8.1768E-06	6.377E-06	4.4278E-06	3.3913E-06	2.74796E-06	2.3098E-06	1.99E-06	1.75E-06	1.56E-06	1.41E-06	1.29E-06
0.54	3.20E-06	6.40E-05	8.0523E-06	6.3593E-06	4.4768E-06	3.4542E-06	2.81195E-06	2.3711E-06	2.05E-06	1.81E-06	1.61E-06	1.46E-06	1.33E-06
0.55	3.20E-06	6.40E-05	7.9257E-06	6.3366E-06	4.523E-06	3.5165E-06	2.8764E-06	2.4335E-06	2.11E-06	1.86E-06	1.66E-06	1.51E-06	1.37E-06
0.56	3.20E-06	6.40E-05	7.7973E-06	6.3091E-06	4.5662E-06	3.5778E-06	2.94118E-06	2.4969E-06	2.17E-06	1.92E-06	1.72E-06	1.56E-06	1.42E-06
0.57	3.20E-06	6.40E-05	7.6674E-06	6.277E-06	4.6063E-06	3.638E-06	3.00611E-06	2.5612E-06	2.23E-06	1.98E-06	1.77E-06	1.61E-06	1.47E-06
0.58	3.20E-06	6.40E-05	7.5365E-06	6.2402E-06	4.6431E-06	3.6969E-06	3.07102E-06	2.6264E-06	2.29E-06	2.04E-06	1.83E-06	1.66E-06	1.52E-06
0.59	3.20E-06	6.40E-05	7.4048E-06	6.1991E-06	4.6763E-06	3.7541E-06	3.13572E-06	2.6922E-06	2.36E-06	2.10E-06	1.89E-06	1.72E-06	1.58E-06
0.6	3.20E-06	6.40E-05	7.2727E-06	6.1538E-06	4.7059E-06	3.8095E-06	0.0000032	2.7586E-06	2.42E-06	2.16E-06	1.95E-06	1.78E-06	1.63E-06
0.61	3.20E-06	6.40E-05	7.1405E-06	6.1045E-06	4.7316E-06	3.8629E-06	3.000064	2.8254E-06	2.49E-06	2.23E-06	2.01E-06	1.84E-06	1.69E-06
0.62	3.20E-06	6.40E-05	7.0083E-06	6.0514E-06	4.7534E-06	3.9139E-06	3.3264E-06	2.8923E-06	2.56E-06	2.29E-06	2.08E-06	1.90E-06	1.75E-06
0.63	3.20E-06	6.40E-05	6.8765E-06	5.9948E-06	4.7711E-06	3.9624E-06	3.38804E-06	2.9591E-06	2.63E-06	2.36E-06	2.14E-06	1.96E-06	1.81E-06
0.64	3.20E-06	6.40E-05	6.7454E-06	5.9347E-06	4.7847E-06	4.008E-06	3.44828E-06	3.0257E-06	2.70E-06	2.43E-06	2.21E-06	2.03E-06	1.88E-06
0.65	3.20E-06	6.40E-05	6.615E-06	5.8716E-06	4.794E-06	4.0506E-06	3.50685E-06	3.0918E-06	2.76E-06	2.50E-06	2.28E-06	2.10E-06	1.94E-06
0.66	3.20E-06	6.40E-05	6.4856E-06	5.8055E-06	4.799E-06	4.09E-06	3.56347E-06	3.1571E-06	2.83E-06	2.57E-06	2.35E-06	2.17E-06	2.01E-06
0.67	3.20E-06	6.40E-05	6.3574E-06	5.7368E-06	4.7998E-06	4.1258E-06	3.61786E-06	3.2213E-06	2.90E-06	2.64E-06	2.42E-06	2.24E-06	2.08E-06
0.68	3.20E-06	6.40E-05	6.2305E-06	5.6657E-06	4.7962E-06	4.158E-06	3.66972E-06	3.2841E-06	2.97E-06	2.71E-06	2.50E-06	2.31E-06	2.15E-06
0.69	3.20E-06	6.40E-05	6.1051E-06	5.5925E-06	4.7883E-06	4.1863E-06	3.71877E-06	3.3452E-06	3.04E-06	2.79E-06	2.57E-06	2.39E-06	2.23E-06
0.7	3.20E-06	6.40E-05	5.9813E-06	5.5172E-06	4.7761E-06	4.2105E-06	3.76471E-06	3.4043E-06	3.11E-06	2.86E-06	2.64E-06	2.46E-06	2.30E-06
0.71	3.20E-06	6.40E-05	5.8592E-06	5.4403E-06	4.7598E-06	4.2306E-06	3.80726E-06	3.461E-06	3.17E-06	2.93E-06	2.72E-06	2.54E-06	2.38E-06
0.72	3.20E-06	6.40E-05	5.7389E-06	5.3619E-06	4.7393E-06	4.2463E-06	3.84615E-06	3.5149E-06	3.24E-06	3.00E-06	2.79E-06	2.61E-06	2.46E-06
0.73	3.20E-06	6.40E-05	5.6204E-06	5.2823E-06	4.7149E-06	4.2576E-06	3.88114E-06	3.5659E-06	3.30E-06	3.07E-06	2.87E-06	2.69E-06	2.54E-06
0.74	3.20E-06	6.40E-05	5.504E-06	5.2016E-06	4.6866E-06	4.2644E-06	3.91198E-06	3.6134E-06	3.36E-06	3.13E-06	2.94E-06	2.77E-06	2.62E-06
0.75	3.20E-06	6.40E-05	5.3895E-06	0.00000512	4.6545E-06	4.2667E-06	3.93846E-06	3.6571E-06	3.41E-06	3.20E-06	3.01E-06	2.84E-06	2.69E-06
0.76	3.20E-06	6.40E-05	5.277E-06	5.0378E-06	4.6189E-06	4.2644E-06	3.9604E-06	3.6969E-06	3.47E-06	3.26E-06	3.08E-06	2.92E-06	2.77E-06
0.77	3.20E-06	6.40E-05	5.1667E-06	4.9551E-06	4.5799E-06	4.2576E-06	3.97763E-06	3.7322E-06	3.52E-06	3.32E-06	3.15E-06	2.99E-06	2.85E-06
0.78	3.20E-06	6.40E-05	5.0585E-06	4.8721E-06	4.5377E-06	4.2463E-06	3.99002E-06	3.7629E-06	3.56E-06	3.38E-06	3.21E-06	3.07E-06	2.93E-06
0.79	3.20E-06	6.40E-05	4.9524E-06	4.789E-06	4.4925E-06	4.2306E-06	3.9975E-06	3.7888E-06	3.60E-06	3.43E-06	3.28E-06	3.13E-06	3.00E-06
0.8	3.20E-06	6.40E-05	4.8485E-06	4.7059E-06	4.4444E-06	4.2105E-06	0.000004	3.8095E-06	3.64E-06	3.48E-06	3.33E-06	3.20E-06	3.08E-06
0.81	3.20E-06	6.40E-05	4.7467E-06	4.6229E-06	4.3938E-06	4.1863E-06	3.9975E-06	3.825E-06	3.67E-06	3.52E-06	3.39E-06	3.26E-06	3.15E-06
0.82	3.20E-06	6.40E-05	4.6471E-06	4.5403E-06	4.3407E-06	4.158E-06	3.99002E-06	3.8351E-06	3.69E-06	3.56E-06	3.43E-06	3.32E-06	3.21E-06
0.83	3.20E-06	6.40E-05	4.5497E-06	4.4581E-06	4.2855E-06	4.1258E-06	3.97763E-06	3.8397E-06	3.71E-06	3.59E-06	3.48E-06	3.37E-06	3.27E-06
0.84	3.20E-06	6.40E-05	4.4543E-06	4.3764E-06	4.2283E-06	4.09E-06	3.9604E-06	3.8388E-06	3.72E-06	3.62E-06	3.51E-06	3.42E-06	3.33E-06
0.85	3.20E-06	6.40E-05	4.3612E-06	4.2953E-06	4.1694E-06	4.0506E-06	3.93846E-06	3.8323E-06	3.73E-06	3.64E-06	3.55E-06	3.46E-06	3.38E-06
0.86	3.20E-06	6.40E-05	4.2701E-06	4.215E-06	4.1089E-06	4.008E-06	3.91198E-06	3.8204E-06	3.73E-06	3.65E-06	3.57E-06	3.49E-06	3.42E-06
0.87	3.20E-06	6.40E-05	4.1811E-06	4.1354E-06	4.047E-06	3.9624E-06	3.88114E-06	3.8032E-06	3.73E-06	3.66E-06	3.59E-06	3.52E-06	3.46E-06
0.88	3.20E-06	6.40E-05	4.0942E-06	4.0568E-06	3.9841E-06	3.9139E-06	3.84615E-06	3.7807E-06	3.72E-06	3.66E-06	3.60E-06	3.54E-06	3.48E-06
0.89	3.20E-06	6.40E-05	4.0093E-06	3.9791E-06	3.9201E-06	3.8629E-06	3.80726E-06	3.7532E-06	3.70E-06	3.65E-06	3.60E-06	3.55E-06	3.50E-06
0.9	3.20E-06	6.40E-05	3.9264E-06	3.9024E-06	3.8554E-06	3.8095E-06	3.76471E-06	3.7209E-06	3.68E-06	3.64E-06	3.60E-06	3.56E-06	3.52E-06
0.91	3.20E-06	6.40E-05	3.8455E-06	3.8268E-06	3.7901E-06	3.7541E-06	3.71877E-06	3.6841E-06	3.65E-06	3.62E-06	3.58E-06	3.55E-06	3.52E-06
0.92	3.20E-06	6.40E-05	3.7665E-06	3.7523E-06	3.7244E-06	3.6969E-06	3.66972E-06	3.643E-06	3.62E-06	3.59E-06	3.57E-06	3.54E-06	3.51E-06
0.93	3.20E-06	6.40E-05	3.6894E-06	3.679E-06	3.6584E-06	3.638E-06	3.61786E-06	3.5979E-06	3.58E-06	3.56E-06	3.54E-06	3.52E-06	3.50E-06
0.94	3.20E-06	6.40E-05	3.6142E-06	3.6069E-06	3.5923E-06	3.5778E-06	3.56347E-06	3.5492E-06	3.54E-06	3.52E-06	3.51E-06	3.49E-06	3.48E-06
0.95	3.20E-06	6.40E-05	3.5408E-06	3.5359E-06	3.5262E-06	3.5165E-06	3.50685E-06	3.4973E-06	3.49E-06	3.48E-06	3.47E-06	3.46E-06	3.45E-06
0.96	3.20E-06	6.40E-05	3.4692E-06	3.4662E-06	3.4602E-06	3.4542E-06	3.44828E-06	3.4423E-06	3.44E-06	3.43E-06	3.42E-06	3.42E-06	3.41E-06
0.97	3.20E-06	6.40E-05	3.3994E-06	3.									



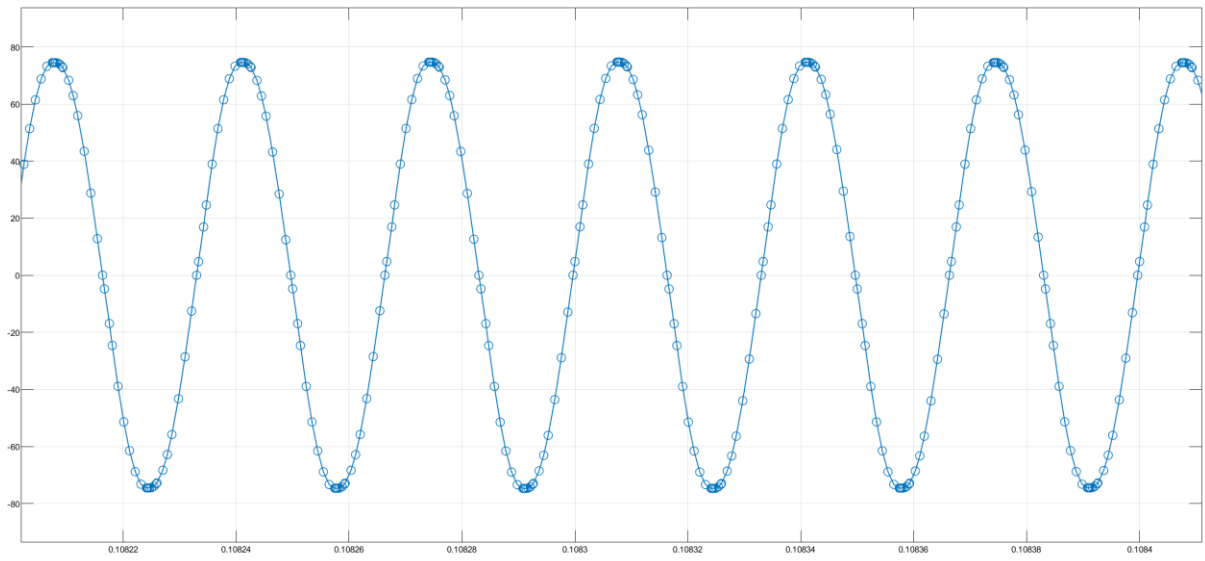
## Appendix C1: Wireless power transfer Design in MATLAB SIMULINK



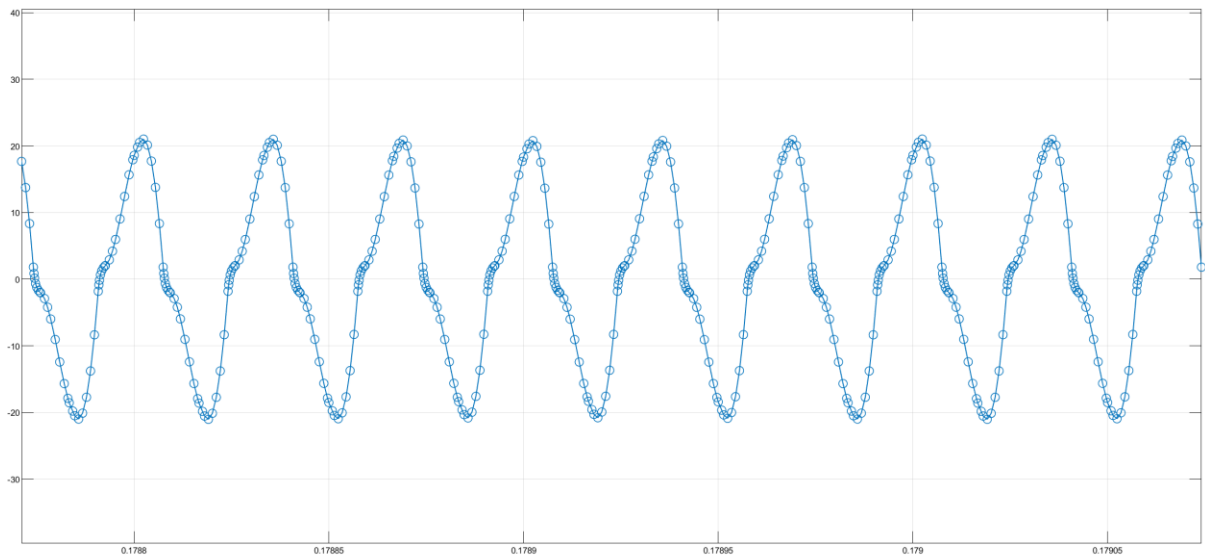
## Appendix C2: H-bridge inverter output voltage waveform



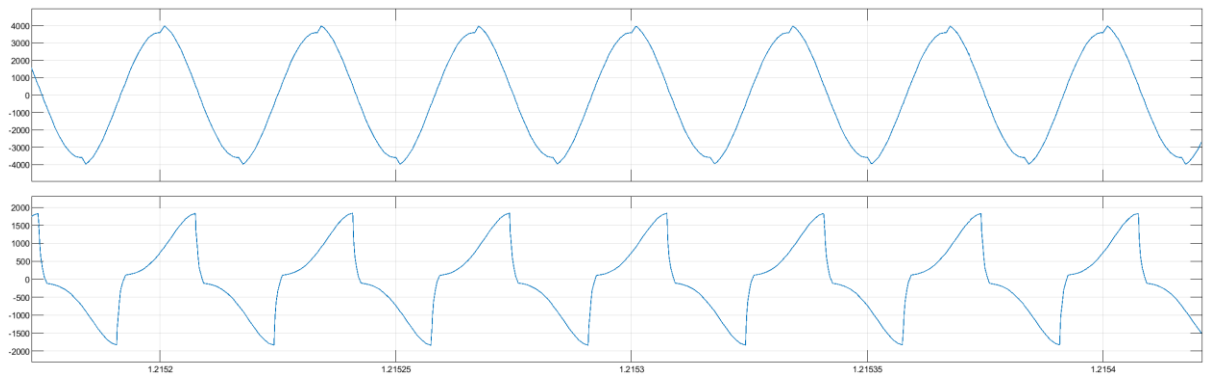
### Appendix C3: Primary side current waveform



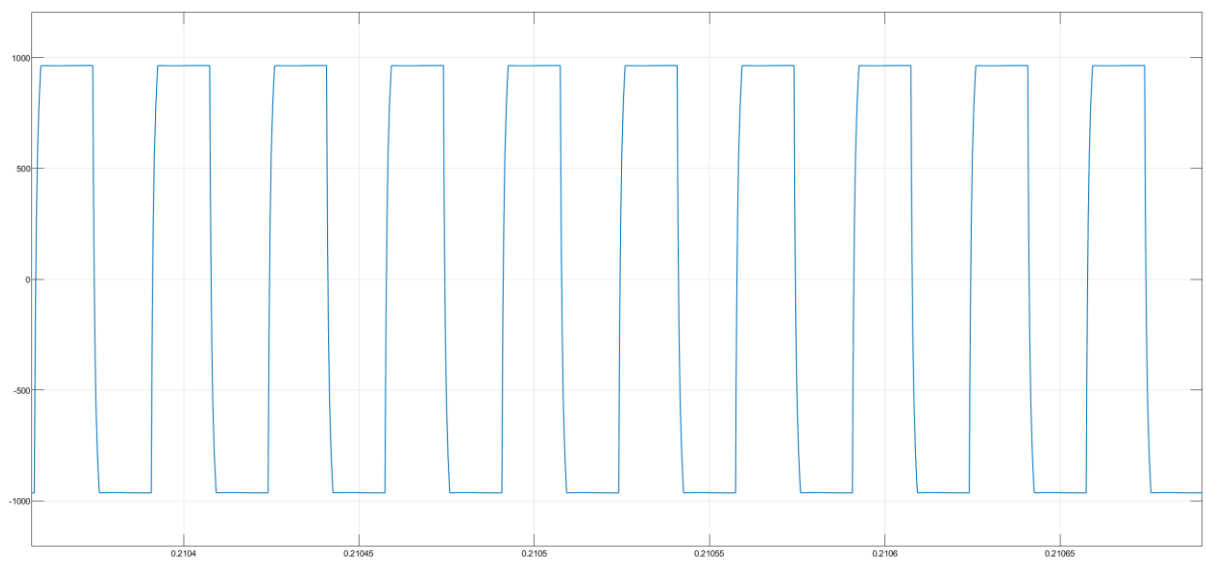
### Appendix C4: Secondary side current waveform



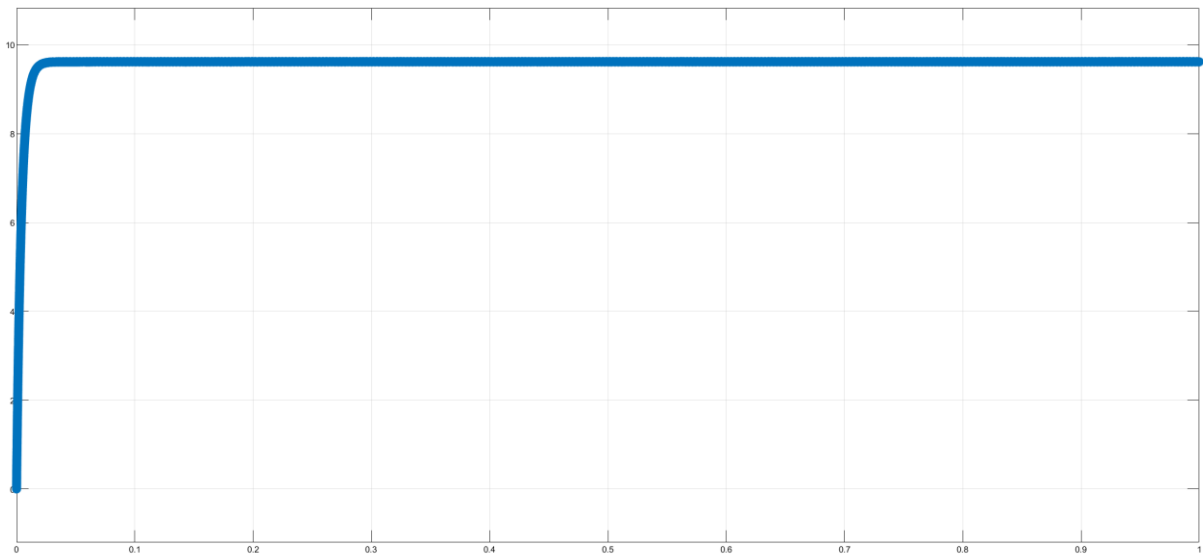
### Appendix C5: Primary and Secondary side voltage waveform



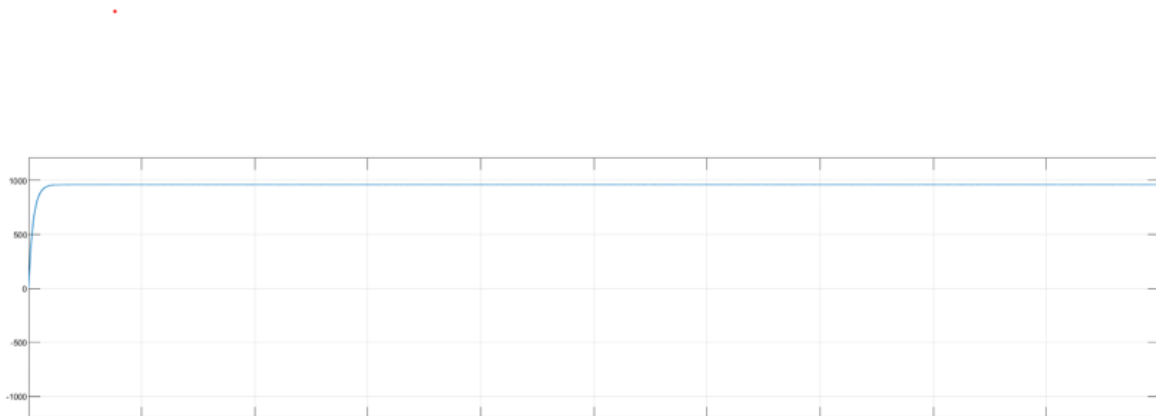
### Appendix C6: Rectifier Output Voltage waveform



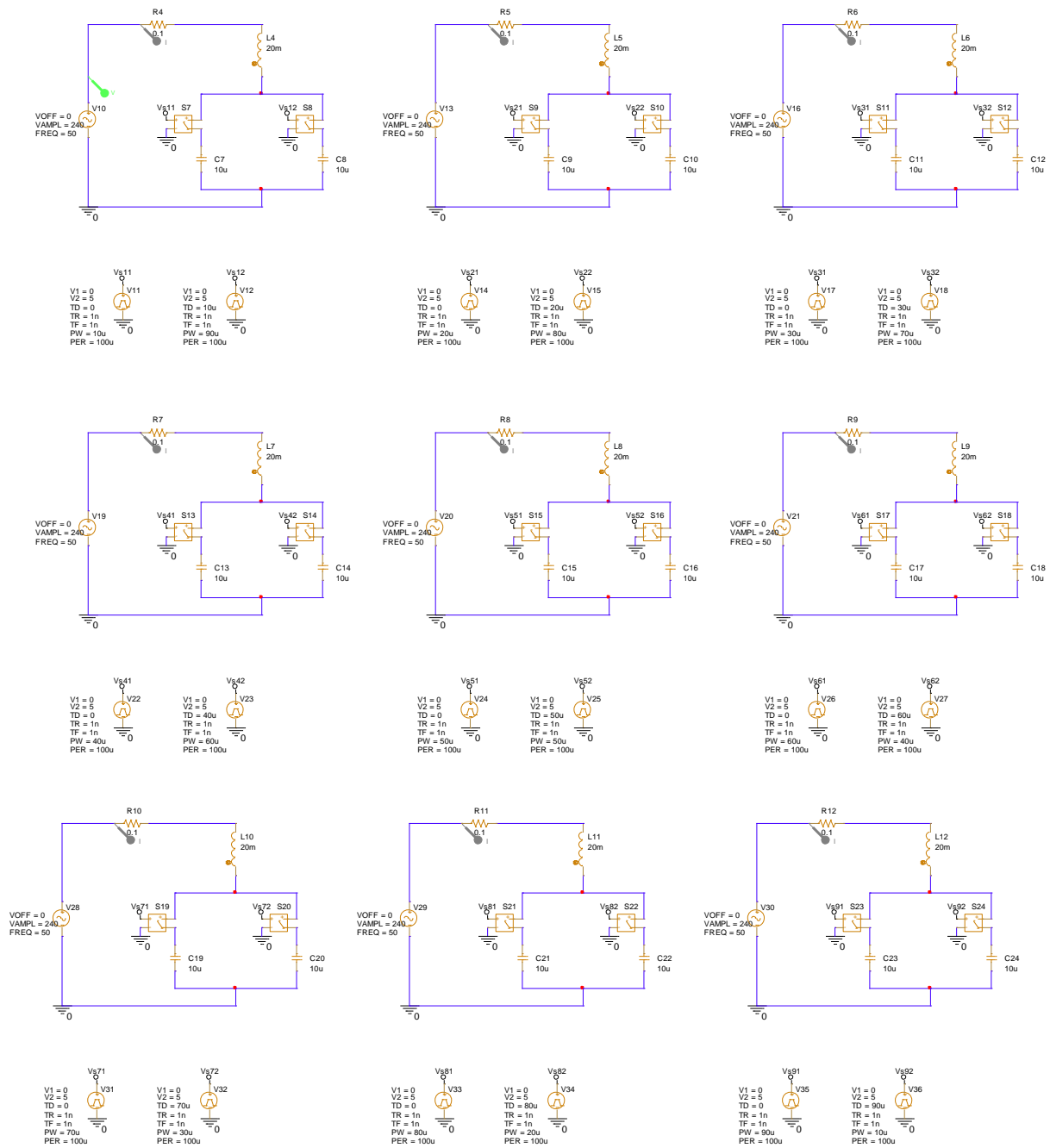
### Appendix C7: At load RL Output Voltage waveform



### Appendix C8: Output Power at load RL waveform



# Appendix D1: Variable capacitor design with same capacitive value at different duty cycles.



## Appendix E1: Power Supply Used in Hardware in its rating



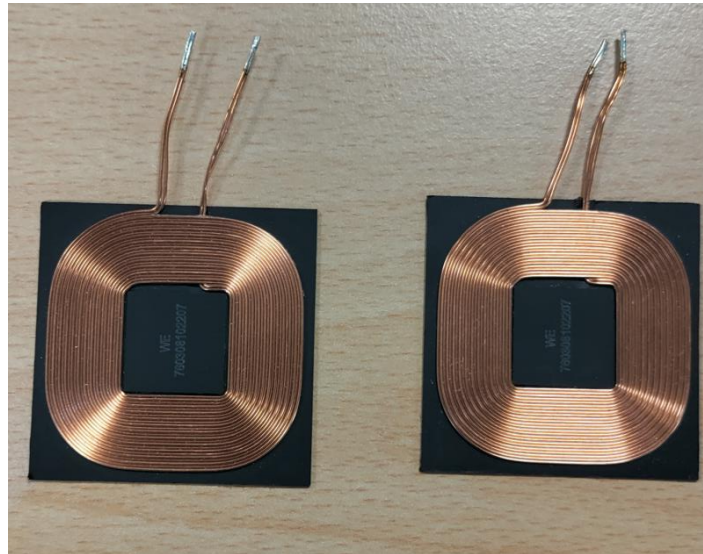
<b>Input Rating</b>	<b>Output Rating</b>
110/220V	24V, 15A

## Appendix E2: Inverter Used in Hardware in its rating



<b>Input Rating</b>	<b>Output Rating</b>
12-40V DC $\leq 20A$	AC High Frequency

### Appendix E3: Coils Used in Hardware in its rating



### Appendix E4: Oscilloscope used in Hardware in its rating



Model	PicoScope 2204A
Bandwidth	10MHz
Maximum sampling rate	100MS/s
Capture memory	8kS
AWG bandwidth	100kHz
Channels	2

